Probing the Wtb vertex structure in t-channel single-top-quark production and decay in pp collisions at $\sqrt{\mathrm{s}} = 8$ TeV with the ATLAS detector

The ATLAS collaboration

E-mail: atlas.publications@cern.ch

ABSTRACT: To probe the Wtb vertex structure, top-quark and W-boson polarisation observables are measured from t-channel single-top-quark events produced in proton-proton collisions at a centre-of-mass energy of 8 TeV. The dataset corresponds to an integrated luminosity of $20.2\,\mathrm{fb}^{-1}$, recorded with the ATLAS detector at the LHC. Selected events contain one isolated electron or muon, large missing transverse momentum and exactly two jets, with one of them identified as likely to contain a b-hadron. Stringent selection requirements are applied to discriminate t-channel single-top-quark events from background. The polarisation observables are extracted from asymmetries in angular distributions measured with respect to spin quantisation axes appropriately chosen for the top quark and the W boson. The asymmetry measurements are performed at parton level by correcting the observed angular distributions for detector effects and hadronisation after subtracting the background contributions. The measured top-quark and W-boson polarisation values are in agreement with the Standard Model predictions. Limits on the imaginary part of the anomalous coupling g_{R} are also set from model-independent measurements.

Contents

1 Introduction

At hadron colliders, top quarks are predominantly produced in pairs ($t\bar{t}$) via the flavour-conserving strong interaction, but single top-quark production can occur via charged-current electroweak processes involving a Wtb vertex. At leading order in QCD perturbation theory, three sub-processes contribute to single top-quark production: an exchange of a virtual W boson either in the t-channel or in the s-channel, or the associated production of a top quark with an on-shell W boson (Wt). The t-channel and s-channel processes do not interfere at next-to-leading-order in QCD and are thus well defined with that precision [1].

In proton-proton (pp) collisions, the t-channel exchange, depicted in figure 1, is the dominant production process of single top quarks. The exchange of a space-like W boson due to the interaction of a light quark with a b-quark produces a top quark and a forward light-quark (called the spectator quark) in the final state. Furthermore, as a consequence of the vector minus axial-vector (V-A) form of the Wtb vertex in the Standard Model, the
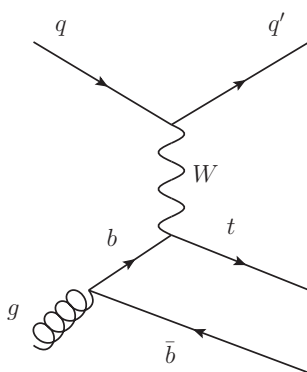
Figure 1. Leading-order Feynman diagram for *t*-channel production of single top quarks in *pp* collisions. In the depicted four-flavour scheme $(2 \rightarrow 3$ process) the initial *b*-quark arises from a gluon splitting into a $b\bar{b}$ pair.

produced top quarks are highly polarised, in particular along the direction of the spectator-quark momentum [2, 3].

Within the Standard Model the top quark decays through the electroweak interaction into an on-shell W boson and a *b*-quark, with a lifetime much shorter than the time scale necessary to depolarise the spin. The information on the top-quark spin can thus be obtained from its decay products. The produced real W boson also possesses a polarisation (or helicity state), which can be extracted from angular distributions of its decay products through the measurement of spin-dependent observables [4].

Measuring the top-quark polarisation and the W-boson spin observables in *t*-channel single top-quark production provides a powerful probe for studying the Wtb vertex in both top-quark production and decay. New physics effects resulting in corrections to the Wtb vertex would affect the top-quark and W-boson polarisations. In the effective operator formalism the most general Wtb Lagrangian can be written as [5]:

$$\mathcal{L}_{Wtb} = -\frac{g}{\sqrt{2}} \bar{b}\gamma^{\mu} \left(V_{\mathrm{L}}P_{\mathrm{L}} + V_{\mathrm{R}}P_{\mathrm{R}}\right) t W_{\mu}^{-} - \frac{g}{\sqrt{2}} \bar{b} \frac{i\sigma^{\mu\nu}q_{\nu}}{m_W} \left(g_{\mathrm{L}}P_{\mathrm{L}} + g_{\mathrm{R}}P_{\mathrm{R}}\right) t W_{\mu}^{-} + \mathrm{h.c.} \quad (1.1)$$

In this expression g is the weak coupling constant, m_W and q_{ν} are the mass and the four-momentum of the W boson, respectively, $P_{\mathrm{L,R}} \equiv (1 \mp \gamma^5)/2$ are the left- and right-handed projection operators, and $\sigma^{\mu\nu} = [\gamma^{\mu}, \gamma^{\nu}]/2$. The constants $V_{\mathrm{L,R}}$ and $g_{\mathrm{L,R}}$ are the left- and right-handed vector and tensor couplings, respectively. In the Standard Model at tree level the coupling V_{L} is the V_{tb} element of the quark-mixing Cabibbo-Kobayashi-Maskawa (CKM) matrix that is close to one, while the anomalous couplings V_{R} and $g_{\mathrm{L,R}}$ are all zero. Deviations from these values would provide hints of physics beyond the Standard Model, and complex values would imply that the top-quark decay has a CP-violating component [5]. The imaginary part of g_{R} (Im g_{R}) can be probed with the best precision in the *t*-channel production of single top quarks through the measurement of polarisation observables [5]. Limits on Im g_{R} have been set at the LHC by the ATLAS Collaboration at a centre-of-mass energy of 7 TeV from the analysis of the double-differential angular decay rates of the produced *t*-channel single-top-quark events [6]. Searches for anomalous

Wtb couplings in single-top-quark production and decay at 7 and 8 TeV have also been published by the CMS Collaboration [7–9].

The top-quark polarisation and the W-boson spin observables can be extracted in an alternative way from the measurement of asymmetries in various angular distributions of the top-quark decay products [4, 5]. Firstly, this article reports a determination of the top-quark polarisation as well as the W-boson spin observables extracted from the measured angular asymmetries. Such measurements serve as a consistency check with the Standard Model predictions. Secondly, limits on Im g_R are presented from the measurement of the so-called normal forward-backward asymmetry, which is the asymmetry predicted to have the highest sensitivity to Im g_R [5], and the asymmetry related to the top-quark polarisation. Here Standard Model values are assumed for all other couplings.

The measurements reported in this article use $20.2\,\mathrm{fb}^{-1}$ of data collected at a centre-of-mass energy of 8 TeV with the ATLAS detector at the LHC. Stringent selection requirements are applied in order to separate signal from background. The W boson from the top-quark decay is identified through its decay modes leading to a final state with an electron or a muon, and missing transverse momentum for the neutrino. The measurement at parton level of the asymmetries is performed by unfolding the observed angular distributions from detector and physics effects after subtracting the background contributions. For all reported results the electron and muon channels are merged, and the analysis is carried out independently of the lepton charge, in order to measure the polarisation observables associated with the combined production and decay of top quarks and top antiquarks.

2   Polarisation observables and asymmetries

The top-quark polarisation is determined from angular distributions of the decay products reconstructed in the top-quark rest frame, while the W-boson spin observables are determined from angular distributions of the charged lepton reconstructed in the W-boson rest frame.

In the top-quark rest frame, the angular distribution of any decay product X of the top quark is given by

$$\frac{1}{\Gamma}\frac{\mathrm{d}\Gamma}{\mathrm{d}(\cos\theta_X)} = \frac{1}{2}\left(1 + \alpha_X P \cos\theta_X\right),\tag{2.1}$$

where θ_X is the angle between the top-quark spin axis and the direction of motion of the chosen decay product in the top-quark rest frame, Γ is the total decay width of the top quark, α_X is the spin analysing power associated with X, and P is the top-quark degree of polarisation. The charged lepton is the most sensitive spin analyser; at next-to-leading-order (NLO) precision in QCD its spin analysing power is $\alpha_{\ell^\pm} = \pm 0.998$ [10]. In the t-channel, single top quarks are produced with a large degree of polarisation in the direction of motion of the spectator quark [3, 11]. This direction is used to define the top-quark spin axis in this measurement. The corresponding degrees of polarisation calculated at NLO in QCD are 0.91 and -0.86 for top-quark and top-antiquark production, respectively [3].

In the framework of a general formalism developed in ref. [4], the spin-density matrix elements for the W-boson helicity components 0, ± 1, resulting from the decay of polarised
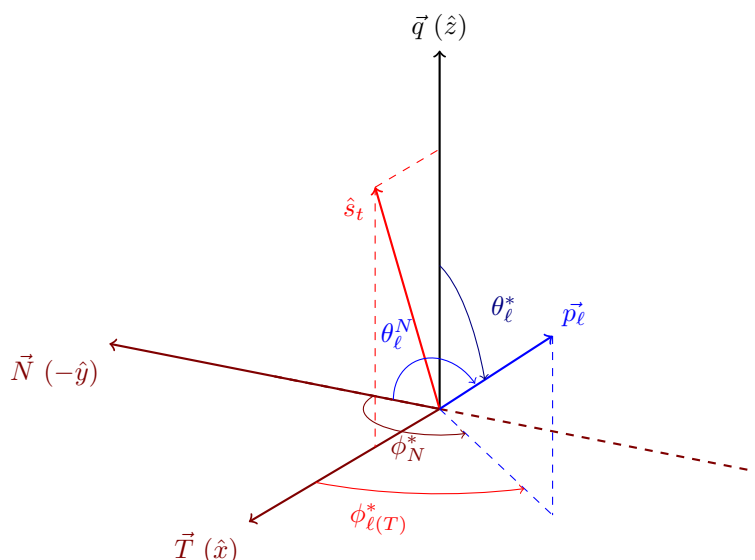
Figure 2. Coordinate system and angles used to define the W-boson spin observables and their related angular asymmetries in the decay of polarised top quarks. The W-boson momentum $\vec{q}$ in the top-quark rest frame defines the $\hat{z}$-axis; the top-quark spin direction $\hat{s}_t$, taken along the spectator-quark momentum in the top-quark rest frame, defines the $\hat{x}$–$\hat{z}$ plane. The polar and azimuthal angles of the charged-lepton momentum $\vec{p}_\ell$ in the W-boson rest frame are labelled θ_ℓ^* and ϕ_ℓ^*, respectively. The normal and transverse axes are defined relatively to $\vec{q}$ and $\hat{s}_t$ according to $\vec{N} = \hat{s}_t \times \vec{q}$ and $\vec{T} = \vec{q} \times \vec{N}$; they are along the $-\hat{y}$ and $\hat{x}$ axes of the coordinate system, respectively. The azimuthal angles ϕ_N^* and ϕ_T^* of the charged lepton in the W-boson rest frame are defined relatively to the $\vec{N}$ and $\vec{T}$ axes, respectively ($\phi_T^* \equiv \phi_\ell^*$), while θ_ℓ^N and θ_ℓ^T (not shown in the figure) are the relative angles between $\vec{p}_\ell$ and the $\vec{N}$ and $\vec{T}$ axes, respectively.

top-quarks, can be parameterised in terms of expectation values of six independent spin observables: $\langle S_{1,2,3}\rangle$, $\langle T_0\rangle$ and $\langle A_{1,2}\rangle$. With $(\theta_\ell^*, \phi_\ell^*)$ denoting the polar and azimuthal angles of the charged-lepton momentum in the W-boson rest frame, the fully differential decay width of a W boson can be written as

$$\frac{1}{\Gamma}\frac{d\Gamma}{d(\cos\theta_\ell^*)d\phi_\ell^*} = \frac{3}{8\pi}\left\{\frac{2}{3} + \frac{1}{\sqrt{6}}\langle T_0\rangle\left(3\cos^2\theta_\ell^* - 1\right) + \langle S_3\rangle\cos\theta_\ell^* \right.$$
$$+ \langle S_1\rangle\cos\phi_\ell^*\sin\theta_\ell^* + \langle S_2\rangle\sin\phi_\ell^*\sin\theta_\ell^*$$
$$\left. - \langle A_1\rangle\cos\phi_\ell^*\sin 2\theta_\ell^* - \langle A_2\rangle\sin\phi_\ell^*\sin 2\theta_\ell^* \right\}. \tag{2.2}$$

In this formalism the W-boson spin axis is taken along the direction of the W-boson momentum in the top-quark rest frame, or equivalently along the direction opposite to the b-quark momentum in the W-boson rest frame. The coordinate system used and the various angles defined for the charged lepton in the W-boson rest frame are depicted in figure 2.

The angular distribution expressed in equation (2.2) implies an integration over all the possible directions of the top-quark spin relative to the W-boson spin axis. The top-quark polarisation is propagated to the spin observables $\langle S_{1,2}\rangle$ and $\langle A_{1,2}\rangle$, which depend in a

proportional way on the value of P. The spin observables $\langle S_3 \rangle$ and $\langle T_0 \rangle$ do not depend on P, and are related to the W-boson helicity fractions F_R, F_L and F_0 [4].

From the values of the helicity fractions predicted by the Standard Model at next-to-next-to-leading order (NNLO) in QCD assuming a top-quark mass of 172.5 GeV and a b-quark mass of 4.8 GeV [12], one obtains $\langle S_3 \rangle = -0.31$ and $\langle T_0 \rangle = -0.43$. The uncertainties in these predictions due to the theoretical uncertainties in the helicity fractions are lower than 0.01 for both $\langle S_3 \rangle$ and $\langle T_0 \rangle$. Combining the predicted degrees of polarisation $P_t = 0.91$ and $P_{\bar{t}} = -0.86$ with the t-channel single-top cross-sections $\sigma_t = 54.9$ pb and $\sigma_{\bar{t}} = 29.7$ pb calculated at NLO in QCD for top-quark and top-antiquark production [13], the Standard Model predictions for $\langle S_{1,2} \rangle$ and $\langle A_{1,2} \rangle$ are: $\langle S_1 \rangle = 0.46$, $\langle A_1 \rangle = 0.23$ and $\langle S_2 \rangle = \langle A_2 \rangle = 0$. These values are calculated at leading order (LO) in QCD from the expressions of the spin-density matrix elements given in refs. [4, 5]. The uncertainties in these predictions resulting from the uncertainties in the top-quark, b-quark and W-boson masses, and from higher-order effects [14], are all smaller than 0.01. Measured values not equal to zero for the $\langle S_2 \rangle$ and $\langle A_2 \rangle$ spin observables would signal the presence of an imaginary coupling in the Wtb vertex, since $\langle S_2 \rangle$ and $\langle A_2 \rangle$ are only sensitive to $\mathrm{Im}\, g_R$ [4].[1] However, $\langle S_2 \rangle$ is twice as sensitive as $\langle A_2 \rangle$ to $\mathrm{Im}\, g_R$, making this observable more suitable for determining this coupling. The other four W-boson spin observables are mainly sensitive to $\mathrm{Re}\, g_R$, with a poor sensitivity to $\mathrm{Im}\, g_R$ [4, 5].

The top-quark polarisation and the W-boson spin observables can be extracted from asymmetries derived by integrating the angular distributions expressed in equations (2.1) and (2.2). These asymmetries are based on single or combined angular observables. They are listed in table 1, together with their associated angular observables and their relation to the polarisation observables.[2] The asymmetry values predicted by the Standard Model are also reported in the table.

Most of the polarisation observables are based on a forward-backward asymmetry, which is generically defined as a function of a given angular observable $\cos\theta$ according to

$$A_{\mathrm{FB}} = \frac{N(\cos\theta > 0) - N(\cos\theta < 0)}{N(\cos\theta > 0) + N(\cos\theta < 0)}, \tag{2.3}$$

where N is the number of events. One of the W-boson spin observables is determined from an asymmetry called edge-central and defined as follows

$$A_{\mathrm{EC}} = \frac{N\left(|\cos\theta| > \frac{1}{2}\right) - N\left(|\cos\theta| < \frac{1}{2}\right)}{N\left(|\cos\theta| > \frac{1}{2}\right) + N\left(|\cos\theta| < \frac{1}{2}\right)}. \tag{2.4}$$

The product $\alpha_\ell P$ is extracted from the forward-backward asymmetry A_{FB}^ℓ of the $\cos\theta_\ell$ angular distribution, where θ_ℓ is the angle between the lepton momentum in the top-quark rest frame and the top-quark spin axis. The measurement of P can also be performed from

---

[1]Including one-loop QCD and electroweak corrections the prediction for g_R in the Standard Model is $(-7.17 - 1.23\mathrm{i}) \times 10^{-3}$ [15], leading to values of the order of 10^{-3} for the $\langle S_2 \rangle$ and $\langle A_2 \rangle$ spin observables.

[2]The asymmetries used in this article and in ref. [5] are related to the ones defined in refs. [4, 16] through the equations $A_{\mathrm{FB}}^T = A_{\mathrm{FB}}^x$, $A_{\mathrm{FB}}^N = -A_{\mathrm{FB}}^y$, $A_{\mathrm{FB}}^{T,\phi} = A_{\mathrm{FB}}^1$, $A_{\mathrm{FB}}^{N,\phi} = -A_{\mathrm{FB}}^2$, $A_{\mathrm{FB}} = A_{\mathrm{FB}}^z$.

Asymmetry	Angular observable	Polarisation observable	SM prediction
A_{FB}^{ℓ}	$\cos\theta_{\ell}$	$\frac{1}{2}\alpha_{\ell}P$	0.45
A_{FB}^{tW}	$\cos\theta_W\cos\theta_{\ell}^*$	$\frac{3}{8}P\left(F_{\mathrm{R}}+F_{\mathrm{L}}\right)$	0.10
A_{FB}	$\cos\theta_{\ell}^*$	$\frac{3}{4}\langle S_3\rangle=\frac{3}{4}\left(F_{\mathrm{R}}-F_{\mathrm{L}}\right)$	-0.23
A_{EC}	$\cos\theta_{\ell}^*$	$\frac{3}{8}\sqrt{\frac{3}{2}}\langle T_0\rangle=\frac{3}{16}\left(1-3F_0\right)$	-0.20
A_{FB}^{T}	$\cos\theta_{\ell}^T$	$\frac{3}{4}\langle S_1\rangle$	0.34
A_{FB}^{N}	$\cos\theta_{\ell}^N$	$-\frac{3}{4}\langle S_2\rangle$	0
$A_{\mathrm{FB}}^{T,\phi}$	$\cos\theta_{\ell}^*\cos\phi_T^*$	$-\frac{2}{\pi}\langle A_1\rangle$	-0.14
$A_{\mathrm{FB}}^{N,\phi}$	$\cos\theta_{\ell}^*\cos\phi_N^*$	$\frac{2}{\pi}\langle A_2\rangle$	0

Table 1. Asymmetries with their associated angular observables and their relation to the top-quark polarisation and W-boson spin observables. The values predicted by the Standard Model are also given. They are calculated using the predictions at NLO in QCD for P and α_{ℓ}, the predictions at NNLO for the helicity fractions, and the predictions at LO for $\langle S_{1,2}\rangle$ and $\langle A_{1,2}\rangle$. The uncertainties in these values are all lower than 0.01. They are estimated from the uncertainties in the top-quark, b-quark and W-boson masses, added in quadrature, including the uncertainty in α_{s} and an estimate of the higher-order effects for the asymmetries related to the W-boson spin observables.

the forward-backward asymmetry A_{FB}^{tW} defined with respect to the combined angular observable $\cos\theta_W\cos\theta_{\ell}^*$ [17], where θ_W is the angle between the W-boson momentum in the top-quark rest frame and the top-quark spin axis. This asymmetry is proportional to the product of P and the sum of two W-boson helicity fractions, as reported in table 1. The W-boson spin observables $\langle S_3\rangle$ and $\langle T_0\rangle$ are derived from the forward-backward asymmetry A_{FB} and from the edge-central asymmetry A_{EC} of the $\cos\theta_{\ell}^*$ angular distribution, respectively. Using the definition [5] of the normal axis $\vec{N}=\vec{s}_t\times\vec{q}$ and transverse axis $\vec{T}=\vec{q}\times\vec{N}$, as illustrated in figure 2, $\langle S_1\rangle$ and $\langle S_2\rangle$ are determined from the forward-backward asymmetries A_{FB}^T and A_{FB}^N in the angular observables $\cos\theta_{\ell}^T$ and $\cos\theta_{\ell}^N$, respectively. The $\langle A_1\rangle$ and $\langle A_2\rangle$ spin observables are determined from the forward-backward asymmetries $A_{\mathrm{FB}}^{T,\phi}$ and $A_{\mathrm{FB}}^{N,\phi}$ based on the combination of $\cos\theta_{\ell}^*$ with the cosine of the azimuthal angles ϕ_T^* and ϕ_N^* defined relatively to $\vec{T}$ and $\vec{N}$, respectively.

Limits on $\mathrm{Im}\,g_{\mathrm{R}}$ can be extracted from the measurement of the A_{FB}^N asymmetry, which has the highest sensitivity to this coupling. For small $\mathrm{Im}\,g_{\mathrm{R}}$ values, taking $V_{\mathrm{L}}=1$ and $V_{\mathrm{R}}=g_{\mathrm{L}}=0$, a linear dependence on $\mathrm{Im}\,g_{\mathrm{R}}$ is obtained for this asymmetry: $A_{\mathrm{FB}}^N=0.64\,P\,\mathrm{Im}\,g_{\mathrm{R}}$ [5]. In this relation the weak dependence of P on $\mathrm{Im}\,g_{\mathrm{R}}$, which is of quadratic form, is not included. As A_{FB}^N depends on P, the measured value of the A_{FB}^{ℓ} asymmetry is required to constrain P for the limit computation. The quadratic variation of P and α_{ℓ} as a function of $\mathrm{Im}\,g_{\mathrm{R}}$ [5, 18] is taken into account when setting the limits through the

procedure explained in section 11. The A_{FB}^{ℓ} asymmetry is chosen to constrain P because its measurement is found to be independent of the value of Im g_{R} assumed when unfolding the corresponding angular distribution; this is discussed in section 9.

3 The ATLAS detector

The ATLAS detector [19] is a multi-purpose particle detector with a forward-backward symmetric, cylindrical geometry and a near 4π coverage in solid angle around the collision point.[3] It consists of an inner tracking detector surrounded by a thin superconducting solenoid, electromagnetic and hadronic calorimeters, and a muon spectrometer. The inner detector is immersed in a 2 T axial magnetic field, and provides charged-particle tracking in the pseudorapidity range $|\eta| < 2.5$. It contains a high-granularity silicon pixel detector, a silicon microstrip tracker, and a straw-tube transition radiation tracker. Lead/liquid-argon sampling calorimeters provide electromagnetic energy measurements with high granularity in the pseudorapidity ranges $|\eta| < 1.5$ (barrel region) and $1.4 < |\eta| < 3.2$ (endcap region). Hadronic energy measurements are provided by steel/scintillator-tile calorimeters in the central pseudorapidity range $|\eta| < 1.7$ and by copper/liquid-argon calorimeters in the endcap region $1.5 < |\eta| < 3.2$. The forward region is instrumented with liquid-argon calorimeters for electromagnetic and hadronic energy measurements, extending the coverage to $|\eta| = 4.9$. The muon spectrometer surrounds the calorimeters and incorporates three large air-core toroid superconducting magnets with eight coils each. It includes separate trigger detectors and high-precision tracking chambers, providing muon momentum measurement for $|\eta| < 2.7$ and muon triggering up to $|\eta| = 2.4$.

A three-level trigger system is used to select interesting events [20]. The first-level trigger is hardware-based and uses a subset of the detector information to reduce the accepted event rate to less than 75 kHz. The second and third levels are software-based and together reduce the event rate to about 400 Hz.

4 Data and simulation samples

The analysis is performed using pp collision data collected in 2012 by the ATLAS detector at a centre-of-mass energy of 8 TeV. The events are required to pass single-electron or single-muon triggers [20, 21], resulting, after detector and data-quality requirements, in a data sample corresponding to an integrated luminosity of $20.2\,\mathrm{fb}^{-1}$. The electron and muon triggers impose a threshold of 24 GeV on the transverse momentum (p_{T}), along with isolation requirements. To recover efficiency for higher-p_{T} leptons, the isolated lepton triggers are complemented by triggers without isolation requirements, but with a threshold raised to 60 GeV for electrons and to 36 GeV for muons.

---

[3]ATLAS uses a right-handed coordinate system with its origin at the nominal interaction point in the centre of the detector and the z-axis along the beam pipe. The x-axis points from the interaction point to the centre of the LHC ring, and the y-axis points upwards. Cylindrical coordinates (r, ϕ) are used in the transverse plane, ϕ being the azimuthal angle around the z-axis. The pseudorapidity is defined in terms of the polar angle θ as $\eta = -\ln\tan(\theta/2)$.

Samples of signal and background events are simulated using various Monte Carlo generators. The generated events are passed through a simulation of the ATLAS detector [22] based on the GEANT4 framework [23]. For some samples a faster simulation (ATLFAST-II [24]), making use of a parameterised response of the electromagnetic and hadronic calorimeters, is performed instead. Minimum-bias events simulated with the PYTHIA (8.1) [25] generator are overlaid to model the pile-up effects from additional pp collisions in the same and nearby bunch crossings. All simulated events are then processed using the same reconstruction and analysis chain as for data events.

Signal t-channel single-top-quark events are generated with the NLO POWHEG-BOX (r2556) [26–28] generator, which uses the four-flavour scheme (figure 1) for the matrix-element calculations [29]. Events are generated with the CT10f4 [30] parton distribution functions (PDFs), and the renormalisation and factorisation scales are set to $\mu_{\mathrm{R}}^2 = \mu_{\mathrm{F}}^2 = 16\left(m_b^2 + p_{\mathrm{T},b}^2\right)$, where m_b is the mass of the b-quark and $p_{\mathrm{T},b}$ is the transverse momentum of the b-quark from the initial gluon splitting (called the spectator b-quark) [29]. Additional t-channel samples are produced with the LO PROTOS (2.2) [31] generator using the CTEQ6L1 PDFs [32]. PROTOS events are generated using the four-flavour scheme, as well, and anomalous couplings are enabled in both the production and the decay vertices, varying $\mathrm{Re}\,V_{\mathrm{L}}$ and $\mathrm{Im}\,g_{\mathrm{R}}$ simultaneously to keep the top-quark width invariant. The factorisation scale is set to $\mu_{\mathrm{F}}^2 = -p_W^2$ for the light quark, where p_W is the four-momentum of the exchanged W boson, and to $\mu_{\mathrm{F}}^2 = m_b^2 + p_{\mathrm{T},b}^2$ for the gluon. Eight PROTOS samples generated with $\mathrm{Im}\,g_{\mathrm{R}}$ in the range $[-0.144, 0.144]$ and $\mathrm{Re}\,V_{\mathrm{L}}$ in the range $[0.982, 1]$ are used, including the Standard Model configuration $\mathrm{Im}\,g_{\mathrm{R}} = 0$ and $\mathrm{Re}\,V_{\mathrm{L}} = 1$. These PROTOS samples are used to compute the parton-level unfolding corrections and to check the reliability of the unfolding method, while the POWHEG-BOX sample is used to determine the expected event yields and template distributions.

Samples of $t\bar{t}$ [33], s-channel single-top-quark and Wt [34] background events are produced using the POWHEG-BOX (r2819, r3026) generator with the CT10 PDFs. To generate the $t\bar{t}$ sample, the model parameter h_{damp}, which effectively regulates the high-p_{T} gluon radiation, is set to the top-quark mass m_t [35].

For the above samples, parton showering, hadronisation and the underlying event are simulated with PYTHIA (6.426) [36] using parameter values set to the Perugia 2011C tune [37], and the CTEQ6L1 PDFs.

To study the modelling uncertainties of all processes involving top quarks, either alternative generators or parameter variations in the POWHEG-BOX and PYTHIA settings are used. For the estimation of the uncertainty in the t-channel matrix-element calculation, a sample is produced using the MADGRAPH5_aMC@NLO (2.0) [38] generator, interfaced to HERWIG (6.52) [39, 40] for parton showering and to JIMMY (4.31) [41] for the underlying-event modelling with the ATLAS AUET2 tuned parameter settings [42] and the CT10f4 PDFs. The events are generated using the four-flavour scheme. For the $t\bar{t}$, s-channel and Wt processes, alternative samples are produced using the MC@NLO (4.03) [43–46] generator interfaced to HERWIG (6.52) for parton showering and JIMMY (4.31) for the underlying-event modelling with the ATLAS AUET2 tune and the CT10 PDFs. To specif-

ically study the impact of the parton-shower modelling, a t-channel sample and a Wt sample both generated with Powheg-Box and coupled to Herwig (6.52) and Jimmy (4.31) with the AUET2 tune are used. For the $t\bar{t}$ process, samples generated using Powheg-Box with the CT10 PDFs, interfaced to Herwig (6.52) with the AUET2 tune or to Pythia (6.426) with the AUET2B tune, are used. Effects of varying the amount of radiation are studied by changing the hard-process and parton-shower scales simultaneously in the Powheg-Box and Pythia (6.426, 6.427) simulations. In the single-top-quark samples the factorisation and renormalisation scales are increased or decreased by a factor of two or one-half, respectively, in combination with the Perugia 2012 radLo and radHi tunes [37]. In the $t\bar{t}$ samples, h_{damp} is set to m_t or $2m_t$ in combination with the radLo and radHi parameterisations, respectively.

All top-quark processes are simulated assuming a top-quark mass of 172.5 GeV, and the top-quark decay is assumed to proceed exclusively through $t \to Wb$. The baseline Powheg-Box samples are passed through the fully Geant4-based simulation of the ATLAS detector, while the Protos samples and all samples used in studies of modelling uncertainties are processed through the ATLFAST-II simulation.

Vector-boson production in association with jets is simulated using the multileg LO Sherpa (1.4.1) [47] generator with its own parameter tune and the CT10 PDFs. Sherpa is used not only to generate the hard process, but also for the parton shower and the modelling of the underlying event. W+jets and Z+jets events with up to four additional partons are generated. The CKKW method [48] is used to remove overlaps between the partonic configurations generated by the matrix element and by the parton showering. Diboson samples of WW, WZ and ZZ events are also produced, using the Sherpa (1.4.1) generator with the CT10 PDFs. All the generated Sherpa single-boson and diboson events are passed through the ATLFAST-II simulation of the detector.

5   Event reconstruction and selection

The analysis considers only W-boson decay modes to an electron or a muon. Events in which the W boson decays to a τ lepton are thus included if the τ lepton subsequently decays to an electron or a muon.

The signal event candidates are selected by requiring a single isolated electron or muon, significant missing transverse momentum, and exactly two jets with one of them identified as likely to contain a b-hadron (b-tagged jet). In fact, the presence of a third jet is not required in the event selection. Indeed, the additional jet resulting from the spectator b-quark originating from the gluon splitting as shown in figure 1 is expected to have a softer p_{T} spectrum and a broader $|\eta|$ distribution than the b-tagged jet produced in the top-quark decay, and, therefore, is in general not detected.

Electron candidates are reconstructed from isolated energy deposits in the electromagnetic calorimeter which are associated with inner-detector tracks fulfilling strict quality requirements [49]. They are required to satisfy $p_{\mathrm{T}} > 25$ GeV and $|\eta| < 2.47$, excluding the barrel-endcap transition region, corresponding to $1.37 < |\eta| < 1.52$. Muon candidates are reconstructed using combined tracking information from the inner detector and the muon

spectrometer [50]. They are required to have $p_T > 25\,\text{GeV}$ and $|\eta| < 2.5$. The electron and muon candidates must fulfil additional isolation requirements, as described in ref. [51], in order to reduce contributions from misidentified jets, non-prompt leptons from the decay of heavy-flavour quarks and electrons from photon conversions.

Jets are reconstructed using the anti-k_t algorithm [52] with a radius parameter of 0.4, from topological clusters [53], calibrated with a local cluster weighting method [54]. Jets are calibrated using an energy- and η-dependent simulation-based scheme, with in situ corrections based on data. The jet energy is further corrected for the effect of multiple pp interactions. To reject jets from pile-up events, a so-called jet-vertex-fraction criterion [55] is applied to the jets with $p_T < 50\,\text{GeV}$ and $|\eta| < 2.4$: at least 50% of the scalar sum of the p_T of the tracks associated with a jet is required to be from tracks compatible with the primary vertex.[4] Only events containing two reconstructed jets with $p_T > 30\,\text{GeV}$ are selected. In addition, one of them must be b-tagged with $|\eta| < 2.5$, while the second jet is required to be untagged and to have $|\eta| < 4.5$. The b-tagging is performed using a neural network which combines three different algorithms exploiting the properties of a b-hadron decay in a jet [56]. The b-tagging algorithm is optimised to improve the rejection of c-quark jets, since W-boson production in association with c-quarks is a major background for the selected final state. The requirement applied to the neural-network discriminant corresponds to a b-tagging efficiency of 50%, and mistagging rates of 3.9% and 0.07% for c-quark jets and light-flavour jets, respectively, as predicted in simulated $t\bar{t}$ events [57, 58].

The missing transverse momentum, with magnitude E_T^{miss}, is reconstructed from the vector sum of energy deposits in the calorimeter projected onto the transverse plane [59]. All cluster energies are corrected using the local cluster weighting method. Clusters associated with high-p_T jets and electrons are further calibrated using their respective energy corrections. Contributions from the p_T of the selected muons are also included in the calculation.

Events are required to contain at least one good primary-vertex candidate, and no jets failing to satisfy reconstruction quality criteria. The magnitude of the missing transverse momentum is required to be larger than $30\,\text{GeV}$. In addition, the transverse mass of the lepton–E_T^{miss} system must be greater than $50\,\text{GeV}$ in order to reduce the multijet background contribution.[5] Further reduction of this background is achieved by imposing an additional requirement on events where the lepton and the leading jet in p_T have opposite directions in the transverse plane [60]. To reduce the $t\bar{t}$ dilepton background, events containing an additional lepton, identified with less stringent criteria (referred to as a loose lepton) and with a p_T threshold lowered to $10\,\text{GeV}$, are rejected.

The lepton and neutrino four-momenta are used to reconstruct the W boson. Since the neutrino escapes undetected, the x- and y-components of the missing transverse momentum

---

[4]A primary-vertex candidate is defined as a reconstructed vertex with at least five associated tracks with $p_T > 400\,\text{MeV}$. The primary vertex associated with the hard-scattering collision is the candidate with the largest sum of the squared p_T of the associated tracks.

[5]The transverse mass of the lepton–E_T^{miss} system is defined as $m_T(\ell, E_T^{\text{miss}}) = \sqrt{2p_T(\ell)E_T^{\text{miss}}(1 - \cos\Delta\phi(\ell, E_T^{\text{miss}}))}$, where $\Delta\phi(\ell, E_T^{\text{miss}})$ is the difference in azimuthal angle between the lepton transverse momentum and the missing transverse momentum.

are assumed to correspond to the transverse momentum of the neutrino. The unmeasured longitudinal component of the neutrino momentum is computed by imposing a W-boson mass constraint on the lepton-neutrino system. If there are two real solutions, the solution giving the smallest magnitude of the longitudinal neutrino momentum is taken. If there are complex solutions, the magnitude of the measured missing transverse momentum is rescaled in order to obtain a physical solution [6]. The top-quark candidate is reconstructed by combining the four-momenta of the reconstructed W boson and the b-tagged jet.

Additional requirements, defining the signal region, are finally applied to the preselected events:

- The pseudorapidity of the untagged jet must satisfy $|\eta| > 2.0$, since the spectator quark tends to be produced in the forward direction in the t-channel process.

- The separation in η between the untagged jet and the b-tagged jet must be larger than 1.5, to reduce the contribution from $t\bar{t}$ background events.

- The mass of the reconstructed top quark is required to be between 130 GeV and 200 GeV, to reject background events from processes not involving top quarks.

- The scalar sum (H_{T}) of the p_{T} of the lepton, the p_{T} of the jets and $E_{\mathrm{T}}^{\mathrm{miss}}$ must be larger than 195 GeV, to further reduce the number of background events, in particular the W+jets contribution.

Figure 3 shows the distributions of the four variables relevant for these requirements, comparing data to the predicted signal and background distributions normalised to the results of the maximum-likelihood fit described in section 7. The cuts that define the signal region are indicated for each of the variables. The multijet background estimate shown in the figure is discussed in section 6.

6   Background normalisation and modelling

The largest background contributions to t-channel single top-quark production arise from $t\bar{t}$ and W+jets production. The former is difficult to distinguish from the signal since $t\bar{t}$ events contain real top quarks in the final state. The W+jets production contributes to the background if there is a b-quark in the final state or due to mistagging of jets containing other quark flavours. Multijet production via the strong interaction can contribute as well if, in addition to two reconstructed jets, an extra jet is misidentified as an isolated lepton, or if a non-prompt lepton appears to be isolated (both referred to as fake leptons). Other minor backgrounds originate from Wt, s-channel single top-quark, Z+jets and diboson production.

For all processes, except multijet production, the normalisation is initially estimated by using the Monte Carlo simulation scaled to the theoretical cross-section predictions, and the event distribution modelling is taken from simulation.

The $t\bar{t}$ production cross-section is calculated at NNLO in QCD including resummation of next-to-next-to-leading-logarithm (NNLL) soft gluon terms with Top++2.0 [61–66]. Its
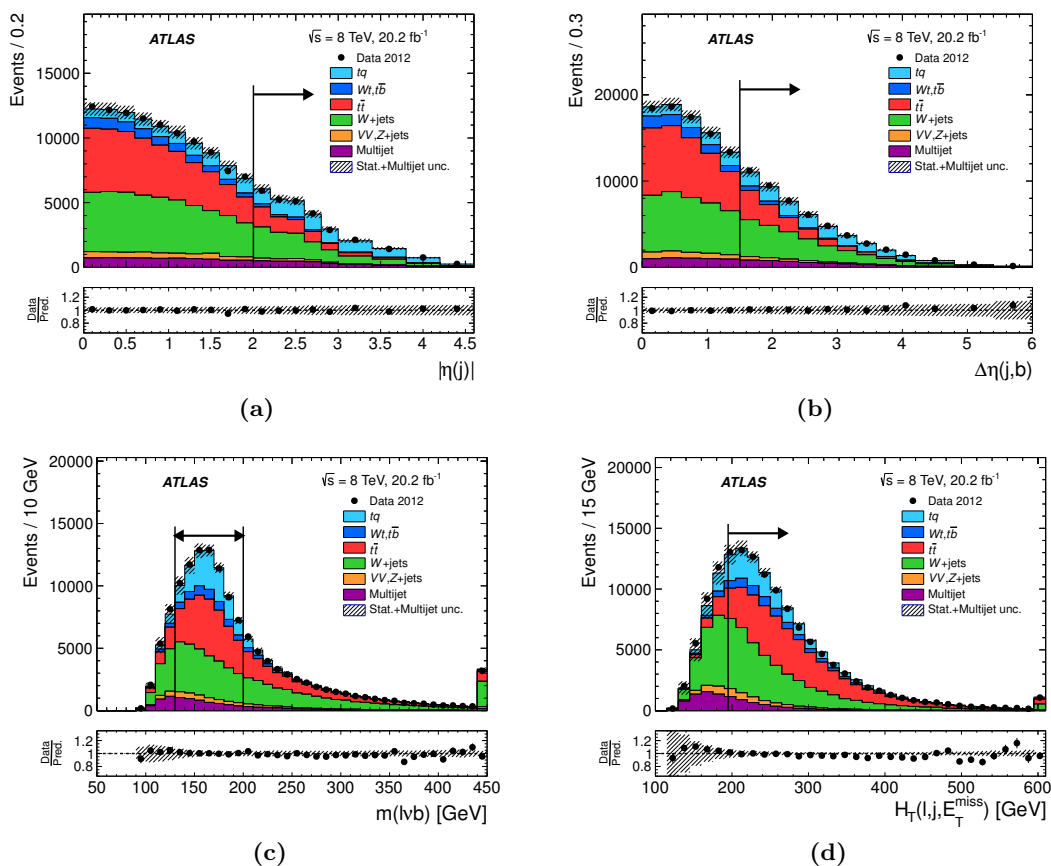
Figure 3. Distributions of the selection variables in the preselected signal region: (a) $|\eta|$ of the untagged jet, (b) separation in η between the untagged and b-tagged jets, (c) reconstructed top-quark mass, and (d) scalar sum of the p_{T} of the lepton, the p_{T} of the jets and $E_{\mathrm{T}}^{\mathrm{miss}}$. The observed distributions are compared to the predicted signal and background distributions, normalised to the results of the maximum-likelihood fit. The labels tq and $t\bar{b}$ refer to the t-channel and s-channel single-top-quark processes, respectively, and VV to diboson production. The vertical lines and the arrows define the signal region. The uncertainty bands include the statistical post-fit uncertainty, the uncertainty due to the limited size of the simulation samples and the uncertainty in the normalisation of the multijet background, added in quadrature. The last bin of the histograms includes overflows. The lower panels show the ratio of data to prediction.

predicted value is 253^{+13}_{-15} pb [61]. The quoted uncertainties include the PDF and α_{s} uncertainties calculated according to the PDF4LHC prescription [67] with the MSTW2008 NNLO [68, 69], CT10 NNLO [30, 70] and NNPDF2.3 5f FFN [71] PDF sets, and the QCD scale uncertainty. The t-channel, Wt and s-channel single-top-quark production cross-sections are calculated at NLO precision in QCD through NNLL resummation, leading to $87.7^{+3.4}_{-1.9}$ pb [72], 22.4 ± 1.5 pb [73] and 5.6 ± 0.2 pb [74], respectively. The calculations assume a top-quark mass of $172.5\,\mathrm{GeV}$ and use the MSTW2008 NNLO [68] PDFs. The quoted uncertainties include those due to the QCD scale uncertainty and the correlated PDF–α_{s} uncertainty.

The cross-sections for inclusive W- and Z-boson production are estimated with NNLO precision using the FEWZ program [75, 76] and the MSTW2008 NNLO PDFs. The diboson samples are normalised to the NLO cross-section predictions calculated with MCFM [77]. A normalisation uncertainty of 20% is assigned to the W+jets background. This uncertainty is estimated from parameter variations of the SHERPA generator covering the measured W+jets cross-sections [78]. A normalisation uncertainty of 20% is also assumed for the Z+jets and diboson processes.

The normalisation as well as the event modelling of the multijet background is estimated from data using the matrix method [51, 79]. This method allows the derivation of the true composition of the data sample in terms of prompt (real) and fake leptons from its observed composition in terms of tight (signal selection) and loose leptons. An alternative normalisation and modelling based on the mixed data-simulation jet-electron method [60, 80] and the purely data-driven anti-muon selection [51] are used to estimate the systematic uncertainties. From the comparison an overall normalisation uncertainty of 70% is assigned to the multijet contribution.

To check the modelling of the $t\bar{t}$ and W+jets background contributions, the simulated events are compared to the data in two dedicated background-dominated regions. Samples enriched in $t\bar{t}$ events ($t\bar{t}$ control region) are defined by considering events preselected as explained in section 5, but containing two additional jets that are required to be untagged. This control region is also used in the normalisation fit described in section 7. Samples enriched in W+jets events (W+jets control region) are selected by applying a relaxed b-tagging requirement corresponding to an efficiency of 80%. In addition, all events satisfying the signal b-tagging requirement are excluded. For these two control regions the dilepton rejection and the four final selection cuts are not applied. An additional category of events is defined by selecting all events not passing any of the four signal selection cuts (anti-signal region). This region is only used in the normalisation fit, in combination with the $t\bar{t}$ control region. It is preferred to the W+jets control region to constrain the W+jets normalisation because it has a flavour composition more similar to that of the signal region. The predicted fraction of heavy-flavour events in the W+jets contribution is around 95% for both the signal and anti-signal selections, whereas it is 55% in the W+jets control region.

Good overall data-prediction agreement is found in the $t\bar{t}$, W+jets and anti-signal control regions for the relevant kinematic observables, as well as for the various angular observables used in the measurements. Figure 4 shows the distributions in the $t\bar{t}$ control region of the four variables used to define the final selections. The distributions obtained in the W+jets control region are displayed in figure 5.

7 Signal and background event yields

The signal and background event yields are estimated through a simultaneous maximum-likelihood fit to the numbers of data events observed in the signal and anti-signal regions, and in the $t\bar{t}$ control region.

The likelihood function [60] is given by the product of Poisson probability terms associated with the fitted regions, combined with the product of Gaussian priors to constrain
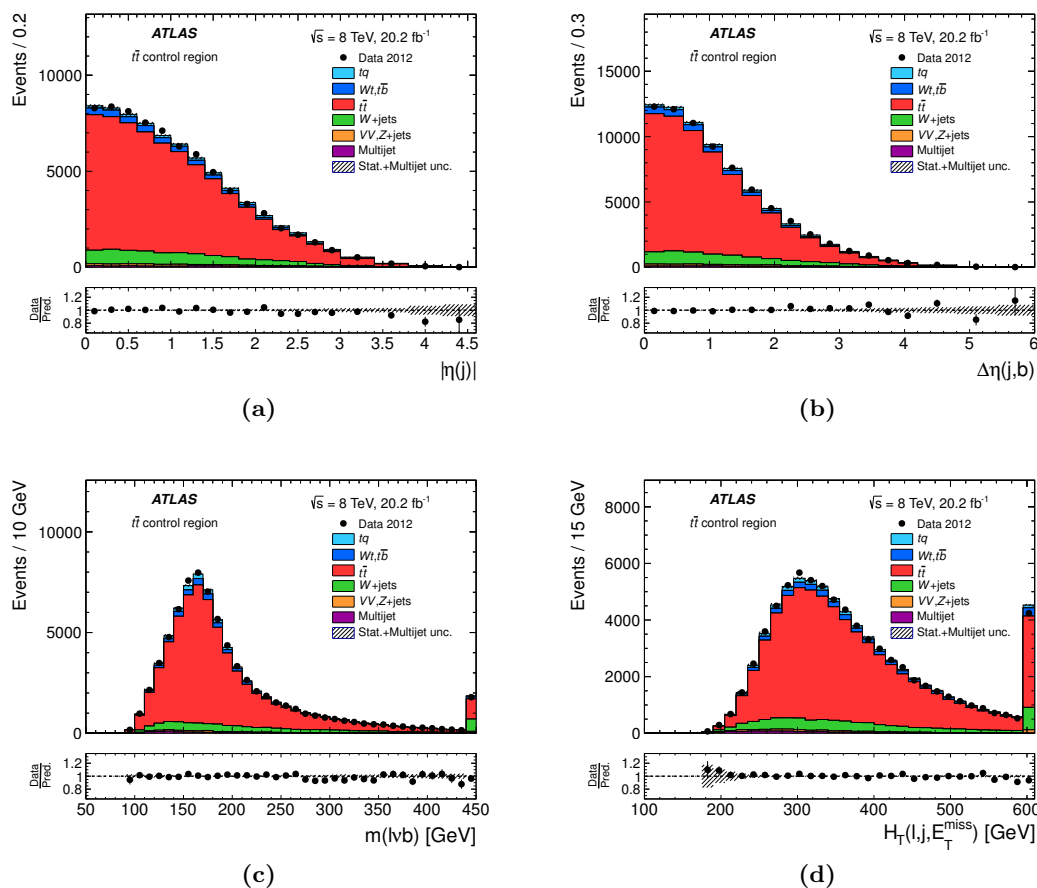
Figure 4. Distributions of the selection variables in the $t\bar{t}$ control region: (a) $|\eta|$ of the untagged jet, (b) separation in η between the untagged and b-tagged jets, (c) reconstructed top-quark mass, and (d) scalar sum of the p_{T} of the lepton, the p_{T} of the jets and $E_{\mathrm{T}}^{\mathrm{miss}}$. The observed distributions are compared to the predicted signal and background distributions, normalised to the results of the maximum-likelihood fit. The labels tq and $t\bar{b}$ refer to the t-channel and s-channel single-top-quark processes, respectively, and VV to diboson production. The uncertainty bands include the statistical post-fit uncertainty, the uncertainty due to the limited size of the simulation samples and the uncertainty in the normalisation of the multijet background, added in quadrature. The last bin of the histograms includes overflows. The lower panels show the ratio of data to prediction.

the background rates to their predictions within the associated uncertainties. In the fit the t-channel single-top-quark contribution is treated as unconstrained. The top-quark background contributions ($t\bar{t}$, Wt and s-channel single top-quark production) are merged with their relative fractions taken from simulation, and the applied constraint is derived from the combination of their cross-section uncertainties presented in section 6. The flavour composition of the W+jets contribution is taken from simulation. In all fitted regions the production of a W boson in association with heavy-flavour jets is the dominant contribution to the W+jets background, predicted to be around 95% in the three regions. The Z+jets and diboson contributions, which are very low in the signal region (2% of the total
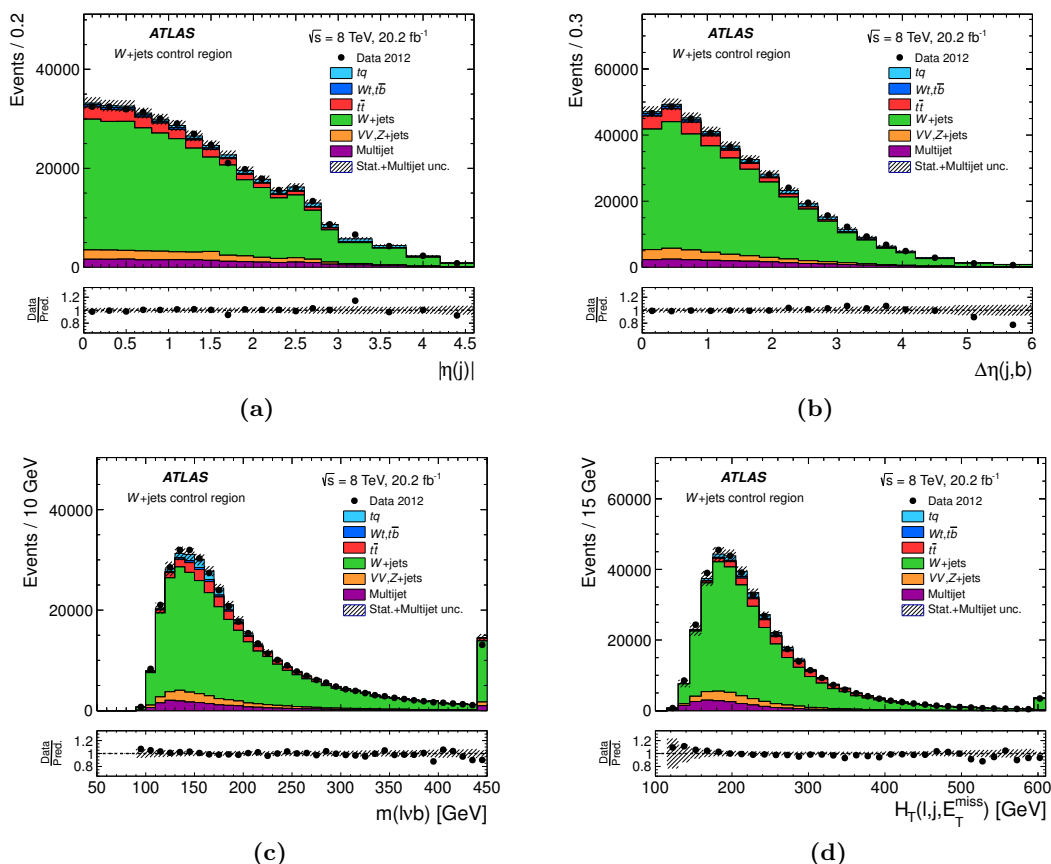
Figure 5. Distributions of the selection variables in the W+jets control region: (a) $|\eta|$ of the untagged jet, (b) separation in η between the untagged and b-tagged jets, (c) reconstructed top-quark mass, and (d) scalar sum of the p_T of the lepton, the p_T of the jets and E_T^{miss}. The observed distributions are compared to the predicted signal and background distributions. The W+jets distributions are normalised to match the observed number of events. The labels tq and $t\bar{b}$ refer to the t-channel and s-channel single-top-quark processes, respectively, and VV to diboson production. The uncertainty bands include the uncertainty due to the limited size of the simulation samples and the uncertainty in the normalisation of the multijet background, added in quadrature. The last bin of the histograms includes overflows. The lower panels show the ratio of data to prediction.

expectation), are merged and fixed to the predictions. The multijet contribution is kept fixed to its data-driven estimate.

The results of the maximum-likelihood fit together with the associated statistical uncertainties (referred to as statistical post-fit uncertainties) are shown in table 2. They are presented as scale factors to be applied to the predicted event yields. The results are found to be stable when the constraints imposed on the top-quark and W+jets backgrounds are significantly relaxed. Table 3 provides the signal and background event yields in the signal region after scaling to the results of the fit to the data. The signal-to-background ratio is 1.2, the t-channel single top-quark production representing 54% of the total expectation. The two main background contributions come from W+jets (19%) and $t\bar{t}$ production (18%).

Process	Scale factor
t-channel	0.95 ± 0.02
$t\bar{t}$, Wt, s-channel	1.01 ± 0.01
W+jets	1.10 ± 0.01

Table 2. Scale factors and uncertainties extracted for the signal and background processes from the simultaneous maximum-likelihood fit of the event yields in the signal, anti-signal and $t\bar{t}$ regions. The quoted uncertainties are statistical only.

Process	Event yield
t-channel	5700 ± 110
Wt, s-channel	265 ± 12
$t\bar{t}$	1914 ± 15
W+jets	2044 ± 57
Z+jets, diboson	188 ± 9
Multijet	420 ± 290
Total expectation	10530 ± 320
Data	10527

Table 3. Signal and background event yields in the signal region after scaling to the results of the maximum-likelihood fit. The quoted uncertainties add in quadrature the post-fit uncertainties and the uncertainties due to the limited size of the simulation samples, except for the data-driven multijet contribution to which the normalisation uncertainty of 70% is applied. The total expectation is compared to the observed number of events.

8 Angular distributions

The distributions observed at reconstruction level for the angular observables used to measure the various asymmetries are shown in figures 6 and 7. They are compared to the predicted signal and background distributions, normalised to the results of the maximum-likelihood fit. To minimise the unfolding corrections that are applied after background subtraction, two bins are chosen for the angular distributions from which forward-backward asymmetries are extracted, while four bins are used for the angular distribution from which the A_{EC} asymmetry is determined.

Depending on the angular observable, as described in section 2, the charged-lepton four-momentum is computed in the rest frame of the reconstructed top quark or in the rest frame of the reconstructed W boson. The angular observables related to the top-quark polarisation are defined by taking the momentum of the untagged jet as the spectator-quark direction, whereas those related to the W-boson spin observables are defined by considering the reverse momentum of the b-tagged jet as the W-boson direction.
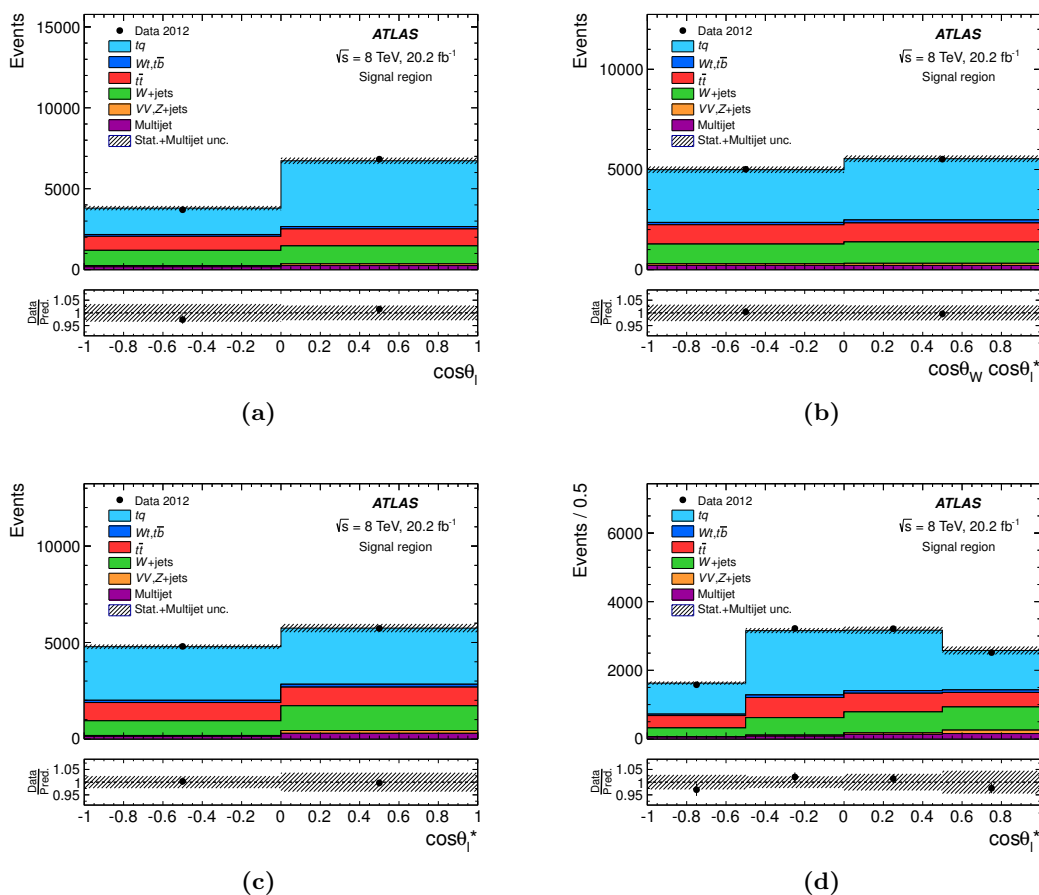
Figure 6. Distributions in the signal region of the angular observables used to measure the various asymmetries: (a) $\cos\theta_\ell$ for A_{FB}^ℓ, (b) $\cos\theta_W \cos\theta_\ell^*$ for A_{FB}^{tW}, (c) $\cos\theta_\ell^*$ with two bins for A_{FB}, and (d) $\cos\theta_\ell^*$ with four bins for A_{EC}. The observed distributions are compared to the predicted signal and background distributions, normalised to the results of the maximum-likelihood fit. The template t-channel distributions are taken from the baseline POWHEG-BOX sample. The labels tq and $t\bar{b}$ refer to the t-channel and s-channel single-top-quark processes, respectively, and VV to diboson production. The uncertainty bands include the statistical post-fit uncertainty, the uncertainty due to the limited size of the simulation samples and the uncertainty in the normalisation of the multijet background, added in quadrature. The lower panels show the ratio of data to prediction.

9 Unfolding

The measured angular distributions are unfolded to the parton level,[6] so that the asymmetries extracted from the corrected angular distributions can be directly compared to theoretical calculations. The unfolding corrections account for distortions due to detector resolution, selection efficiencies, and reconstruction of the W boson and top quark. They also include the effects due to hadronisation and parton showering.

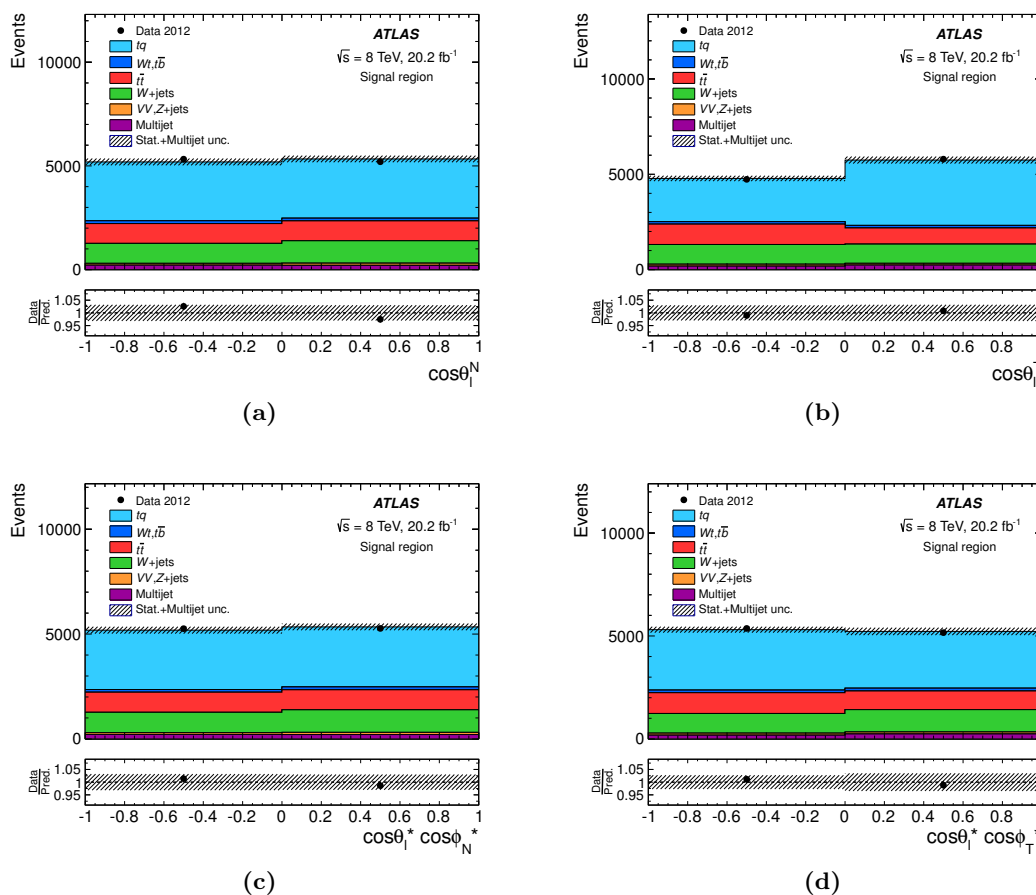[6]Partons are defined from the matrix-element hard process and immediate decays.

Figure 7. Distributions in the signal region of the angular observables used to measure the various asymmetries: (a) $\cos\theta_\ell^N$ for A_{FB}^N, (b) $\cos\theta_\ell^T$ for A_{FB}^T, (c) $\cos\theta_\ell^* \cos\phi_N^*$ for $A_{\mathrm{FB}}^{N,\phi}$, and (d) $\cos\theta_\ell^* \cos\phi_T^*$ for $A_{\mathrm{FB}}^{T,\phi}$. The observed distributions are compared to the predicted signal and background distributions, normalised to the results of the maximum-likelihood fit. The template t-channel distributions are taken from the baseline POWHEG-BOX sample. The labels tq and $t\bar{b}$ refer to the t-channel and s-channel single-top-quark processes, respectively, and VV to diboson production. The uncertainty bands include the statistical post-fit uncertainty, the uncertainty due to the limited size of the simulation samples and the uncertainty in the normalisation of the multijet background, added in quadrature. The lower panels show the ratio of data to prediction.

The unfolding procedure is applied to the angular distributions after subtracting the background contributions, and is based on a matrix inversion combined with an efficiency correction. The number of unfolded signal events N_j^{unfolded} in each bin j of the parton-level distribution is obtained from the background-subtracted yields N_i^{measured} measured in all bins i of the reconstructed distribution, according to

$$N_j^{\mathrm{unfolded}} = \frac{\sum_i M_{ji}^{-1} N_i^{\mathrm{measured}}}{\epsilon_j}, \tag{9.1}$$

where M_{ji} is the migration matrix which relates the parton-level and reconstructed values of the considered angular variable, and ϵ_j is the event selection efficiency. Both the mi-

gration matrix and the selection efficiency are computed using samples of t-channel events simulated with the PROTOS generator, as described below. For the chosen numbers of bins, the fractions of simulated events belonging to the diagonal elements of the migration matrices are found to be between 68% and 90%, depending on the angular observable. The selection efficiencies are between 0.6% and 1.6%, depending on the angular observable and on the bin range. The matrix inversion is performed by using the iterative Bayesian method [81] as implemented in the RooUnfold framework [82]. The number of iterations is chosen such that the absolute change in the extracted asymmetry between two successive steps becomes lower than 0.0005. The unfolding procedure has been validated through convergence and closure tests performed by using template distributions constructed from the t-channel POWHEG-BOX and PROTOS samples presented in section 4. The closure tests showed that the residual bias induced by the unfolding method is negligible, whatever the measured asymmetry.

With the aim of testing their compatibility with the Standard Model predictions, all asymmetries described in section 2, except A_{FB}^N, are extracted using the PROTOS simulation generated with the Standard Model values of the Wtb couplings to determine the migration matrix and the selection efficiency. For all the asymmetry measurements, the Standard Model Wtb couplings, as implemented in the POWHEG-BOX generator, are considered for the subtracted top-quark backgrounds.

To constrain $\mathrm{Im}\,g_{\mathrm{R}}$ using the method explained in section 2, the A_{FB}^N and A_{FB}^ℓ asymmetries must be measured without any assumption about $\mathrm{Im}\,g_{\mathrm{R}}$. It is observed that the presence of anomalous couplings in general modifies the kinematics in such a way that the efficiency corrections are dependent on the Wtb couplings. While the measurement of A_{FB}^ℓ is found to be independent of the value of $\mathrm{Im}\,g_{\mathrm{R}}$ assumed in the unfolding corrections, the measurement of A_{FB}^N is found to depend on the unfolding corrections used. By applying an interpolation technique it is possible to unfold the $\cos\theta_\ell^N$ angular distribution independently of any assumption about $\mathrm{Im}\,g_{\mathrm{R}}$, so that the extracted A_{FB}^N asymmetry, combined with A_{FB}^ℓ, can be used to constrain this coupling.

The interpolation method is based on determining the unfolding corrections using a linear combination of the migration and efficiency corrections provided by five Protos samples in which $\mathrm{Im}\,g_{\mathrm{R}}$ is varied ($\mathrm{Im}\,g_{\mathrm{R}} = 0, \pm 0.094, \pm 0.23$). An iterative procedure is applied to determine the coefficients of the linear combination until convergence is reached in the extracted A_{FB}^N asymmetry. The method proceeds as follows. An initial value of A_{FB}^N is first extracted using the standard Protos unfolding corrections. This value is then used to determine, via a Lagrange interpolation, the weights to be applied to the five predicted corrections. A new value of A_{FB}^N is obtained after unfolding the $\cos\theta_\ell^N$ angular distribution with these corrections using the Bayesian method. The chosen convergence criterion for the interpolation procedure requires that the difference between the extracted A_{FB}^N from two successive steps is smaller than 0.0005. By using template distributions given by PROTOS samples not used in the linear combination of the unfolding corrections ($\mathrm{Im}\,g_{\mathrm{R}} = \pm 0.043, \pm 0.144$), it has been checked that this method recovers the generated asymmetries at parton level.
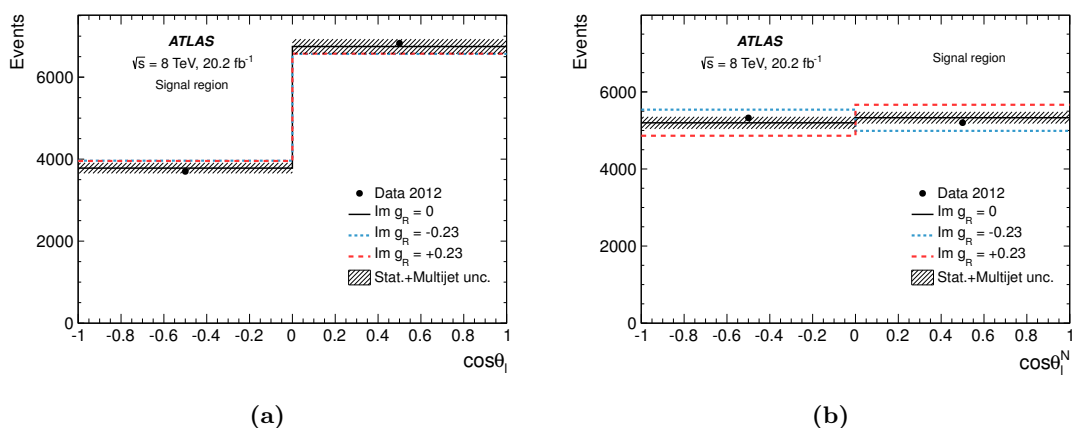
Figure 8. Comparison of the distributions observed in the signal region with the distributions predicted as a function of $\mathrm{Im}\, g_{\mathrm{R}}$ for the angular observables from which the asymmetries used to set limits on this coupling are measured: (a) $\cos\theta_\ell$ for A_{FB}^ℓ and (b) $\cos\theta_\ell^N$ for A_{FB}^N. The predicted distributions are determined by adding the signal and background contributions normalised to the results of the maximum-likelihood fit. The template signal distributions are taken from the PROTOS samples generated with $\mathrm{Im}\, g_{\mathrm{R}} = 0$ (Standard Model parameterisation) and $\mathrm{Im}\, g_{\mathrm{R}} = \pm 0.23$. The corresponding parton-level values for the A_{FB}^N asymmetry are 0 and ± 0.10, respectively. For A_{FB}^ℓ the predicted values are 0.45 for $\mathrm{Im}\, g_{\mathrm{R}} = 0$ and 0.34 for $\mathrm{Im}\, g_{\mathrm{R}} = \pm 0.23$. The uncertainty bands include the statistical post-fit uncertainty, the uncertainty due to the limited size of the simulation samples and the uncertainty in the normalisation of the multijet background, added in quadrature.

The sensitivity to $\mathrm{Im}\, g_{\mathrm{R}}$ of the $\cos\theta_\ell$ and $\cos\theta_\ell^N$ distributions, which are used to set limits on this coupling, is illustrated in figure 8. In this figure the observed distributions are compared to the signal-plus-background predictions built by adding the signal templates given by the PROTOS samples generated with $\mathrm{Im}\, g_{\mathrm{R}} = 0$ (Standard Model parameterisation) and $\mathrm{Im}\, g_{\mathrm{R}} = \pm 0.23$, the latter corresponding to the maximum values considered in the interpolation method described above.

10 Systematic uncertainties

Several sources of systematic uncertainty affect the asymmetry measurements, modifying the signal and background event yields and angular distributions. To evaluate the impact of each source the asymmetries are extracted by unfolding the template distributions after varying them to reflect that source of uncertainty. In each case a new background estimation is performed before subtraction, using the fitting procedure described in section 7. For all sources of systematic uncertainty other than those associated with the limited size of the simulation samples, the nominal unfolding corrections are considered. The systematic uncertainty is evaluated as the difference between the nominal asymmetry value and the one measured using the varied normalisations and shapes.

The sources of systematic uncertainty are split into the following categories:

Background normalisation. The uncertainties in the normalisation of the top-quark and W+jets background processes are determined from the maximum-likelihood fit. For the merged Z+jets and diboson processes the normalisation uncertainty of 20% introduced in section 6 is applied to the predictions. For the data-driven normalisation of the multijet background the uncertainty of 70% estimated from the comparison of the matrix-method estimates with those given by the jet-electron and anti-muon methods is used.

The uncertainty in the integrated luminosity is 1.9% [83]. It is propagated to the asymmetry measurements through the normalisation of the simulated backgrounds.

Detector modelling. Systematic uncertainties in the reconstruction and energy calibration of jets, electrons and muons are propagated in the analysis through variations in the modelling of the detector response. For the jets, the main source of uncertainty is the energy scale, evaluated using a combination of in situ techniques [54]. Other jet-related uncertainty sources are the modelling of the energy resolution [84] and reconstruction efficiency [54] (both referred to as jet reconstruction uncertainties), and the modelling of the tagging efficiencies of b-quark jets, c-quark jets and light-flavour jets [57, 58]. Uncertainties related to leptons come from trigger, identification and isolation efficiencies, as well as from the energy scale and resolution [49, 50] (all referred to as lepton reconstruction uncertainties). The uncertainties in the energy scale and resolution corrections applied to leptons and jets are propagated to the computation of the missing transverse momentum. The scale and resolution uncertainties due to soft jets and to contributions of calorimeter energy deposits not associated with any reconstructed objects are also considered and evaluated independently (they are labelled $E_{\mathrm{T}}^{\mathrm{miss}}$ reconstruction uncertainties). For all detector modelling uncertainties, positive and negative uncertainties are estimated separately from the corresponding shifts.

Signal and background modelling. Systematic uncertainties associated with the signal and background modelling are estimated by comparing event samples from different generators and by varying parameters in the event generation.

The uncertainty in the matrix-element calculation in the simulation of the t-channel single-top-quark process is estimated by comparing MADGRAPH5_aMC@NLO+HERWIG with POWHEG-BOX+HERWIG. For the $t\bar{t}$ and Wt processes, MC@NLO is compared with POWHEG-BOX, both generators interfaced to HERWIG. The uncertainty in the parton shower is estimated by comparing POWHEG-BOX interfaced with PYTHIA and HERWIG for the t-channel, $t\bar{t}$ and Wt processes. For the s-channel single-top-quark contribution the uncertainty due to the choice of generator and parton shower is estimated in a combined way by comparing MC@NLO+HERWIG with POWHEG-BOX+PYTHIA.

An additional modelling uncertainty is considered for the signal process by comparing the NLO Powheg-Box sample to the LO Protos sample implementing the Standard Model parameterisation of the Wtb couplings. To estimate this uncertainty, only the shapes of the distributions are varied in order to assess the impact of using a LO generator to determine the unfolding corrections.

The uncertainty in the amount of QCD radiation is evaluated for all top-quark processes by comparing the POWHEG-BOX samples generated with the varied hard-process and

parton-shower scales presented in section 4. The largest shift in the measured asymmetries is taken as uncertainty.

The dependence of the measured asymmetries on the top-quark mass is estimated using POWHEG-BOX samples generated with different top-quark masses. Variations lower than 0.01 per GeV are found for the measured asymmetry values. Therefore, these variations are not included in the total systematic uncertainty.

The impact of the flavour composition on the modelling of the W+jets distributions is determined by propagating an uncertainty of 50% in the ratio of W+$b\bar{b}$ to W+$c\bar{c}$ events. As reported in section 7, W+light-flavour jets events give a small contribution in the signal region and no associated modelling uncertainty is taken into account. An additional shape-modelling uncertainty is considered for the W+jets distributions. Indeed, in the W+jets control region a few kinematic variables are slightly mismodelled, and the impact of this mismodelling is evaluated by reweighting the W+jets angular distributions in the signal region. The applied event weights are derived from matching to data (after subtraction of all processes other than W+jets) the mismodelled kinematic variables in the W+jets control region. This procedure leads to a conservative estimate since it also accounts for mismodelling of the W+light-flavour jets events, which have a much more important contribution in the W+jets control region than in the signal region.

The systematic uncertainty associated with the data-driven shape modelling of the multijet events is estimated by comparing the shapes provided by the baseline matrix method and the alternative modelling given by the jet-electron and anti-muon methods.

All the signal and background modelling uncertainties, except that associated with the W+jets flavour composition, are symmetrised by taking the difference between the nominal and varied measurements as positive and negative uncertainties.

Systematic uncertainties related to the parton distribution functions are estimated for all processes, except for the multijet contribution. The uncertainty is estimated, following the PDF4LHC prescription [67], by calculating the envelope of the uncertainties at 68% confidence level of the CT10 [30], MSTW2008NLO [68] and NNPDF2.3 [71] sets.

Limited size of simulation samples. The uncertainty due to the limited size of the Monte Carlo samples is evaluated by varying the background normalisation and shape, as well as the unfolding corrections, through Gaussian fluctuations. The standard deviation of the distribution of the measured asymmetry provided by an ensemble test of pseudo-experiments built from these variations is taken as a systematic uncertainty.

Tables 4 and 5 show the contribution of each source of systematic uncertainty to the asymmetry measurements. The total uncertainties are obtained from the sum in quadrature of all contributions. Tables 4 and 5 also include the statistical uncertainty from the data sample. It is evaluated using a procedure similar to that used for the uncertainty associated with the size of the simulation samples, but varying the observed numbers of events and the shape of the angular distributions through Poisson fluctuations.

The asymmetry measurements are dominated by the systematic uncertainties. The largest contributions are from the uncertainties in the modelling of the t-channel and $t\bar{t}$ processes, and in the jet reconstruction and energy scale. Significant contributions also

come from the uncertainty in the modelling of the multijet or W+jets events, depending on the measured asymmetry, and from the limited size of the simulation samples. The statistical uncertainty of the data sample, although lower than the systematic uncertainty, also has a sizeable impact on the measurement precision.

11 Results

The values of the asymmetries related to the top-quark polarisation and to the W-boson spin observables, measured using the Standard Model Wtb couplings for the signal unfolding corrections and for the top-quark background modelling, are

$$
\begin{aligned}
A_{\mathrm{FB}}^{\ell} &= 0.49 \pm 0.03(\mathrm{stat.}) \pm 0.05(\mathrm{syst.}) = 0.49 \pm 0.06 \,, \\
A_{\mathrm{FB}}^{tW} &= 0.10 \pm 0.03(\mathrm{stat.}) \pm 0.05(\mathrm{syst.}) = 0.10 \pm 0.06 \,, \\
A_{\mathrm{FB}} &= -0.26 \pm 0.02(\mathrm{stat.}) \pm 0.07(\mathrm{syst.}) = -0.26 \pm 0.08 \,, \\
A_{\mathrm{EC}} &= -0.25 \pm 0.03(\mathrm{stat.}) \pm 0.05(\mathrm{syst.}) = -0.25 \pm 0.06 \,, \\
A_{\mathrm{FB}}^{T} &= 0.39 \pm 0.03(\mathrm{stat.}) \pm 0.09(\mathrm{syst.}) = 0.39 \pm 0.09 \,, \\
A_{\mathrm{FB}}^{N,\phi} &= -0.03 \pm 0.03(\mathrm{stat.}) \pm 0.05(\mathrm{syst.}) = -0.03 \pm 0.06 \,, \\
A_{\mathrm{FB}}^{T,\phi} &= -0.17 \pm 0.05(\mathrm{stat.})^{+0.11}_{-0.10}(\mathrm{syst.}) = -0.17^{+0.12}_{-0.11} \,.
\end{aligned}
$$

The values for the top-quark polarisation combined with the charged-lepton spin analysing power and with the sum of the W-boson helicity fractions, derived from the measured A_{FB}^{ℓ} and A_{FB}^{tW} asymmetries using the relations given in table 1, are

$$
\begin{aligned}
\alpha_{\ell}P &= 0.97 \pm 0.05(\mathrm{stat.}) \pm 0.11(\mathrm{syst.}) = 0.97 \pm 0.12 \,, \\
P(F_{\mathrm{R}} + F_{\mathrm{L}}) &= 0.25 \pm 0.08(\mathrm{stat.}) \pm 0.14(\mathrm{syst.}) = 0.25 \pm 0.16 \,.
\end{aligned}
$$

The values of the W-boson spin observables derived from the measured A_{FB}, A_{EC}, A_{FB}^{T}, $A_{\mathrm{FB}}^{N,\phi}$ and $A_{\mathrm{FB}}^{T,\phi}$ asymmetries through the relations given in table 1 are

$$
\begin{aligned}
\langle S_3 \rangle &= -0.35 \pm 0.03(\mathrm{stat.}) \pm 0.10(\mathrm{syst.}) = -0.35 \pm 0.10 \,, \\
\langle T_0 \rangle &= -0.55 \pm 0.06(\mathrm{stat.}) \pm 0.12(\mathrm{syst.}) = -0.55 \pm 0.13 \,, \\
\langle S_1 \rangle &= 0.52 \pm 0.04(\mathrm{stat.}) \pm 0.12(\mathrm{syst.}) = 0.52 \pm 0.12 \,, \\
\langle A_2 \rangle &= -0.05 \pm 0.05(\mathrm{stat.}) \pm 0.09(\mathrm{syst.}) = -0.05 \pm 0.10 \,, \\
\langle A_1 \rangle &= 0.27 \pm 0.07(\mathrm{stat.})^{+0.16}_{-0.17}(\mathrm{syst.}) = 0.27^{+0.17}_{-0.19} \,.
\end{aligned}
$$

The results for the A_{FB}^{N} asymmetry, which has the highest sensitivity to the anomalous Wtb coupling $\mathrm{Im}\,g_{\mathrm{R}}$, and for its associated W-boson spin observable are

$$
\begin{aligned}
A_{\mathrm{FB}}^{N} &= -0.04 \pm 0.02(\mathrm{stat.}) \pm 0.03(\mathrm{syst.}) = -0.04 \pm 0.04 \,, \\
\langle S_2 \rangle &= 0.06 \pm 0.03(\mathrm{stat.}) \pm 0.04(\mathrm{syst.}) = 0.06 \pm 0.05 \,.
\end{aligned}
$$

These observables are measured using the signal corrections interpolated with respect to $\mathrm{Im}\,g_{\mathrm{R}}$ as explained in section 9, and using the Standard Model couplings for the top-quark background modelling.

Uncertainty source	$\Delta A_{\mathrm{FB}}^{\ell} \times 10^2$	$\Delta A_{\mathrm{FB}}^{tW} \times 10^2$	$\Delta A_{\mathrm{FB}} \times 10^2$	$\Delta A_{\mathrm{EC}} \times 10^2$
Statistical uncertainty	± 2.6	± 3.1	± 2.3	± 2.8
Simulation statistics	± 1.7	± 1.9	± 1.4	± 1.7
Luminosity	<0.1	<0.1	<0.1	<0.1
Background normalisation	± 0.5	± 0.5	± 0.9	± 0.7
$E_{\mathrm{T}}^{\mathrm{miss}}$ reconstruction	$+0.9 \atop -0.1$	$+0.4 \atop -0.7$	$+1.1 \atop -0.7$	$+0.8 \atop -0.2$
Lepton reconstruction	$+1.0 \atop -0.4$	$+0.1 \atop -1.3$	± 1.4	$+0.6 \atop -0.3$
Jet reconstruction	± 2.1	± 2.5	± 1.2	± 1.8
Jet energy scale	$+1.3 \atop -1.2$	$+2.0 \atop -1.6$	$+3.4 \atop -2.7$	$+2.0 \atop -0.7$
Jet flavour tagging	± 0.9	± 0.3	± 0.6	± 0.4
PDF	± 0.2	<0.1	<0.1	± 0.2
$t\bar{t}$ generator	± 2.3	± 1.0	± 0.2	± 1.2
$t\bar{t}$ parton shower	± 0.6	± 0.5	± 2.7	± 0.3
$t\bar{t}$ scales	± 0.2	± 0.4	± 1.2	± 0.3
Wt, s-channel generator	± 1.0	± 1.1	± 0.4	± 0.3
Wt, s-channel scales	± 0.9	± 0.3	± 0.3	± 0.3
t-channel NLO generator	± 1.4	± 0.6	± 0.6	± 2.7
t-channel LO-NLO generator	± 1.5	± 2.0	± 2.6	± 1.8
t-channel parton shower	± 0.5	± 1.0	± 3.5	± 0.2
t-channel scales	± 1.1	± 2.0	± 0.6	± 1.6
W+jets, multijet modelling	$+1.9 \atop -2.4$	$+0.9 \atop -1.0$	$+2.2 \atop -2.1$	$+1.3 \atop -1.2$
Total systematic uncertainty	$+5.4 \atop -5.4$	$+5.2 \atop -5.3$	$+7.3 \atop -6.9$	$+5.3 \atop -4.8$

Table 4. Uncertainties contributing to the measurements of the A_{FB}^{ℓ}, A_{FB}^{tW}, A_{FB} and A_{EC} asymmetries. For better readability the uncertainties are multiplied by 10^2.

Figure 9 shows the measured and predicted values of all asymmetries, while figure 10 compares the derived values for the six W-boson spin observables. Compatibility between the measurements and Standard Model predictions is observed.

The overall compatibility of the measurements with the Standard Model predictions is evaluated through the construction of a χ^2 test statistic taking into account all measured quantities with their correlations. The theoretical uncertainties, which are negligible compared to the measurement uncertainties, are not taken into account in the χ^2 calculation. The overall covariance matrix is computed from the sum of the covariance matrices associated with the various sources of statistical and systematic uncertainty. To calculate the covariance matrices associated with the detector-related and W+jets flavour composition uncertainties, the positive and negative uncertainties are symmetrised by taking the larger value. The overall p-value for the eight asymmetries is found to be 0.94, and it is 0.83 for the six W-boson spin observables.

Uncertainty source	$\Delta A_{\text{FB}}^{N} \times 10^2$	$\Delta A_{\text{FB}}^{T} \times 10^2$	$\Delta A_{\text{FB}}^{N,\phi} \times 10^2$	$\Delta A_{\text{FB}}^{T,\phi} \times 10^2$
Statistical uncertainty	± 2.2	± 3.1	± 3.0	± 4.6
Simulation statistics	± 1.3	± 2.0	± 1.8	± 2.9
Luminosity	<0.1	<0.1	<0.1	<0.1
Background normalisation	± 0.4	± 1.1	± 0.6	± 1.1
$E_{\text{T}}^{\text{miss}}$ reconstruction	$^{+0.3}_{-0.4}$	$^{+0.5}_{-0.3}$	$^{+0.5}_{-0.8}$	$^{+0.4}_{-1.3}$
Lepton reconstruction	$^{+0.1}_{-0.2}$	$^{+1.3}_{-1.5}$	$^{+0.6}_{-0.5}$	$^{+1.6}_{-0.6}$
Jet reconstruction	± 0.8	± 0.5	± 1.6	± 1.3
Jet energy scale	$^{+0.9}_{-0.8}$	$^{+3.9}_{-4.6}$	$^{+0.6}_{-2.5}$	$^{+4.5}_{-2.5}$
Jet flavour tagging	± 0.2	± 0.6	± 0.3	± 0.6
PDF	± 0.1	± 0.1	± 0.1	± 0.4
$t\bar{t}$ generator	± 0.2	± 3.5	± 1.7	± 1.3
$t\bar{t}$ parton shower	± 1.5	± 1.0	± 0.9	± 1.6
$t\bar{t}$ scales	± 0.3	± 0.8	± 0.3	± 1.3
Wt, s-channel generator	± 0.2	± 0.8	± 0.3	± 1.4
Wt, s-channel scales	± 0.6	± 0.5	± 0.4	± 0.9
t-channel NLO generator	± 0.3	± 4.5	± 2.6	± 7.2
t-channel LO-NLO generator	± 0.5	± 1.9	± 1.3	± 3.2
t-channel parton shower	± 0.7	± 0.9	<0.1	± 1.1
t-channel scales	± 0.9	± 2.2	± 1.4	± 2.6
W+jets, multijet modelling	$^{+0.7}_{-0.6}$	$^{+1.3}_{-1.7}$	± 0.6	$^{+2.3}_{-1.7}$
Total systematic uncertainty	$^{+2.9}_{-2.9}$	$^{+8.3}_{-8.8}$	$^{+4.8}_{-5.4}$	$^{+10.9}_{-10.1}$

Table 5. Uncertainties contributing to the measurements of the A_{FB}^{N}, A_{FB}^{T}, $A_{\text{FB}}^{N,\phi}$ and $A_{\text{FB}}^{T,\phi}$ asymmetries. For better readability the uncertainties are multiplied by 10^2.

Limits on the anomalous coupling $\text{Im}\, g_{\text{R}}$ are extracted from the A_{FB}^{N} and A_{FB}^{ℓ} asymmetries, which, as discussed in section 9, are measured independently of any assumption about $\text{Im}\, g_{\text{R}}$ in the unfolding procedure, but assuming the Standard Model couplings for the subtracted top-quark backgrounds. However, for the main $t\bar{t}$ background a negligible dependence on $\text{Im}\, g_{\text{R}}$ is expected.

The limit extraction is based on the TOPFIT code [5, 85]. By taking into account the analytic expressions and parameterisations introduced in refs. [4, 5, 18] for the Wtb coupling dependence of $\langle S_2 \rangle$, α_ℓ and P, it is possible to determine the allowed region for $\text{Im}\, g_{\text{R}}$ from the measured values of A_{FB}^{N} and A_{FB}^{ℓ}. The limit setting is based on the computation of the χ^2 test statistic using the covariance matrix associated with the A_{FB}^{N} and A_{FB}^{ℓ} measurements. An overall correlation coefficient of -0.05 is found.

Assuming $V_{\text{L}} = 1$ and that all anomalous couplings other than $\text{Im}\, g_{\text{R}}$ vanish ($V_{\text{R}} = g_{\text{L}} = 0$ and $\text{Re}\, g_{\text{R}} = 0$), the limits set at the 95% confidence level are $\text{Im}\, g_{\text{R}} \in [-0.18, 0.06]$.
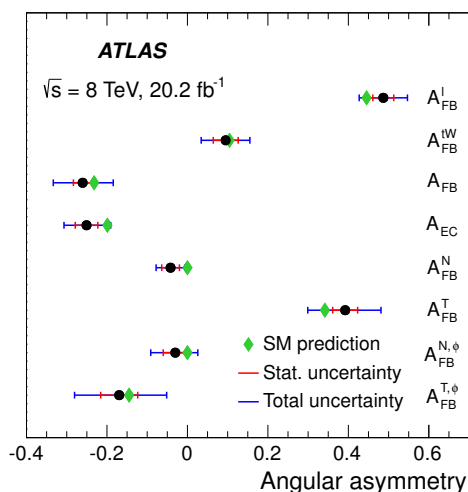
Figure 9. Summary of the measured asymmetries and comparison with the Standard Model predictions.
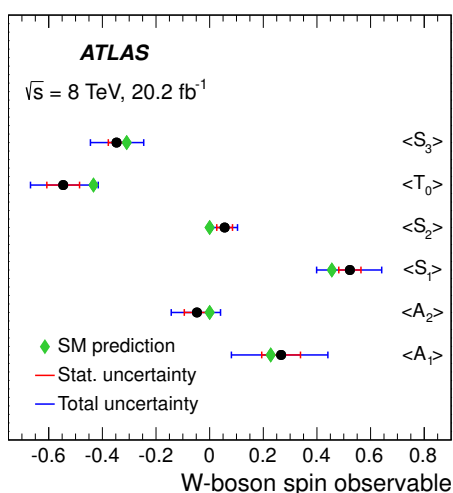

Figure 10. Summary of the measured values of the W-boson spin observables and comparison with the Standard Model predictions.

The measured interval of allowed values slightly improves on the limits set at $7\,\mathrm{TeV}$ by the ATLAS Collaboration from the measurement of double-differential angular decay rates [6].

12 Conclusion

Measurements of the top-quark and W-boson polarisation observables in t-channel single top-quark production at $\sqrt{s} = 8\,\mathrm{TeV}$ with $20.2\,\mathrm{fb}^{-1}$ of pp collision data recorded with the ATLAS detector at the LHC are presented. The selected events contain one isolated elec-

tron or muon, large missing transverse momentum and exactly two jets, of which one is tagged as a b-jet. A cut-based analysis is used to discriminate the signal events from background, and the electron and muon channels are combined. The polarisation observables are measured from asymmetries in various angular distributions unfolded to the parton level. Unfolding corrections based on a Standard Model simulation of the t-channel process are used, as well as model-independent corrections derived through an interpolation method. The measured asymmetries and the measured polarisation observables are in agreement with the predictions of the Standard Model. Limits on the imaginary part of the anomalous coupling g_{R} are also set, giving $\mathrm{Im}\, g_{\mathrm{R}} \in [-0.18, 0.06]$ at the 95% confidence level. The extracted values improve on the most recently published limits for this coupling.

References

[1] S.S.D. Willenbrock and D.A. Dicus, *Production of heavy quarks from W-gluon fusion*, [*Phys. Rev.* **D 34** (1986) 155](#) [ɪɴSPIRE].

[2] G. Mahlon and S.J. Parke, *Single top quark production at the LHC: Understanding spin*, [*Phys. Lett.* **B 476** (2000) 323](#) [`hep-ph/9912458`] [ɪɴSPIRE].

[3] R. Schwienhorst, C.P. Yuan, C. Mueller and Q.-H. Cao, *Single top quark production and decay in the t-channel at next-to-leading order at the LHC*, [*Phys. Rev.* **D 83** (2011) 034019](#) [`arXiv:1012.5132`] [ɪɴSPIRE].

[4] J.A. Aguilar-Saavedra and J. Bernabéu, *Breaking down the entire W boson spin observables from its decay*, [*Phys. Rev.* **D 93** (2016) 011301](#) [`arXiv:1508.04592`] [ɪɴSPIRE].

[5] J.A. Aguilar-Saavedra and J. Bernabéu, *W polarisation beyond helicity fractions in top quark decays*, [*Nucl. Phys.* **B 840** (2010) 349](#) [`arXiv:1005.5382`] [ɪɴSPIRE].

[6] ATLAS collaboration, *Search for anomalous couplings in the Wtb vertex from the measurement of double differential angular decay rates of single top quarks produced in the t-channel with the ATLAS detector*, [*JHEP* **04** (2016) 023](#) [`arXiv:1510.03764`] [ɪɴSPIRE].

[7] CMS collaboration, *Measurement of top quark polarisation in t-channel single top quark production*, [*JHEP* **04** (2016) 073](#) [`arXiv:1511.02138`] [ɪɴSPIRE].

[8] CMS collaboration, *Measurement of the W boson helicity in events with a single reconstructed top quark in pp collisions at $\sqrt{s} = 8\,TeV$*, [*JHEP* **01** (2015) 053](#) [`arXiv:1410.1154`] [ɪɴSPIRE].

[9] CMS collaboration, *Search for anomalous Wtb couplings and flavour-changing neutral currents in t-channel single top quark production in pp collisions at $\sqrt{s} = 7$ and $8\,TeV$*, [*JHEP* **02** (2017) 028](#) [`arXiv:1610.03545`] [ɪɴSPIRE].

[10] A. Brandenburg, Z.G. Si and P. Uwer, *QCD corrected spin analyzing power of jets in decays of polarized top quarks*, [*Phys. Lett.* **B 539** (2002) 235](#) [`hep-ph/0205023`] [ɪɴSPIRE].

[11] G. Mahlon and S.J. Parke, *Improved spin basis for angular correlation studies in single top quark production at the Tevatron*, [*Phys. Rev.* **D 55** (1997) 7249](#) [`hep-ph/9611367`] [ɪɴSPIRE].

[12] A. Czarnecki, J.G. Körner and J.H. Piclum, *Helicity fractions of W bosons from top quark decays at NNLO in QCD*, [*Phys. Rev.* **D 81** (2010) 111503](#) [`arXiv:1005.2625`] [ɪɴSPIRE].

[13] J.M. Campbell, R. Frederix, F. Maltoni and F. Tramontano, *Next-to-Leading-Order Predictions for t-Channel Single-Top Production at Hadron Colliders*, [*Phys. Rev. Lett.* **102** (2009) 182003](#) [`arXiv:0903.0005`] [ɪɴSPIRE].

[14] M. Fischer, S. Groote, J.G. Körner and M.C. Mauser, *Complete angular analysis of polarized top decay at $O(\alpha_s)$*, [*Phys. Rev.* **D 65** (2002) 054036](#) [`hep-ph/0101322`] [ɪɴSPIRE].

[15] G.A. González-Sprinberg, R. Martinez and J. Vidal, *Top quark tensor couplings*, [*JHEP* **07** (2011) 094](#) [*Erratum ibid.* **1305** (2013) 117] [`arXiv:1105.5601`] [ɪɴSPIRE].

[16] J.A. Aguilar-Saavedra, J. Bernabéu, V.A. Mitsou and A. Segarra, *The Z boson spin observables as messengers of new physics*, [`arXiv:1701.03115`](#) [ɪɴSPIRE].

[17] J.A. Aguilar-Saavedra and R.V. Herrero-Hahn, *Model-independent measurement of the top quark polarisation*, *Phys. Lett.* **B 718** (2013) 983 [arXiv:1208.6006] [INSPIRE].

[18] J.A. Aguilar-Saavedra and S. Amor dos Santos, *New directions for top quark polarization in the t-channel process*, *Phys. Rev.* **D 89** (2014) 114009 [arXiv:1404.1585] [INSPIRE].

[19] ATLAS collaboration, *The ATLAS Experiment at the CERN Large Hadron Collider*, 2008 *JINST* **3** S08003 [INSPIRE].

[20] ATLAS collaboration, *Performance of the ATLAS Trigger System in 2010*, *Eur. Phys. J.* **C 72** (2012) 1849 [arXiv:1110.1530] [INSPIRE].

[21] ATLAS collaboration, *Performance of the ATLAS muon trigger in pp collisions at* $\sqrt{s} = 8\,TeV$, *Eur. Phys. J.* **C 75** (2015) 120 [arXiv:1408.3179] [INSPIRE].

[22] ATLAS collaboration, *The ATLAS Simulation Infrastructure*, *Eur. Phys. J.* **C 70** (2010) 823 [arXiv:1005.4568] [INSPIRE].

[23] GEANT4 collaboration, S. Agostinelli et al., *GEANT4: a simulation toolkit*, *Nucl. Instrum. Meth.* **A 506** (2003) 250 [INSPIRE].

[24] ATLAS collaboration, *The simulation principle and performance of the ATLAS fast calorimeter simulation FastCaloSim*, ATL-PHYS-PUB-2010-13 (2013).

[25] T. Sjöstrand, S. Mrenna and P.Z. Skands, *A brief introduction to PYTHIA 8.1*, *Comput. Phys. Commun.* **178** (2008) 852 [arXiv:0710.3820] [INSPIRE].

[26] P. Nason, *A new method for combining NLO QCD with shower Monte Carlo algorithms*, *JHEP* **11** (2004) 040 [hep-ph/0409146] [INSPIRE].

[27] S. Frixione, P. Nason and C. Oleari, *Matching NLO QCD computations with parton shower simulations: the POWHEG method*, *JHEP* **11** (2007) 070 [arXiv:0709.2092] [INSPIRE].

[28] S. Alioli, P. Nason, C. Oleari and E. Re, *A general framework for implementing NLO calculations in shower Monte Carlo programs: the POWHEG BOX*, *JHEP* **06** (2010) 043 [arXiv:1002.2581] [INSPIRE].

[29] R. Frederix, E. Re and P. Torrielli, *Single-top t-channel hadroproduction in the four-flavour scheme with POWHEG and aMC@NLO*, *JHEP* **09** (2012) 130 [arXiv:1207.5391] [INSPIRE].

[30] H.-L. Lai et al., *New parton distributions for collider physics*, *Phys. Rev.* **D 82** (2010) 074024 [arXiv:1007.2241] [INSPIRE].

[31] J.A. Aguilar-Saavedra, *Single top quark production at LHC with anomalous Wtb couplings*, *Nucl. Phys.* **B 804** (2008) 160 [arXiv:0803.3810] [INSPIRE].

[32] J. Pumplin, D.R. Stump, J. Huston, H.L. Lai, P.M. Nadolsky and W.K. Tung, *New generation of parton distributions with uncertainties from global QCD analysis*, *JHEP* **07** (2002) 012 [hep-ph/0201195] [INSPIRE].

[33] S. Frixione, P. Nason and G. Ridolfi, *A positive-weight next-to-leading-order Monte Carlo for heavy flavour hadroproduction*, *JHEP* **09** (2007) 126 [arXiv:0707.3088] [INSPIRE].

[34] E. Re, *Single-top Wt-channel production matched with parton showers using the POWHEG method*, *Eur. Phys. J.* **C 71** (2011) 1547 [arXiv:1009.2450] [INSPIRE].

[35] ATLAS collaboration, *Comparison of Monte Carlo generator predictions to ATLAS measurements of top pair production at* $\sqrt{s} = 7\,TeV$, ATLAS-PHYS-PUB-2015-002 (2015).

[36] T. Sjöstrand, S. Mrenna and P.Z. Skands, *PYTHIA 6.4 physics and manual*, *JHEP* **05** (2006) 026 [hep-ph/0603175] [INSPIRE].

[37] P.Z. Skands, *Tuning Monte Carlo generators: The Perugia tunes*, *Phys. Rev.* **D 82** (2010) 074018 [arXiv:1005.3457] [INSPIRE].

[38] J. Alwall et al., *The automated computation of tree-level and next-to-leading order differential cross sections and their matching to parton shower simulations*, *JHEP* **07** (2014) 079 [arXiv:1405.0301] [INSPIRE].

[39] G. Marchesini, B.R. Webber, G. Abbiendi, I.G. Knowles, M.H. Seymour and L. Stanco, *HERWIG 5.1 — a Monte Carlo event generator for simulating hadron emission reactions with interfering gluons*, *Comput. Phys. Commun.* **67** (1992) 465 [INSPIRE].

[40] G. Corcella et al., *HERWIG 6: An Event generator for hadron emission reactions with interfering gluons (including supersymmetric processes)*, *JHEP* **01** (2001) 010 [hep-ph/0011363] [INSPIRE].

[41] J.M. Butterworth, J.R. Forshaw and M.H. Seymour, *Multiparton interactions in photoproduction at HERA*, *Z. Phys.* **C 72** (1996) 637 [hep-ph/9601371] [INSPIRE].

[42] ATLAS collaboration, *New ATLAS event generator tunes to 2010 data*, ATL-PHYS-PUB-2011-008 (2011).

[43] S. Frixione and B.R. Webber, *Matching NLO QCD computations and parton shower simulations*, *JHEP* **06** (2002) 029 [hep-ph/0204244] [INSPIRE].

[44] S. Frixione, P. Nason and B.R. Webber, *Matching NLO QCD and parton showers in heavy flavor production*, *JHEP* **08** (2003) 007 [hep-ph/0305252] [INSPIRE].

[45] S. Frixione, E. Laenen, P. Motylinski and B.R. Webber, *Single-top production in MC@NLO*, *JHEP* **03** (2006) 092 [hep-ph/0512250] [INSPIRE].

[46] S. Frixione, E. Laenen, P. Motylinski, B.R. Webber and C.D. White, *Single-top hadroproduction in association with a W boson*, *JHEP* **07** (2008) 029 [arXiv:0805.3067] [INSPIRE].

[47] T. Gleisberg et al., *Event generation with SHERPA 1.1*, *JHEP* **02** (2009) 007 [arXiv:0811.4622] [INSPIRE].

[48] S. Hoeche, F. Krauss, S. Schumann and F. Siegert, *QCD matrix elements and truncated showers*, *JHEP* **05** (2009) 053 [arXiv:0903.1219] [INSPIRE].

[49] ATLAS collaboration, *Electron reconstruction and identification efficiency measurements with the ATLAS detector using the 2011 LHC proton-proton collision data*, *Eur. Phys. J.* **C 74** (2014) 2941 [arXiv:1404.2240] [INSPIRE].

[50] ATLAS collaboration, *Measurement of the muon reconstruction performance of the ATLAS detector using 2011 and 2012 LHC proton-proton collision data*, *Eur. Phys. J.* **C 74** (2014) 3130 [arXiv:1407.3935] [INSPIRE].

[51] ATLAS collaboration, *Estimation of non-prompt and fake lepton backgrounds in final states with top quarks produced in proton-proton collisions at $\sqrt{s} = 8$ TeV with the ATLAS detector*, ATLAS-CONF-2014-058 (2014).

[52] M. Cacciari, G.P. Salam and G. Soyez, *The anti-k_t jet clustering algorithm*, *JHEP* **04** (2008) 063 [arXiv:0802.1189] [INSPIRE].

[53] ATLAS collaboration, *Topological cell clustering in the ATLAS calorimeters and its performance in LHC Run 1*, arXiv:1603.02934 [INSPIRE].

[54] ATLAS collaboration, *Jet energy measurement and its systematic uncertainty in proton-proton collisions at $\sqrt{s} = 7\,TeV$ with the ATLAS detector*, *Eur. Phys. J.* **C 75** (2015) 17 [arXiv:1406.0076] [INSPIRE].

[55] ATLAS collaboration, *Performance of pile-up mitigation techniques for jets in pp collisions at $\sqrt{s} = 8\,TeV$ using the ATLAS detector*, *Eur. Phys. J.* **C 76** (2016) 581 [arXiv:1510.03823] [INSPIRE].

[56] ATLAS collaboration, *Performance of b-Jet Identification in the ATLAS Experiment*, 2016 *JINST* **11** P04008 [arXiv:1512.01094] [INSPIRE].

[57] ATLAS collaboration, *Calibration of the performance of b-tagging for c and light-flavour jets in the 2012 ATLAS data*, ATLAS-CONF-2014-046 (2014).

[58] ATLAS collaboration, *Calibration of b-tagging using dileptonic top pair events in a combinatorial likelihood approach with the ATLAS experiment*, ATLAS-CONF-2014-004 (2014).

[59] ATLAS collaboration, *Performance of missing transverse momentum reconstruction in proton-proton collisions at $7\,TeV$ with ATLAS*, *Eur. Phys. J.* **C 72** (2012) 1844 [arXiv:1108.5602] [INSPIRE].

[60] ATLAS collaboration, *Comprehensive measurements of t-channel single top-quark production cross sections at $\sqrt{s} = 7\,TeV$ with the ATLAS detector*, *Phys. Rev.* **D 90** (2014) 112006 [arXiv:1406.7844] [INSPIRE].

[61] M. Cacciari, M. Czakon, M. Mangano, A. Mitov and P. Nason, *Top-pair production at hadron colliders with next-to-next-to-leading logarithmic soft-gluon resummation*, *Phys. Lett.* **B 710** (2012) 612 [arXiv:1111.5869] [INSPIRE].

[62] P. Bärnreuther, M. Czakon and A. Mitov, *Percent Level Precision Physics at the Tevatron: First Genuine NNLO QCD Corrections to $q\bar{q} \to t\bar{t} + X$*, *Phys. Rev. Lett.* **109** (2012) 132001 [arXiv:1204.5201] [INSPIRE].

[63] M. Czakon and A. Mitov, *NNLO corrections to top-pair production at hadron colliders: the all-fermionic scattering channels*, *JHEP* **12** (2012) 054 [arXiv:1207.0236] [INSPIRE].

[64] M. Czakon and A. Mitov, *NNLO corrections to top pair production at hadron colliders: the quark-gluon reaction*, *JHEP* **01** (2013) 080 [arXiv:1210.6832] [INSPIRE].

[65] M. Czakon, P. Fiedler and A. Mitov, *Total Top-Quark Pair-Production Cross section at Hadron Colliders Through $O(\alpha_S^4)$*, *Phys. Rev. Lett.* **110** (2013) 252004 [arXiv:1303.6254] [INSPIRE].

[66] M. Czakon and A. Mitov, *Top++: a program for the calculation of the top-pair cross-section at hadron colliders*, *Comput. Phys. Commun.* **185** (2014) 2930 [arXiv:1112.5675] [INSPIRE].

[67] M. Botje et al., *The PDF4LHC Working Group Interim Recommendations*, arXiv:1101.0538 [INSPIRE].

[68] A.D. Martin, W.J. Stirling, R.S. Thorne and G. Watt, *Parton distributions for the LHC*, *Eur. Phys. J.* **C 63** (2009) 189 [arXiv:0901.0002] [INSPIRE].

[69] A.D. Martin, W.J. Stirling, R.S. Thorne and G. Watt, *Uncertainties on α_s in global PDF analyses and implications for predicted hadronic cross sections*, *Eur. Phys. J.* **C 64** (2009) 653 [arXiv:0905.3531] [INSPIRE].

[70] J. Gao et al., *CT10 next-to-next-to-leading order global analysis of QCD*, *Phys. Rev.* **D 89** (2014) 033009 [arXiv:1302.6246] [INSPIRE].

[71] R.D. Ball et al., *Parton distributions with LHC data*, *Nucl. Phys.* **B 867** (2013) 244 [arXiv:1207.1303] [INSPIRE].

[72] N. Kidonakis, *Next-to-next-to-leading-order collinear and soft gluon corrections for t-channel single top quark production*, *Phys. Rev.* **D 83** (2011) 091503 [arXiv:1103.2792] [INSPIRE].

[73] N. Kidonakis, *Two-loop soft anomalous dimensions for single top quark associated production with a W^- or H^-*, *Phys. Rev.* **D 82** (2010) 054018 [arXiv:1005.4451] [INSPIRE].

[74] N. Kidonakis, *NNLL resummation for s-channel single top quark production*, *Phys. Rev.* **D 81** (2010) 054028 [arXiv:1001.5034] [INSPIRE].

[75] R. Gavin, Y. Li, F. Petriello and S. Quackenbush, *FEWZ 2.0: A code for hadronic Z production at next-to-next-to-leading order*, *Comput. Phys. Commun.* **182** (2011) 2388 [arXiv:1011.3540] [INSPIRE].

[76] R. Gavin, Y. Li, F. Petriello and S. Quackenbush, *W physics at the LHC with FEWZ 2.1*, *Comput. Phys. Commun.* **184** (2013) 208 [arXiv:1201.5896] [INSPIRE].

[77] J.M. Campbell, R.K. Ellis and C. Williams, *Vector boson pair production at the LHC*, *JHEP* **07** (2011) 018 [arXiv:1105.0020] [INSPIRE].

[78] ATLAS collaboration, *Measurements of the W production cross sections in association with jets with the ATLAS detector*, *Eur. Phys. J.* **C 75** (2015) 82 [arXiv:1409.8639] [INSPIRE].

[79] ATLAS collaboration, *Measurement of the top quark pair production cross-section with ATLAS in the single lepton channel*, *Phys. Lett.* **B 711** (2012) 244 [arXiv:1201.1889] [INSPIRE].

[80] ATLAS collaboration, *Measurement of the t-channel single top-quark production cross section in pp collisions at $\sqrt{s} = 7$ TeV with the ATLAS detector*, *Phys. Lett.* **B 717** (2012) 330 [arXiv:1205.3130] [INSPIRE].

[81] G. D'Agostini, *A Multidimensional unfolding method based on Bayes' theorem*, *Nucl. Instrum. Meth.* **A 362** (1995) 487 [INSPIRE].

[82] T. Adye, *Unfolding algorithms and tests using RooUnfold*, arXiv:1105.1160 [INSPIRE].

[83] ATLAS collaboration, *Luminosity determination in pp collisions at $\sqrt{s} = 8$ TeV using the ATLAS detector at the LHC*, *Eur. Phys. J.* **C 76** (2016) 653 [arXiv:1608.03953] [INSPIRE].

[84] ATLAS collaboration, *Jet energy resolution in proton-proton collisions at $\sqrt{s} = 7$ TeV recorded in 2010 with the ATLAS detector*, *Eur. Phys. J.* **C 73** (2013) 2306 [arXiv:1210.6210] [INSPIRE].

[85] C. Bernardo et al., *Studying the Wtb vertex structure using recent LHC results*, *Phys. Rev.* **D 90** (2014) 113007 [arXiv:1408.7063] [INSPIRE].

[86] ATLAS collaboration, *ATLAS Computing Acknowledgements 2016–2017*, ATL-GEN-PUB-2016-002 (2016).

The ATLAS collaboration

M. Aaboud[137d], G. Aad[88], B. Abbott[115], J. Abdallah[8], O. Abdinov[12], B. Abeloos[119],
O.S. AbouZeid[139], N.L. Abraham[151], H. Abramowicz[155], H. Abreu[154], R. Abreu[118],
Y. Abulaiti[148a,148b], B.S. Acharya[167a,167b,a], S. Adachi[157], L. Adamczyk[41a], D.L. Adams[27],
J. Adelman[110], S. Adomeit[102], T. Adye[133], A.A. Affolder[139], T. Agatonovic-Jovin[14],
J.A. Aguilar-Saavedra[128a,128f], S.P. Ahlen[24], F. Ahmadov[68,b], G. Aielli[135a,135b],
H. Akerstedt[148a,148b], T.P.A. Åkesson[84], A.V. Akimov[98], G.L. Alberghi[22a,22b], J. Albert[172],
S. Albrand[58], M.J. Alconada Verzini[74], M. Aleksa[32], I.N. Aleksandrov[68], C. Alexa[28b],
G. Alexander[155], T. Alexopoulos[10], M. Alhroob[115], B. Ali[130], M. Aliev[76a,76b], G. Alimonti[94a],
J. Alison[33], S.P. Alkire[38], B.M.M. Allbrooke[151], B.W. Allen[118], P.P. Allport[19],
A. Aloisio[106a,106b], A. Alonso[39], F. Alonso[74], C. Alpigiani[140], A.A. Alshehri[56], M. Alstaty[88],
B. Alvarez Gonzalez[32], D. Álvarez Piqueras[170], M.G. Alviggi[106a,106b], B.T. Amadio[16],
Y. Amaral Coutinho[26a], C. Amelung[25], D. Amidei[92], S.P. Amor Dos Santos[128a,128c],
A. Amorim[128a,128b], S. Amoroso[32], G. Amundsen[25], C. Anastopoulos[141], L.S. Ancu[52],
N. Andari[19], T. Andeen[11], C.F. Anders[60b], J.K. Anders[77], K.J. Anderson[33], A. Andreazza[94a,94b],
V. Andrei[60a], S. Angelidakis[9], I. Angelozzi[109], A. Angerami[38], F. Anghinolfi[32],
A.V. Anisenkov[111,c], N. Anjos[13], A. Annovi[126a,126b], C. Antel[60a], M. Antonelli[50],
A. Antonov[100,*], D.J. Antrim[166], F. Anulli[134a], M. Aoki[69], L. Aperio Bella[19], G. Arabidze[93],
Y. Arai[69], J.P. Araque[128a], V. Araujo Ferraz[26a], A.T.H. Arce[48], F.A. Arduh[74], J-F. Arguin[97],
S. Argyropoulos[66], M. Arik[20a], A.J. Armbruster[145], L.J. Armitage[79], O. Arnaez[32], H. Arnold[51],
M. Arratia[30], O. Arslan[23], A. Artamonov[99], G. Artoni[122], S. Artz[86], S. Asai[157], N. Asbah[45],
A. Ashkenazi[155], B. Åsman[148a,148b], L. Asquith[151], K. Assamagan[27], R. Astalos[146a],
M. Atkinson[169], N.B. Atlay[143], K. Augsten[130], G. Avolio[32], B. Axen[16], M.K. Ayoub[119],
G. Azuelos[97,d], M.A. Baak[32], A.E. Baas[60a], M.J. Baca[19], H. Bachacou[138], K. Bachas[76a,76b],
M. Backes[122], M. Backhaus[32], P. Bagiacchi[134a,134b], P. Bagnaia[134a,134b], Y. Bai[35a],
J.T. Baines[133], M. Bajic[39], O.K. Baker[179], E.M. Baldin[111,c], P. Balek[175], T. Balestri[150],
F. Balli[138], W.K. Balunas[124], E. Banas[42], Sw. Banerjee[176,e], A.A.E. Bannoura[178], L. Barak[32],
E.L. Barberio[91], D. Barberis[53a,53b], M. Barbero[88], T. Barillari[103], M-S Barisits[32], T. Barklow[145],
N. Barlow[30], S.L. Barnes[87], B.M. Barnett[133], R.M. Barnett[16], Z. Barnovska-Blenessy[36a],
A. Baroncelli[136a], G. Barone[25], A.J. Barr[122], L. Barranco Navarro[170], F. Barreiro[85],
J. Barreiro Guimarães da Costa[35a], R. Bartoldus[145], A.E. Barton[75], P. Bartos[146a],
A. Basalaev[125], A. Bassalat[119,f], R.L. Bates[56], S.J. Batista[161], J.R. Batley[30], M. Battaglia[139],
M. Bauce[134a,134b], F. Bauer[138], H.S. Bawa[145,g], J.B. Beacham[113], M.D. Beattie[75], T. Beau[83],
P.H. Beauchemin[165], P. Bechtle[23], H.P. Beck[18,h], K. Becker[122], M. Becker[86], M. Beckingham[173],
C. Becot[112], A.J. Beddall[20e], A. Beddall[20b], V.A. Bednyakov[68], M. Bedognetti[109], C.P. Bee[150],
L.J. Beemster[109], T.A. Beermann[32], M. Begel[27], J.K. Behr[45], A.S. Bell[81], G. Bella[155],
L. Bellagamba[22a], A. Bellerive[31], M. Bellomo[89], K. Belotskiy[100], O. Beltramello[32],
N.L. Belyaev[100], O. Benary[155,*], D. Benchekroun[137a], M. Bender[102], K. Bendtz[148a,148b],
N. Benekos[10], Y. Benhammou[155], E. Benhar Noccioli[179], J. Benitez[66], D.P. Benjamin[48],
J.R. Bensinger[25], S. Bentvelsen[109], L. Beresford[122], M. Beretta[50], D. Berge[109],
E. Bergeaas Kuutmann[168], N. Berger[5], J. Beringer[16], S. Berlendis[58], N.R. Bernard[89],
C. Bernius[112], F.U. Bernlochner[23], T. Berry[80], P. Berta[131], C. Bertella[86], G. Bertoli[148a,148b],
F. Bertolucci[126a,126b], I.A. Bertram[75], C. Bertsche[45], D. Bertsche[115], G.J. Besjes[39],
O. Bessidskaia Bylund[148a,148b], M. Bessner[45], N. Besson[138], C. Betancourt[51], A. Bethani[58],
S. Bethke[103], A.J. Bevan[79], R.M. Bianchi[127], M. Bianco[32], O. Biebel[102], D. Biedermann[17],
R. Bielski[87], N.V. Biesuz[126a,126b], M. Biglietti[136a], J. Bilbao De Mendizabal[52], T.R.V. Billoud[97],
H. Bilokon[50], M. Bindi[57], A. Bingul[20b], C. Bini[134a,134b], S. Biondi[22a,22b], T. Bisanz[57],

D.M. Bjergaard[48], C.W. Black[152], J.E. Black[145], K.M. Black[24], D. Blackburn[140], R.E. Blair[6],
T. Blazek[146a], I. Bloch[45], C. Blocker[25], A. Blue[56], W. Blum[86,*], U. Blumenschein[57],
S. Blunier[34a], G.J. Bobbink[109], V.S. Bobrovnikov[111,c], S.S. Bocchetta[84], A. Bocci[48], C. Bock[102],
M. Boehler[51], D. Boerner[178], J.A. Bogaerts[32], D. Bogavac[102], A.G. Bogdanchikov[111],
C. Bohm[148a], V. Boisvert[80], P. Bokan[14], T. Bold[41a], A.S. Boldyrev[101], M. Bomben[83], M. Bona[79],
M. Boonekamp[138], A. Borisov[132], G. Borissov[75], J. Bortfeldt[32], D. Bortoletto[122],
V. Bortolotto[62a,62b,62c], K. Bos[109], D. Boscherini[22a], M. Bosman[13], J.D. Bossio Sola[29],
J. Boudreau[127], J. Bouffard[2], E.V. Bouhova-Thacker[75], D. Boumediene[37], C. Bourdarios[119],
S.K. Boutle[56], A. Boveia[113], J. Boyd[32], I.R. Boyko[68], J. Bracinik[19], A. Brandt[8], G. Brandt[57],
O. Brandt[60a], U. Bratzler[158], B. Brau[89], J.E. Brau[118], W.D. Breaden Madden[56],
K. Brendlinger[124], A.J. Brennan[91], L. Brenner[109], R. Brenner[168], S. Bressler[175], T.M. Bristow[49],
D. Britton[56], D. Britzger[45], F.M. Brochu[30], I. Brock[23], R. Brock[93], G. Brooijmans[38],
T. Brooks[80], W.K. Brooks[34b], J. Brosamer[16], E. Brost[110], J.H Broughton[19],
P.A. Bruckman de Renstrom[42], D. Bruncko[146b], R. Bruneliere[51], A. Bruni[22a], G. Bruni[22a],
L.S. Bruni[109], BH Brunt[30], M. Bruschi[22a], N. Bruscino[23], P. Bryant[33], L. Bryngemark[84],
T. Buanes[15], Q. Buat[144], P. Buchholz[143], A.G. Buckley[56], I.A. Budagov[68], F. Buehrer[51],
M.K. Bugge[121], O. Bulekov[100], D. Bullock[8], H. Burckhart[32], S. Burdin[77], C.D. Burgard[51],
A.M. Burger[5], B. Burghgrave[110], K. Burka[42], S. Burke[133], I. Burmeister[46], J.T.P. Burr[122],
E. Busato[37], D. Büscher[51], V. Büscher[86], P. Bussey[56], J.M. Butler[24], C.M. Buttar[56],
J.M. Butterworth[81], P. Butti[32], W. Buttinger[27], A. Buzatu[56], A.R. Buzykaev[111,c],
S. Cabrera Urbán[170], D. Caforio[130], V.M. Cairo[40a,40b], O. Cakir[4a], N. Calace[52], P. Calafiura[16],
A. Calandri[88], G. Calderini[83], P. Calfayan[64], G. Callea[40a,40b], L.P. Caloba[26a],
S. Calvente Lopez[85], D. Calvet[37], S. Calvet[37], T.P. Calvet[88], R. Camacho Toro[33], S. Camarda[32],
P. Camarri[135a,135b], D. Cameron[121], R. Caminal Armadans[169], C. Camincher[58], S. Campana[32],
M. Campanelli[81], A. Camplani[94a,94b], A. Campoverde[143], V. Canale[106a,106b], A. Canepa[163a],
M. Cano Bret[36c], J. Cantero[116], T. Cao[155], M.D.M. Capeans Garrido[32], I. Caprini[28b],
M. Caprini[28b], M. Capua[40a,40b], R.M. Carbone[38], R. Cardarelli[135a], F. Cardillo[51], I. Carli[131],
T. Carli[32], G. Carlino[106a], B.T. Carlson[127], L. Carminati[94a,94b], R.M.D. Carney[148a,148b],
S. Caron[108], E. Carquin[34b], G.D. Carrillo-Montoya[32], J.R. Carter[30], J. Carvalho[128a,128c],
D. Casadei[19], M.P. Casado[13,i], M. Casolino[13], D.W. Casper[166], E. Castaneda-Miranda[147a],
R. Castelijn[109], A. Castelli[109], V. Castillo Gimenez[170], N.F. Castro[128a,j], A. Catinaccio[32],
J.R. Catmore[121], A. Cattai[32], J. Caudron[23], V. Cavaliere[169], E. Cavallaro[13], D. Cavalli[94a],
M. Cavalli-Sforza[13], V. Cavasinni[126a,126b], F. Ceradini[136a,136b], L. Cerda Alberich[170],
A.S. Cerqueira[26b], A. Cerri[151], L. Cerrito[135a,135b], F. Cerutti[16], A. Cervelli[18], S.A. Cetin[20d],
A. Chafaq[137a], D. Chakraborty[110], S.K. Chan[59], Y.L. Chan[62a], P. Chang[169], J.D. Chapman[30],
D.G. Charlton[19], A. Chatterjee[52], C.C. Chau[161], C.A. Chavez Barajas[151], S. Che[113],
S. Cheatham[167a,167c], A. Chegwidden[93], S. Chekanov[6], S.V. Chekulaev[163a], G.A. Chelkov[68,k],
M.A. Chelstowska[92], C. Chen[67], H. Chen[27], S. Chen[35b], S. Chen[157], X. Chen[35c,l], Y. Chen[70],
H.C. Cheng[92], H.J. Cheng[35a], Y. Cheng[33], A. Cheplakov[68], E. Cheremushkina[132],
R. Cherkaoui El Moursli[137e], V. Chernyatin[27,*], E. Cheu[7], L. Chevalier[138], V. Chiarella[50],
G. Chiarelli[126a,126b], G. Chiodini[76a], A.S. Chisholm[32], A. Chitan[28b], Y.H. Chiu[172],
M.V. Chizhov[68], K. Choi[64], A.R. Chomont[37], S. Chouridou[9], B.K.B. Chow[102],
V. Christodoulou[81], D. Chromek-Burckhart[32], J. Chudoba[129], A.J. Chuinard[90],
J.J. Chwastowski[42], L. Chytka[117], A.K. Ciftci[4a], D. Cinca[46], V. Cindro[78], I.A. Cioara[23],
C. Ciocca[22a,22b], A. Ciocio[16], F. Cirotto[106a,106b], Z.H. Citron[175], M. Citterio[94a],
M. Ciubancan[28b], A. Clark[52], B.L. Clark[59], M.R. Clark[38], P.J. Clark[49], R.N. Clarke[16],
C. Clement[148a,148b], Y. Coadou[88], M. Cobal[167a,167c], A. Coccaro[52], J. Cochran[67],
L. Colasurdo[108], B. Cole[38], A.P. Colijn[109], J. Collot[58], T. Colombo[166], P. Conde Muiño[128a,128b],

E. Coniavitis[51], S.H. Connell[147b], I.A. Connelly[80], V. Consorti[51], S. Constantinescu[28b],
G. Conti[32], F. Conventi[106a,m], M. Cooke[16], B.D. Cooper[81], A.M. Cooper-Sarkar[122],
F. Cormier[171], K.J.R. Cormier[161], T. Cornelissen[178], M. Corradi[134a,134b], F. Corriveau[90,n],
A. Cortes-Gonzalez[32], G. Cortiana[103], G. Costa[94a], M.J. Costa[170], D. Costanzo[141], G. Cottin[30],
G. Cowan[80], B.E. Cox[87], K. Cranmer[112], S.J. Crawley[56], G. Cree[31], S. Crépé-Renaudin[58],
F. Crescioli[83], W.A. Cribbs[148a,148b], M. Crispin Ortuzar[122], M. Cristinziani[23], V. Croft[108],
G. Crosetti[40a,40b], A. Cueto[85], T. Cuhadar Donszelmann[141], J. Cummings[179], M. Curatolo[50],
J. Cúth[86], H. Czirr[143], P. Czodrowski[3], G. D'amen[22a,22b], S. D'Auria[56], M. D'Onofrio[77],
M.J. Da Cunha Sargedas De Sousa[128a,128b], C. Da Via[87], W. Dabrowski[41a], T. Dado[146a],
T. Dai[92], O. Dale[15], F. Dallaire[97], C. Dallapiccola[89], M. Dam[39], J.R. Dandoy[33], N.P. Dang[51],
A.C. Daniells[19], N.S. Dann[87], M. Danninger[171], M. Dano Hoffmann[138], V. Dao[51], G. Darbo[53a],
S. Darmora[8], J. Dassoulas[3], A. Dattagupta[118], W. Davey[23], C. David[45], T. Davidek[131],
M. Davies[155], P. Davison[81], E. Dawe[91], I. Dawson[141], K. De[8], R. de Asmundis[106a],
A. De Benedetti[115], S. De Castro[22a,22b], S. De Cecco[83], N. De Groot[108], P. de Jong[109],
H. De la Torre[93], F. De Lorenzi[67], A. De Maria[57], D. De Pedis[134a], A. De Salvo[134a],
U. De Sanctis[151], A. De Santo[151], J.B. De Vivie De Regie[119], W.J. Dearnaley[75], R. Debbe[27],
C. Debenedetti[139], D.V. Dedovich[68], N. Dehghanian[3], I. Deigaard[109], M. Del Gaudio[40a,40b],
J. Del Peso[85], T. Del Prete[126a,126b], D. Delgove[119], F. Deliot[138], C.M. Delitzsch[52],
A. Dell'Acqua[32], L. Dell'Asta[24], M. Dell'Orso[126a,126b], M. Della Pietra[106a,106b], D. della Volpe[52],
M. Delmastro[5], P.A. Delsart[58], D.A. DeMarco[161], S. Demers[179], D. Demichev[68], A. Demilly[83],
S.P. Denisov[132], D. Denysiuk[138], D. Derendarz[42], J.E. Derkaoui[137d], F. Derue[83], P. Dervan[77],
K. Desch[23], C. Deterre[45], K. Dette[46], P.O. Deviveiros[32], A. Dewhurst[133], S. Dhaliwal[25],
A. Di Ciaccio[135a,135b], L. Di Ciaccio[5], W.K. Di Clemente[124], C. Di Donato[106a,106b],
A. Di Girolamo[32], B. Di Girolamo[32], B. Di Micco[136a,136b], R. Di Nardo[32], K.F. Di Petrillo[59],
A. Di Simone[51], R. Di Sipio[161], D. Di Valentino[31], C. Diaconu[88], M. Diamond[161], F.A. Dias[49],
M.A. Diaz[34a], E.B. Diehl[92], J. Dietrich[17], S. Díez Cornell[45], A. Dimitrievska[14], J. Dingfelder[23],
P. Dita[28b], S. Dita[28b], F. Dittus[32], F. Djama[88], T. Djobava[54b], J.I. Djuvsland[60a],
M.A.B. do Vale[26c], D. Dobos[32], M. Dobre[28b], C. Doglioni[84], J. Dolejsi[131], Z. Dolezal[131],
M. Donadelli[26d], S. Donati[126a,126b], P. Dondero[123a,123b], J. Donini[37], J. Dopke[133], A. Doria[106a],
M.T. Dova[74], A.T. Doyle[56], E. Drechsler[57], M. Dris[10], Y. Du[36b], J. Duarte-Campderros[155],
E. Duchovni[175], G. Duckeck[102], O.A. Ducu[97,o], D. Duda[109], A. Dudarev[32], A.Chr. Dudder[86],
E.M. Duffield[16], L. Duflot[119], M. Dührssen[32], M. Dumancic[175], A.K. Duncan[56], M. Dunford[60a],
H. Duran Yildiz[4a], M. Düren[55], A. Durglishvili[54b], D. Duschinger[47], B. Dutta[45], M. Dyndal[45],
C. Eckardt[45], K.M. Ecker[103], R.C. Edgar[92], N.C. Edwards[49], T. Eifert[32], G. Eigen[15],
K. Einsweiler[16], T. Ekelof[168], M. El Kacimi[137c], V. Ellajosyula[88], M. Ellert[168], S. Elles[5],
F. Ellinghaus[178], A.A. Elliot[172], N. Ellis[32], J. Elmsheuser[27], M. Elsing[32], D. Emeliyanov[133],
Y. Enari[157], O.C. Endner[86], J.S. Ennis[173], J. Erdmann[46], A. Ereditato[18], G. Ernis[178], J. Ernst[2],
M. Ernst[27], S. Errede[169], E. Ertel[86], M. Escalier[119], H. Esch[46], C. Escobar[127], B. Esposito[50],
A.I. Etienvre[138], E. Etzion[155], H. Evans[64], A. Ezhilov[125], F. Fabbri[22a,22b], L. Fabbri[22a,22b],
G. Facini[33], R.M. Fakhrutdinov[132], S. Falciano[134a], R.J. Falla[81], J. Faltova[32], Y. Fang[35a],
M. Fanti[94a,94b], A. Farbin[8], A. Farilla[136a], C. Farina[127], E.M. Farina[123a,123b], T. Farooque[13],
S. Farrell[16], S.M. Farrington[173], P. Farthouat[32], F. Fassi[137e], P. Fassnacht[32], D. Fassouliotis[9],
M. Faucci Giannelli[80], A. Favareto[53a,53b], W.J. Fawcett[122], L. Fayard[119], O.L. Fedin[125,p],
W. Fedorko[171], S. Feigl[121], L. Feligioni[88], C. Feng[36b], E.J. Feng[32], H. Feng[92], A.B. Fenyuk[132],
L. Feremenga[8], P. Fernandez Martinez[170], S. Fernandez Perez[13], J. Ferrando[45], A. Ferrari[168],
P. Ferrari[109], R. Ferrari[123a], D.E. Ferreira de Lima[60b], A. Ferrer[170], D. Ferrere[52], C. Ferretti[92],
F. Fiedler[86], A. Filipčič[78], M. Filipuzzi[45], F. Filthaut[108], M. Fincke-Keeler[172], K.D. Finelli[152],
M.C.N. Fiolhais[128a,128c,q], L. Fiorini[170], A. Fischer[2], C. Fischer[13], J. Fischer[178], W.C. Fisher[93],

N. Flaschel[45], I. Fleck[143], P. Fleischmann[92], G.T. Fletcher[141], R.R.M. Fletcher[124], T. Flick[178],
B.M. Flierl[102], L.R. Flores Castillo[62a], M.J. Flowerdew[103], G.T. Forcolin[87], A. Formica[138],
A. Forti[87], A.G. Foster[19], D. Fournier[119], H. Fox[75], S. Fracchia[13], P. Francavilla[83],
M. Franchini[22a,22b], D. Francis[32], L. Franconi[121], M. Franklin[59], M. Frate[166],
M. Fraternali[123a,123b], D. Freeborn[81], S.M. Fressard-Batraneanu[32], F. Friedrich[47],
D. Froidevaux[32], J.A. Frost[122], C. Fukunaga[158], E. Fullana Torregrosa[86], T. Fusayasu[104],
J. Fuster[170], C. Gabaldon[58], O. Gabizon[154], A. Gabrielli[22a,22b], A. Gabrielli[16], G.P. Gach[41a],
S. Gadatsch[32], G. Gagliardi[53a,53b], L.G. Gagnon[97], P. Gagnon[64], C. Galea[108],
B. Galhardo[128a,128c], E.J. Gallas[122], B.J. Gallop[133], P. Gallus[130], G. Galster[39], K.K. Gan[113],
S. Ganguly[37], J. Gao[36a], Y. Gao[49], Y.S. Gao[145,g], F.M. Garay Walls[49], C. García[170],
J.E. García Navarro[170], M. Garcia-Sciveres[16], R.W. Gardner[33], N. Garelli[145], V. Garonne[121],
A. Gascon Bravo[45], K. Gasnikova[45], C. Gatti[50], A. Gaudiello[53a,53b], G. Gaudio[123a],
L. Gauthier[97], I.L. Gavrilenko[98], C. Gay[171], G. Gaycken[23], E.N. Gazis[10], Z. Gecse[171],
C.N.P. Gee[133], Ch. Geich-Gimbel[23], M. Geisen[86], M.P. Geisler[60a], K. Gellerstedt[148a,148b],
C. Gemme[53a], M.H. Genest[58], C. Geng[36a,r], S. Gentile[134a,134b], C. Gentsos[156], S. George[80],
D. Gerbaudo[13], A. Gershon[155], S. Ghasemi[143], M. Ghneimat[23], B. Giacobbe[22a],
S. Giagu[134a,134b], P. Giannetti[126a,126b], S.M. Gibson[80], M. Gignac[171], M. Gilchriese[16],
T.P.S. Gillam[30], D. Gillberg[31], G. Gilles[178], D.M. Gingrich[3,d], N. Giokaris[9,*],
M.P. Giordani[167a,167c], F.M. Giorgi[22a], P.F. Giraud[138], P. Giromini[59], D. Giugni[94a], F. Giuli[122],
C. Giuliani[103], M. Giulini[60b], B.K. Gjelsten[121], S. Gkaitatzis[156], I. Gkialas[9],
E.L. Gkougkousis[139], L.K. Gladilin[101], C. Glasman[85], J. Glatzer[13], P.C.F. Glaysher[49],
A. Glazov[45], M. Goblirsch-Kolb[25], J. Godlewski[42], S. Goldfarb[91], T. Golling[52], D. Golubkov[132],
A. Gomes[128a,128b,128d], R. Gonçalo[128a], R. Goncalves Gama[26a],
J. Goncalves Pinto Firmino Da Costa[138], G. Gonella[51], L. Gonella[19], A. Gongadze[68],
S. González de la Hoz[170], S. Gonzalez-Sevilla[52], L. Goossens[32], P.A. Gorbounov[99],
H.A. Gordon[27], I. Gorelov[107], B. Gorini[32], E. Gorini[76a,76b], A. Gorišek[78], A.T. Goshaw[48],
C. Gössling[46], M.I. Gostkin[68], C.R. Goudet[119], D. Goujdami[137c], A.G. Goussiou[140],
N. Govender[147b,s], E. Gozani[154], L. Graber[57], I. Grabowska-Bold[41a], P.O.J. Gradin[58],
P. Grafström[22a,22b], J. Gramling[52], E. Gramstad[121], S. Grancagnolo[17], V. Gratchev[125],
P.M. Gravila[28e], H.M. Gray[32], E. Graziani[136a], Z.D. Greenwood[82,t], C. Grefe[23], K. Gregersen[81],
I.M. Gregor[45], P. Grenier[145], K. Grevtsov[5], J. Griffiths[8], A.A. Grillo[139], K. Grimm[75],
S. Grinstein[13,u], Ph. Gris[37], J.-F. Grivaz[119], S. Groh[86], E. Gross[175], J. Grosse-Knetter[57],
G.C. Grossi[82], Z.J. Grout[81], L. Guan[92], W. Guan[176], J. Guenther[65], F. Guescini[52], D. Guest[166],
O. Gueta[155], B. Gui[113], E. Guido[53a,53b], T. Guillemin[5], S. Guindon[2], U. Gul[56], C. Gumpert[32],
J. Guo[36c], W. Guo[92], Y. Guo[36a,r], R. Gupta[43], S. Gupta[122], G. Gustavino[134a,134b],
P. Gutierrez[115], N.G. Gutierrez Ortiz[81], C. Gutschow[81], C. Guyot[138], C. Gwenlan[122],
C.B. Gwilliam[77], A. Haas[112], C. Haber[16], H.K. Hadavand[8], A. Hadef[88], S. Hageböck[23],
M. Hagihara[164], H. Hakobyan[180,*], M. Haleem[45], J. Haley[116], G. Halladjian[93], G.D. Hallewell[88],
K. Hamacher[178], P. Hamal[117], K. Hamano[172], A. Hamilton[147a], G.N. Hamity[141], P.G. Hamnett[45],
L. Han[36a], S. Han[35a], K. Hanagaki[69,v], K. Hanawa[157], M. Hance[139], B. Haney[124], P. Hanke[60a],
R. Hanna[138], J.B. Hansen[39], J.D. Hansen[39], M.C. Hansen[23], P.H. Hansen[39], K. Hara[164],
A.S. Hard[176], T. Harenberg[178], F. Hariri[119], S. Harkusha[95], R.D. Harrington[49], P.F. Harrison[173],
F. Hartjes[109], N.M. Hartmann[102], M. Hasegawa[70], Y. Hasegawa[142], A. Hasib[115], S. Hassani[138],
S. Haug[18], R. Hauser[93], L. Hauswald[47], M. Havranek[129], C.M. Hawkes[19], R.J. Hawkings[32],
D. Hayakawa[159], D. Hayden[93], C.P. Hays[122], J.M. Hays[79], H.S. Hayward[77], S.J. Haywood[133],
S.J. Head[19], T. Heck[86], V. Hedberg[84], L. Heelan[8], K.K. Heidegger[51], S. Heim[124], T. Heim[16],
B. Heinemann[45,w], J.J. Heinrich[102], L. Heinrich[112], C. Heinz[55], J. Hejbal[129], L. Helary[32],
S. Hellman[148a,148b], C. Helsens[32], J. Henderson[122], R.C.W. Henderson[75], Y. Heng[176],

S. Henkelmann[171], A.M. Henriques Correia[32], S. Henrot-Versille[119], G.H. Herbert[17], H. Herde[25],
V. Herget[177], Y. Hernández Jiménez[147c], G. Herten[51], R. Hertenberger[102], L. Hervas[32],
G.G. Hesketh[81], N.P. Hessey[163a], J.W. Hetherly[43], E. Higón-Rodriguez[170], E. Hill[172], J.C. Hill[30],
K.H. Hiller[45], S.J. Hillier[19], I. Hinchliffe[16], E. Hines[124], M. Hirose[51], D. Hirschbuehl[178],
O. Hladik[129], X. Hoad[49], J. Hobbs[150], N. Hod[163a], M.C. Hodgkinson[141], P. Hodgson[141],
A. Hoecker[32], M.R. Hoeferkamp[107], F. Hoenig[102], D. Hohn[23], T.R. Holmes[16], M. Homann[46],
S. Honda[164], T. Honda[69], T.M. Hong[127], B.H. Hooberman[169], W.H. Hopkins[118], Y. Horii[105],
A.J. Horton[144], J-Y. Hostachy[58], S. Hou[153], A. Hoummada[137a], J. Howarth[45], J. Hoya[74],
M. Hrabovsky[117], I. Hristova[17], J. Hrivnac[119], T. Hryn'ova[5], A. Hrynevich[96], P.J. Hsu[63],
S.-C. Hsu[140], Q. Hu[36a], S. Hu[36c], Y. Huang[45], Z. Hubacek[130], F. Hubaut[88], F. Huegging[23],
T.B. Huffman[122], E.W. Hughes[38], G. Hughes[75], M. Huhtinen[32], P. Huo[150], N. Huseynov[68,b],
J. Huston[93], J. Huth[59], G. Iacobucci[52], G. Iakovidis[27], I. Ibragimov[143], L. Iconomidou-Fayard[119],
E. Ideal[179], P. Iengo[32], O. Igonkina[109,x], T. Iizawa[174], Y. Ikegami[69], M. Ikeno[69], Y. Ilchenko[11,y],
D. Iliadis[156], N. Ilic[145], G. Introzzi[123a,123b], P. Ioannou[9,*], M. Iodice[136a], K. Iordanidou[38],
V. Ippolito[59], N. Ishijima[120], M. Ishino[157], M. Ishitsuka[159], C. Issever[122], S. Istin[20a], F. Ito[164],
J.M. Iturbe Ponce[87], R. Iuppa[162a,162b], H. Iwasaki[69], J.M. Izen[44], V. Izzo[106a], S. Jabbar[3],
B. Jackson[124], P. Jackson[1], V. Jain[2], K.B. Jakobi[86], K. Jakobs[51], S. Jakobsen[32], T. Jakoubek[129],
D.O. Jamin[116], D.K. Jana[82], R. Jansky[65], J. Janssen[23], M. Janus[57], P.A. Janus[41a],
G. Jarlskog[84], N. Javadov[68,b], T. Javůrek[51], M. Javurkova[51], F. Jeanneau[138], L. Jeanty[16],
J. Jejelava[54a,z], G.-Y. Jeng[152], P. Jenni[51,aa], C. Jeske[173], S. Jézéquel[5], H. Ji[176], J. Jia[150],
H. Jiang[67], Y. Jiang[36a], Z. Jiang[145], S. Jiggins[81], J. Jimenez Pena[170], S. Jin[35a], A. Jinaru[28b],
O. Jinnouchi[159], H. Jivan[147c], P. Johansson[141], K.A. Johns[7], C.A. Johnson[64], W.J. Johnson[140],
K. Jon-And[148a,148b], G. Jones[173], R.W.L. Jones[75], S. Jones[7], T.J. Jones[77], J. Jongmanns[60a],
P.M. Jorge[128a,128b], J. Jovicevic[163a], X. Ju[176], A. Juste Rozas[13,u], M.K. Köhler[175],
A. Kaczmarska[42], M. Kado[119], H. Kagan[113], M. Kagan[145], S.J. Kahn[88], T. Kaji[174],
E. Kajomovitz[48], C.W. Kalderon[122], A. Kaluza[86], S. Kama[43], A. Kamenshchikov[132],
N. Kanaya[157], S. Kaneti[30], L. Kanjir[78], V.A. Kantserov[100], J. Kanzaki[69], B. Kaplan[112],
L.S. Kaplan[176], A. Kapliy[33], D. Kar[147c], K. Karakostas[10], A. Karamaoun[3], N. Karastathis[10],
M.J. Kareem[57], E. Karentzos[10], S.N. Karpov[68], Z.M. Karpova[68], K. Karthik[112],
V. Kartvelishvili[75], A.N. Karyukhin[132], K. Kasahara[164], L. Kashif[176], R.D. Kass[113],
A. Kastanas[149], Y. Kataoka[157], C. Kato[157], A. Katre[52], J. Katzy[45], K. Kawade[105],
K. Kawagoe[73], T. Kawamoto[157], G. Kawamura[57], V.F. Kazanin[111,c], R. Keeler[172], R. Kehoe[43],
J.S. Keller[45], J.J. Kempster[80], H. Keoshkerian[161], O. Kepka[129], B.P. Kerševan[78], S. Kersten[178],
R.A. Keyes[90], M. Khader[169], F. Khalil-zada[12], A. Khanov[116], A.G. Kharlamov[111,c],
T. Kharlamova[111,c], T.J. Khoo[52], V. Khovanskiy[99,*], E. Khramov[68], J. Khubua[54b,ab], S. Kido[70],
C.R. Kilby[80], H.Y. Kim[8], S.H. Kim[164], Y.K. Kim[33], N. Kimura[156], O.M. Kind[17], B.T. King[77],
M. King[170], D. Kirchmeier[47], J. Kirk[133], A.E. Kiryunin[103], T. Kishimoto[157], D. Kisielewska[41a],
F. Kiss[51], K. Kiuchi[164], O. Kivernyk[138], E. Kladiva[146b], T. Klapdor-Kleingrothaus[51],
M.H. Klein[38], M. Klein[77], U. Klein[77], K. Kleinknecht[86], P. Klimek[110], A. Klimentov[27],
R. Klingenberg[46], T. Klioutchnikova[32], E.-E. Kluge[60a], P. Kluit[109], S. Kluth[103], J. Knapik[42],
E. Kneringer[65], E.B.F.G. Knoops[88], A. Knue[103], A. Kobayashi[157], D. Kobayashi[159],
T. Kobayashi[157], M. Kobel[47], M. Kocian[145], P. Kodys[131], T. Koffas[31], E. Koffeman[109],
N.M. Köhler[103], T. Koi[145], H. Kolanoski[17], M. Kolb[60b], I. Koletsou[5], A.A. Komar[98,*],
Y. Komori[157], T. Kondo[69], N. Kondrashova[36c], K. Köneke[51], A.C. König[108], T. Kono[69,ac],
R. Konoplich[112,ad], N. Konstantinidis[81], R. Kopeliansky[64], S. Koperny[41a], A.K. Kopp[51],
K. Korcyl[42], K. Kordas[156], A. Korn[81], A.A. Korol[111,c], I. Korolkov[13], E.V. Korolkova[141],
O. Kortner[103], S. Kortner[103], T. Kosek[131], V.V. Kostyukhin[23], A. Kotwal[48], A. Koulouris[10],
A. Kourkoumeli-Charalampidi[123a,123b], C. Kourkoumelis[9], V. Kouskoura[27], A.B. Kowalewska[42],

R. Kowalewski[172], T.Z. Kowalski[41a], C. Kozakai[157], W. Kozanecki[138], A.S. Kozhin[132],
V.A. Kramarenko[101], G. Kramberger[78], D. Krasnopevtsev[100], M.W. Krasny[83],
A. Krasznahorkay[32], A. Kravchenko[27], M. Kretz[60c], J. Kretzschmar[77], K. Kreutzfeldt[55],
P. Krieger[161], K. Krizka[33], K. Kroeninger[46], H. Kroha[103], J. Kroll[124], J. Kroseberg[23],
J. Krstic[14], U. Kruchonak[68], H. Krüger[23], N. Krumnack[67], M.C. Kruse[48], M. Kruskal[24],
T. Kubota[91], H. Kucuk[81], S. Kuday[4b], J.T. Kuechler[178], S. Kuehn[51], A. Kugel[60c], F. Kuger[177],
T. Kuhl[45], V. Kukhtin[68], R. Kukla[138], Y. Kulchitsky[95], S. Kuleshov[34b], M. Kuna[134a,134b],
T. Kunigo[71], A. Kupco[129], O. Kuprash[155], H. Kurashige[70], L.L. Kurchaninov[163a],
Y.A. Kurochkin[95], M.G. Kurth[44], V. Kus[129], E.S. Kuwertz[172], M. Kuze[159], J. Kvita[117],
T. Kwan[172], D. Kyriazopoulos[141], A. La Rosa[103], J.L. La Rosa Navarro[26d], L. La Rotonda[40a,40b],
C. Lacasta[170], F. Lacava[134a,134b], J. Lacey[31], H. Lacker[17], D. Lacour[83], E. Ladygin[68],
R. Lafaye[5], B. Laforge[83], T. Lagouri[179], S. Lai[57], S. Lammers[64], W. Lampl[7], E. Lançon[138],
U. Landgraf[51], M.P.J. Landon[79], M.C. Lanfermann[52], V.S. Lang[60a], J.C. Lange[13],
A.J. Lankford[166], F. Lanni[27], K. Lantzsch[23], A. Lanza[123a], A. Lapertosa[53a,53b], S. Laplace[83],
C. Lapoire[32], J.F. Laporte[138], T. Lari[94a], F. Lasagni Manghi[22a,22b], M. Lassnig[32], P. Laurelli[50],
W. Lavrijsen[16], A.T. Law[139], P. Laycock[77], T. Lazovich[59], M. Lazzaroni[94a,94b], B. Le[91],
O. Le Dortz[83], E. Le Guirriec[88], E.P. Le Quilleuc[138], M. LeBlanc[172], T. LeCompte[6],
F. Ledroit-Guillon[58], C.A. Lee[27], S.C. Lee[153], L. Lee[1], B. Lefebvre[90], G. Lefebvre[83],
M. Lefebvre[172], F. Legger[102], C. Leggett[16], A. Lehan[77], G. Lehmann Miotto[32], X. Lei[7],
W.A. Leight[31], A.G. Leister[179], M.A.L. Leite[26d], R. Leitner[131], D. Lellouch[175], B. Lemmer[57],
K.J.C. Leney[81], T. Lenz[23], B. Lenzi[32], R. Leone[7], S. Leone[126a,126b], C. Leonidopoulos[49],
S. Leontsinis[10], G. Lerner[151], C. Leroy[97], A.A.J. Lesage[138], C.G. Lester[30], M. Levchenko[125],
J. Levêque[5], D. Levin[92], L.J. Levinson[175], M. Levy[19], D. Lewis[79], M. Leyton[44], B. Li[36a,r],
C. Li[36a], H. Li[150], L. Li[48], L. Li[36c], Q. Li[35a], S. Li[48], X. Li[87], Y. Li[143], Z. Liang[35a],
B. Liberti[135a], A. Liblong[161], P. Lichard[32], K. Lie[169], J. Liebal[23], W. Liebig[15], A. Limosani[152],
S.C. Lin[153,ae], T.H. Lin[86], B.E. Lindquist[150], A.E. Lionti[52], E. Lipeles[124], A. Lipniacka[15],
M. Lisovyi[60b], T.M. Liss[169], A. Lister[171], A.M. Litke[139], B. Liu[153,af], D. Liu[153], H. Liu[92],
H. Liu[27], J. Liu[36b], J.B. Liu[36a], K. Liu[88], L. Liu[169], M. Liu[36a], Y.L. Liu[36a], Y. Liu[36a],
M. Livan[123a,123b], A. Lleres[58], J. Llorente Merino[35a], S.L. Lloyd[79], F. Lo Sterzo[153],
E.M. Lobodzinska[45], P. Loch[7], F.K. Loebinger[87], K.M. Loew[25], A. Loginov[179,*], T. Lohse[17],
K. Lohwasser[45], M. Lokajicek[129], B.A. Long[24], J.D. Long[169], R.E. Long[75], L. Longo[76a,76b],
K.A. Looper[113], J.A. Lopez[34b], D. Lopez Mateos[59], B. Lopez Paredes[141], I. Lopez Paz[13],
A. Lopez Solis[83], J. Lorenz[102], N. Lorenzo Martinez[64], M. Losada[21], P.J. Lösel[102], X. Lou[35a],
A. Lounis[119], J. Love[6], P.A. Love[75], H. Lu[62a], N. Lu[92], H.J. Lubatti[140], C. Luci[134a,134b],
A. Lucotte[58], C. Luedtke[51], F. Luehring[64], W. Lukas[65], L. Luminari[134a], O. Lundberg[148a,148b],
B. Lund-Jensen[149], P.M. Luzi[83], D. Lynn[27], R. Lysak[129], E. Lytken[84], V. Lyubushkin[68],
H. Ma[27], L.L. Ma[36b], Y. Ma[36b], G. Maccarrone[50], A. Macchiolo[103], C.M. Macdonald[141],
B. Maček[78], J. Machado Miguens[124,128b], D. Madaffari[88], R. Madar[37], H.J. Maddocks[168],
W.F. Mader[47], A. Madsen[45], J. Maeda[70], S. Maeland[15], T. Maeno[27], A. Maevskiy[101],
E. Magradze[57], J. Mahlstedt[109], C. Maiani[119], C. Maidantchik[26a], A.A. Maier[103], T. Maier[102],
A. Maio[128a,128b,128d], S. Majewski[118], Y. Makida[69], N. Makovec[119], B. Malaescu[83],
Pa. Malecki[42], V.P. Maleev[125], F. Malek[58], U. Mallik[66], D. Malon[6], C. Malone[30], S. Maltezos[10],
S. Malyukov[32], J. Mamuzic[170], G. Mancini[50], L. Mandelli[94a], I. Mandić[78], J. Maneira[128a,128b],
L. Manhaes de Andrade Filho[26b], J. Manjarres Ramos[163b], A. Mann[102], A. Manousos[32],
B. Mansoulie[138], J.D. Mansour[35a], R. Mantifel[90], M. Mantoani[57], S. Manzoni[94a,94b],
L. Mapelli[32], G. Marceca[29], L. March[52], G. Marchiori[83], M. Marcisovsky[129], M. Marjanovic[14],
D.E. Marley[92], F. Marroquim[26a], S.P. Marsden[87], Z. Marshall[16], S. Marti-Garcia[170],
B. Martin[93], T.A. Martin[173], V.J. Martin[49], B. Martin dit Latour[15], M. Martinez[13,u],

V.I. Martinez Outschoorn[169], S. Martin-Haugh[133], V.S. Martoiu[28b], A.C. Martyniuk[81],
A. Marzin[32], L. Masetti[86], T. Mashimo[157], R. Mashinistov[98], J. Masik[87], A.L. Maslennikov[111,c],
I. Massa[22a,22b], L. Massa[22a,22b], P. Mastrandrea[5], A. Mastroberardino[40a,40b], T. Masubuchi[157],
P. Mättig[178], J. Mattmann[86], J. Maurer[28b], S.J. Maxfield[77], D.A. Maximov[111,c], R. Mazini[153],
I. Maznas[156], S.M. Mazza[94a,94b], N.C. Mc Fadden[107], G. Mc Goldrick[161], S.P. Mc Kee[92],
A. McCarn[92], R.L. McCarthy[150], T.G. McCarthy[103], L.I. McClymont[81], E.F. McDonald[91],
J.A. Mcfayden[81], G. Mchedlidze[57], S.J. McMahon[133], R.A. McPherson[172,n], M. Medinnis[45],
S. Meehan[140], S. Mehlhase[102], A. Mehta[77], K. Meier[60a], C. Meineck[102], B. Meirose[44],
D. Melini[170,ag], B.R. Mellado Garcia[147c], M. Melo[146a], F. Meloni[18], S.B. Menary[87], L. Meng[77],
X.T. Meng[92], A. Mengarelli[22a,22b], S. Menke[103], E. Meoni[165], S. Mergelmeyer[17], P. Mermod[52],
L. Merola[106a,106b], C. Meroni[94a], F.S. Merritt[33], A. Messina[134a,134b], J. Metcalfe[6], A.S. Mete[166],
C. Meyer[86], C. Meyer[124], J-P. Meyer[138], J. Meyer[109], H. Meyer Zu Theenhausen[60a], F. Miano[151],
R.P. Middleton[133], S. Miglioranzi[53a,53b], L. Mijović[49], G. Mikenberg[175], M. Mikestikova[129],
M. Mikuž[78], M. Milesi[91], A. Milic[27], D.W. Miller[33], C. Mills[49], A. Milov[175],
D.A. Milstead[148a,148b], A.A. Minaenko[132], Y. Minami[157], I.A. Minashvili[68], A.I. Mincer[112],
B. Mindur[41a], M. Mineev[68], Y. Minegishi[157], Y. Ming[176], L.M. Mir[13], K.P. Mistry[124],
T. Mitani[174], J. Mitrevski[102], V.A. Mitsou[170], A. Miucci[18], P.S. Miyagawa[141], A. Mizukami[69],
J.U. Mjörnmark[84], M. Mlynarikova[131], T. Moa[148a,148b], K. Mochizuki[97], P. Mogg[51],
S. Mohapatra[38], S. Molander[148a,148b], R. Moles-Valls[23], R. Monden[71], M.C. Mondragon[93],
K. Mönig[45], J. Monk[39], E. Monnier[88], A. Montalbano[150], J. Montejo Berlingen[32],
F. Monticelli[74], S. Monzani[94a,94b], R.W. Moore[3], N. Morange[119], D. Moreno[21],
M. Moreno Llácer[57], P. Morettini[53a], S. Morgenstern[32], D. Mori[144], T. Mori[157], M. Morii[59],
M. Morinaga[157], V. Morisbak[121], S. Moritz[86], A.K. Morley[152], G. Mornacchi[32], J.D. Morris[79],
L. Morvaj[150], P. Moschovakos[10], M. Mosidze[54b], H.J. Moss[141], J. Moss[145,ah], K. Motohashi[159],
R. Mount[145], E. Mountricha[27], E.J.W. Moyse[89], S. Muanza[88], R.D. Mudd[19], F. Mueller[103],
J. Mueller[127], R.S.P. Mueller[102], T. Mueller[30], D. Muenstermann[75], P. Mullen[56], G.A. Mullier[18],
F.J. Munoz Sanchez[87], J.A. Murillo Quijada[19], W.J. Murray[173,133], H. Musheghyan[57],
M. Muškinja[78], A.G. Myagkov[132,ai], M. Myska[130], B.P. Nachman[16], O. Nackenhorst[52],
K. Nagai[122], R. Nagai[69,ac], K. Nagano[69], Y. Nagasaka[61], K. Nagata[164], M. Nagel[51], E. Nagy[88],
A.M. Nairz[32], Y. Nakahama[105], K. Nakamura[69], T. Nakamura[157], I. Nakano[114],
R.F. Naranjo Garcia[45], R. Narayan[11], D.I. Narrias Villar[60a], I. Naryshkin[125], T. Naumann[45],
G. Navarro[21], R. Nayyar[7], H.A. Neal[92], P.Yu. Nechaeva[98], T.J. Neep[87], A. Negri[123a,123b],
M. Negrini[22a], S. Nektarijevic[108], C. Nellist[119], A. Nelson[166], S. Nemecek[129], P. Nemethy[112],
A.A. Nepomuceno[26a], M. Nessi[32,aj], M.S. Neubauer[169], M. Neumann[178], R.M. Neves[112],
P. Nevski[27], P.R. Newman[19], T. Nguyen Manh[97], R.B. Nickerson[122], R. Nicolaidou[138],
J. Nielsen[139], V. Nikolaenko[132,ai], I. Nikolic-Audit[83], K. Nikolopoulos[19], J.K. Nilsen[121],
P. Nilsson[27], Y. Ninomiya[157], A. Nisati[134a], R. Nisius[103], T. Nobe[157], M. Nomachi[120],
I. Nomidis[31], T. Nooney[79], S. Norberg[115], M. Nordberg[32], N. Norjoharuddeen[122],
O. Novgorodova[47], S. Nowak[103], M. Nozaki[69], L. Nozka[117], K. Ntekas[166], E. Nurse[81], F. Nuti[91],
D.C. O'Neil[144], A.A. O'Rourke[45], V. O'Shea[56], F.G. Oakham[31,d], H. Oberlack[103],
T. Obermann[23], J. Ocariz[83], A. Ochi[70], I. Ochoa[38], J.P. Ochoa-Ricoux[34a], S. Oda[73], S. Odaka[69],
H. Ogren[64], A. Oh[87], S.H. Oh[48], C.C. Ohm[16], H. Ohman[168], H. Oide[53a,53b], H. Okawa[164],
Y. Okumura[157], T. Okuyama[69], A. Olariu[28b], L.F. Oleiro Seabra[128a], S.A. Olivares Pino[49],
D. Oliveira Damazio[27], A. Olszewski[42], J. Olszowska[42], A. Onofre[128a,128e], K. Onogi[105],
P.U.E. Onyisi[11,y], M.J. Oreglia[33], Y. Oren[155], D. Orestano[136a,136b], N. Orlando[62b], R.S. Orr[161],
B. Osculati[53a,53b,*], R. Ospanov[87], G. Otero y Garzon[29], H. Otono[73], M. Ouchrif[137d],
F. Ould-Saada[121], A. Ouraou[138], K.P. Oussoren[109], Q. Ouyang[35a], M. Owen[56], R.E. Owen[19],
V.E. Ozcan[20a], N. Ozturk[8], K. Pachal[144], A. Pacheco Pages[13], L. Pacheco Rodriguez[138],

C. Padilla Aranda[13], S. Pagan Griso[16], M. Paganini[179], F. Paige[27], P. Pais[89], K. Pajchel[121],
G. Palacino[64], S. Palazzo[40a,40b], S. Palestini[32], M. Palka[41b], D. Pallin[37],
E.St. Panagiotopoulou[10], I. Panagoulias[10], C.E. Pandini[83], J.G. Panduro Vazquez[80],
P. Pani[148a,148b], S. Panitkin[27], D. Pantea[28b], L. Paolozzi[52], Th.D. Papadopoulou[10],
K. Papageorgiou[9], A. Paramonov[6], D. Paredes Hernandez[179], A.J. Parker[75], M.A. Parker[30],
K.A. Parker[141], F. Parodi[53a,53b], J.A. Parsons[38], U. Parzefall[51], V.R. Pascuzzi[161],
E. Pasqualucci[134a], S. Passaggio[53a], Fr. Pastore[80], G. Pásztor[31,ak], S. Pataraia[178], J.R. Pater[87],
T. Pauly[32], J. Pearce[172], B. Pearson[115], L.E. Pedersen[39], S. Pedraza Lopez[170], R. Pedro[128a,128b],
S.V. Peleganchuk[111,c], O. Penc[129], C. Peng[35a], H. Peng[36a], J. Penwell[64], B.S. Peralva[26b],
M.M. Perego[138], D.V. Perepelitsa[27], E. Perez Codina[163a], L. Perini[94a,94b], H. Pernegger[32],
S. Perrella[106a,106b], R. Peschke[45], V.D. Peshekhonov[68], K. Peters[45], R.F.Y. Peters[87],
B.A. Petersen[32], T.C. Petersen[39], E. Petit[58], A. Petridis[1], C. Petridou[156], P. Petroff[119],
E. Petrolo[134a], M. Petrov[122], F. Petrucci[136a,136b], N.E. Pettersson[89], A. Peyaud[138], R. Pezoa[34b],
P.W. Phillips[133], G. Piacquadio[150], E. Pianori[173], A. Picazio[89], E. Piccaro[79], M. Piccinini[22a,22b],
M.A. Pickering[122], R. Piegaia[29], J.E. Pilcher[33], A.D. Pilkington[87], A.W.J. Pin[87],
M. Pinamonti[167a,167c,al], J.L. Pinfold[3], A. Pingel[39], S. Pires[83], H. Pirumov[45], M. Pitt[175],
L. Plazak[146a], M.-A. Pleier[27], V. Pleskot[86], E. Plotnikova[68], D. Pluth[67], R. Poettgen[148a,148b],
L. Poggioli[119], D. Pohl[23], G. Polesello[123a], A. Poley[45], A. Policicchio[40a,40b], R. Polifka[161],
A. Polini[22a], C.S. Pollard[56], V. Polychronakos[27], K. Pommès[32], L. Pontecorvo[134a], B.G. Pope[93],
G.A. Popeneciu[28c], A. Poppleton[32], S. Pospisil[130], K. Potamianos[16], I.N. Potrap[68], C.J. Potter[30],
C.T. Potter[118], G. Poulard[32], J. Poveda[32], V. Pozdnyakov[68], M.E. Pozo Astigarraga[32],
P. Pralavorio[88], A. Pranko[16], S. Prell[67], D. Price[87], L.E. Price[6], M. Primavera[76a], S. Prince[90],
K. Prokofiev[62c], F. Prokoshin[34b], S. Protopopescu[27], J. Proudfoot[6], M. Przybycien[41a],
D. Puddu[136a,136b], M. Purohit[27,am], P. Puzo[119], J. Qian[92], G. Qin[56], Y. Qin[87], A. Quadt[57],
W.B. Quayle[167a,167b], M. Queitsch-Maitland[45], D. Quilty[56], S. Raddum[121], V. Radeka[27],
V. Radescu[122], S.K. Radhakrishnan[150], P. Radloff[118], P. Rados[91], F. Ragusa[94a,94b], G. Rahal[181],
J.A. Raine[87], S. Rajagopalan[27], M. Rammensee[32], C. Rangel-Smith[168], M.G. Ratti[94a,94b],
D.M. Rauch[45], F. Rauscher[102], S. Rave[86], T. Ravenscroft[56], I. Ravinovich[175], M. Raymond[32],
A.L. Read[121], N.P. Readioff[77], M. Reale[76a,76b], D.M. Rebuzzi[123a,123b], A. Redelbach[177],
G. Redlinger[27], R. Reece[139], R.G. Reed[147c], K. Reeves[44], L. Rehnisch[17], J. Reichert[124],
A. Reiss[86], C. Rembser[32], H. Ren[35a], M. Rescigno[134a], S. Resconi[94a], E.D. Resseguie[124],
O.L. Rezanova[111,c], P. Reznicek[131], R. Rezvani[97], R. Richter[103], S. Richter[81], E. Richter-Was[41b],
O. Ricken[23], M. Ridel[83], P. Rieck[103], C.J. Riegel[178], J. Rieger[57], O. Rifki[115], M. Rijssenbeek[150],
A. Rimoldi[123a,123b], M. Rimoldi[18], L. Rinaldi[22a], B. Ristić[52], E. Ritsch[32], I. Riu[13],
F. Rizatdinova[116], E. Rizvi[79], C. Rizzi[13], R.T. Roberts[87], S.H. Robertson[90,n],
A. Robichaud-Veronneau[90], D. Robinson[30], J.E.M. Robinson[45], A. Robson[56], C. Roda[126a,126b],
Y. Rodina[88,an], A. Rodriguez Perez[13], D. Rodriguez Rodriguez[170], S. Roe[32], C.S. Rogan[59],
O. Røhne[121], J. Roloff[59], A. Romaniouk[100], M. Romano[22a,22b], S.M. Romano Saez[37],
E. Romero Adam[170], N. Rompotis[140], M. Ronzani[51], L. Roos[83], E. Ros[170], S. Rosati[134a],
K. Rosbach[51], P. Rose[139], N.-A. Rosien[57], V. Rossetti[148a,148b], E. Rossi[106a,106b], L.P. Rossi[53a],
J.H.N. Rosten[30], R. Rosten[140], M. Rotaru[28b], I. Roth[175], J. Rothberg[140], D. Rousseau[119],
A. Rozanov[88], Y. Rozen[154], X. Ruan[147c], F. Rubbo[145], M.S. Rudolph[161], F. Rühr[51],
A. Ruiz-Martinez[31], Z. Rurikova[51], N.A. Rusakovich[68], A. Ruschke[102], H.L. Russell[140],
J.P. Rutherfoord[7], N. Ruthmann[32], Y.F. Ryabov[125], M. Rybar[169], G. Rybkin[119], S. Ryu[6],
A. Ryzhov[132], G.F. Rzehorz[57], A.F. Saavedra[152], G. Sabato[109], S. Sacerdoti[29],
H.F-W. Sadrozinski[139], R. Sadykov[68], F. Safai Tehrani[134a], P. Saha[110], M. Sahinsoy[60a],
M. Saimpert[138], T. Saito[157], H. Sakamoto[157], Y. Sakurai[174], G. Salamanna[136a,136b],
A. Salamon[135a,135b], J.E. Salazar Loyola[34b], D. Salek[109], P.H. Sales De Bruin[140], D. Salihagic[103],

A. Salnikov[145], J. Salt[170], D. Salvatore[40a,40b], F. Salvatore[151], A. Salvucci[62a,62b,62c],
A. Salzburger[32], D. Sammel[51], D. Sampsonidis[156], J. Sánchez[170], V. Sanchez Martinez[170],
A. Sanchez Pineda[106a,106b], H. Sandaker[121], R.L. Sandbach[79], M. Sandhoff[178], C. Sandoval[21],
D.P.C. Sankey[133], M. Sannino[53a,53b], A. Sansoni[50], C. Santoni[37], R. Santonico[135a,135b],
H. Santos[128a], I. Santoyo Castillo[151], K. Sapp[127], A. Sapronov[68], J.G. Saraiva[128a,128d],
B. Sarrazin[23], O. Sasaki[69], K. Sato[164], E. Sauvan[5], G. Savage[80], P. Savard[161,d], N. Savic[103],
C. Sawyer[133], L. Sawyer[82,t], J. Saxon[33], C. Sbarra[22a], A. Sbrizzi[22a,22b], T. Scanlon[81],
D.A. Scannicchio[166], M. Scarcella[152], V. Scarfone[40a,40b], J. Schaarschmidt[175], P. Schacht[103],
B.M. Schachtner[102], D. Schaefer[32], L. Schaefer[124], R. Schaefer[45], J. Schaeffer[86], S. Schaepe[23],
S. Schaetzel[60b], U. Schäfer[86], A.C. Schaffer[119], D. Schaile[102], R.D. Schamberger[150], V. Scharf[60a],
V.A. Schegelsky[125], D. Scheirich[131], M. Schernau[166], C. Schiavi[53a,53b], S. Schier[139], C. Schillo[51],
M. Schioppa[40a,40b], S. Schlenker[32], K.R. Schmidt-Sommerfeld[103], K. Schmieden[32], C. Schmitt[86],
S. Schmitt[45], S. Schmitz[86], B. Schneider[163a], U. Schnoor[51], L. Schoeffel[138], A. Schoening[60b],
B.D. Schoenrock[93], E. Schopf[23], M. Schott[86], J.F.P. Schouwenberg[108], J. Schovancova[8],
S. Schramm[52], M. Schreyer[177], N. Schuh[86], A. Schulte[86], M.J. Schultens[23],
H.-C. Schultz-Coulon[60a], H. Schulz[17], M. Schumacher[51], B.A. Schumm[139], Ph. Schune[138],
A. Schwartzman[145], T.A. Schwarz[92], H. Schweiger[87], Ph. Schwemling[138], R. Schwienhorst[93],
J. Schwindling[138], T. Schwindt[23], G. Sciolla[25], F. Scuri[126a,126b], F. Scutti[91], J. Searcy[92],
P. Seema[23], S.C. Seidel[107], A. Seiden[139], F. Seifert[130], J.M. Seixas[26a], G. Sekhniaidze[106a],
K. Sekhon[92], S.J. Sekula[43], N. Semprini-Cesari[22a,22b], C. Serfon[121], L. Serin[119],
L. Serkin[167a,167b], M. Sessa[136a,136b], R. Seuster[172], H. Severini[115], T. Sfiligoj[78], F. Sforza[32],
A. Sfyrla[52], E. Shabalina[57], N.W. Shaikh[148a,148b], L.Y. Shan[35a], R. Shang[169], J.T. Shank[24],
M. Shapiro[16], P.B. Shatalov[99], K. Shaw[167a,167b], S.M. Shaw[87], A. Shcherbakova[148a,148b],
C.Y. Shehu[151], P. Sherwood[81], L. Shi[153,ao], S. Shimizu[70], C.O. Shimmin[166], M. Shimojima[104],
S. Shirabe[73], M. Shiyakova[68,ap], A. Shmeleva[98], D. Shoaleh Saadi[97], M.J. Shochet[33],
S. Shojaii[94a], D.R. Shope[115], S. Shrestha[113], E. Shulga[100], M.A. Shupe[7], P. Sicho[129],
A.M. Sickles[169], P.E. Sidebo[149], E. Sideras Haddad[147c], O. Sidiropoulou[177], D. Sidorov[116],
A. Sidoti[22a,22b], F. Siegert[47], Dj. Sijacki[14], J. Silva[128a,128d], S.B. Silverstein[148a], V. Simak[130],
Lj. Simic[14], S. Simion[119], E. Simioni[86], B. Simmons[81], D. Simon[37], M. Simon[86], P. Sinervo[161],
N.B. Sinev[118], M. Sioli[22a,22b], G. Siragusa[177], I. Siral[92], S.Yu. Sivoklokov[101], J. Sjölin[148a,148b],
M.B. Skinner[75], H.P. Skottowe[59], P. Skubic[115], M. Slater[19], T. Slavicek[130], M. Slawinska[109],
K. Sliwa[165], R. Slovak[131], V. Smakhtin[175], B.H. Smart[5], L. Smestad[15], J. Smiesko[146a],
S.Yu. Smirnov[100], Y. Smirnov[100], L.N. Smirnova[101,aq], O. Smirnova[84], J.W. Smith[57],
M.N.K. Smith[38], R.W. Smith[38], M. Smizanska[75], K. Smolek[130], A.A. Snesarev[98], I.M. Snyder[118],
S. Snyder[27], R. Sobie[172,n], F. Socher[47], A. Soffer[155], D.A. Soh[153], G. Sokhrannyi[78],
C.A. Solans Sanchez[32], M. Solar[130], E.Yu. Soldatov[100], U. Soldevila[170], A.A. Solodkov[132],
A. Soloshenko[68], O.V. Solovyanov[132], V. Solovyev[125], P. Sommer[51], H. Son[165], H.Y. Song[36a,ar],
A. Sood[16], A. Sopczak[130], V. Sopko[130], V. Sorin[13], D. Sosa[60b], C.L. Sotiropoulou[126a,126b],
R. Soualah[167a,167c], A.M. Soukharev[111,c], D. South[45], B.C. Sowden[80], S. Spagnolo[76a,76b],
M. Spalla[126a,126b], M. Spangenberg[173], F. Spanò[80], D. Sperlich[17], F. Spettel[103], R. Spighi[22a],
G. Spigo[32], L.A. Spiller[91], M. Spousta[131], R.D. St. Denis[56,*], A. Stabile[94a], R. Stamen[60a],
S. Stamm[17], E. Stanecka[42], R.W. Stanek[6], C. Stanescu[136a], M. Stanescu-Bellu[45],
M.M. Stanitzki[45], S. Stapnes[121], E.A. Starchenko[132], G.H. Stark[33], J. Stark[58], S.H Stark[39],
P. Staroba[129], P. Starovoitov[60a], S. Stärz[32], R. Staszewski[42], P. Steinberg[27], B. Stelzer[144],
H.J. Stelzer[32], O. Stelzer-Chilton[163a], H. Stenzel[55], G.A. Stewart[56], J.A. Stillings[23],
M.C. Stockton[90], M. Stoebe[90], G. Stoicea[28b], P. Stolte[57], S. Stonjek[103], A.R. Stradling[8],
A. Straessner[47], M.E. Stramaglia[18], J. Strandberg[149], S. Strandberg[148a,148b], A. Strandlie[121],
M. Strauss[115], P. Strizenec[146b], R. Ströhmer[177], D.M. Strom[118], R. Stroynowski[43], A. Strubig[108],

S.A. Stucci[27], B. Stugu[15], N.A. Styles[45], D. Su[145], J. Su[127], S. Suchek[60a], Y. Sugaya[120], M. Suk[130], V.V. Sulin[98], S. Sultansoy[4c], T. Sumida[71], S. Sun[59], X. Sun[3], J.E. Sundermann[51], K. Suruliz[151], C.J.E. Suster[152], M.R. Sutton[151], S. Suzuki[69], M. Svatos[129], M. Swiatlowski[33], S.P. Swift[2], I. Sykora[146a], T. Sykora[131], D. Ta[51], K. Tackmann[45], J. Taenzer[155], A. Taffard[166], R. Tafirout[163a], N. Taiblum[155], H. Takai[27], R. Takashima[72], T. Takeshita[142], Y. Takubo[69], M. Talby[88], A.A. Talyshev[111,c], J. Tanaka[157], M. Tanaka[159], R. Tanaka[119], S. Tanaka[69], R. Tanioka[70], B.B. Tannenwald[113], S. Tapia Araya[34b], S. Tapprogge[86], S. Tarem[154], G.F. Tartarelli[94a], P. Tas[131], M. Tasevsky[129], T. Tashiro[71], E. Tassi[40a,40b], A. Tavares Delgado[128a,128b], Y. Tayalati[137e], A.C. Taylor[107], G.N. Taylor[91], P.T.E. Taylor[91], W. Taylor[163b], F.A. Teischinger[32], P. Teixeira-Dias[80], D. Temple[144], H. Ten Kate[32], P.K. Teng[153], J.J. Teoh[120], F. Tepel[178], S. Terada[69], K. Terashi[157], J. Terron[85], S. Terzo[13], M. Testa[50], R.J. Teuscher[161,n], T. Theveneaux-Pelzer[88], J.P. Thomas[19], J. Thomas-Wilsker[80], P.D. Thompson[19], A.S. Thompson[56], L.A. Thomsen[179], E. Thomson[124], M.J. Tibbetts[16], R.E. Ticse Torres[88], V.O. Tikhomirov[98,as], Yu.A. Tikhonov[111,c], S. Timoshenko[100], P. Tipton[179], S. Tisserant[88], K. Todome[159], T. Todorov[5,*], T. Todorova-Nova[131], J. Tojo[73], S. Tokár[146a], K. Tokushuku[69], E. Tolley[59], L. Tomlinson[87], M. Tomoto[105], L. Tompkins[145,at], K. Toms[107], B. Tong[59], P. Tornambe[51], E. Torrence[118], H. Torres[144], E. Torró Pastor[140], J. Toth[88,au], F. Touchard[88], D.R. Tovey[141], T. Trefzger[177], A. Tricoli[27], I.M. Trigger[163a], S. Trincaz-Duvoid[83], M.F. Tripiana[13], W. Trischuk[161], B. Trocmé[58], A. Trofymov[45], C. Troncon[94a], M. Trottier-McDonald[16], M. Trovatelli[172], L. Truong[167a,167c], M. Trzebinski[42], A. Trzupek[42], J.C-L. Tseng[122], P.V. Tsiareshka[95], G. Tsipolitis[10], N. Tsirintanis[9], S. Tsiskaridze[13], V. Tsiskaridze[51], E.G. Tskhadadze[54a], K.M. Tsui[62a], I.I. Tsukerman[99], V. Tsulaia[16], S. Tsuno[69], D. Tsybychev[150], Y. Tu[62b], A. Tudorache[28b], V. Tudorache[28b], T.T. Tulbure[28a], A.N. Tuna[59], S.A. Tupputi[22a,22b], S. Turchikhin[68], D. Turgeman[175], I. Turk Cakir[4b,av], R. Turra[94a,94b], P.M. Tuts[38], G. Ucchielli[22a,22b], I. Ueda[157], M. Ughetto[148a,148b], F. Ukegawa[164], G. Unal[32], A. Undrus[27], G. Unel[166], F.C. Ungaro[91], Y. Unno[69], C. Unverdorben[102], J. Urban[146b], P. Urquijo[91], P. Urrejola[86], G. Usai[8], J. Usui[69], L. Vacavant[88], V. Vacek[130], B. Vachon[90], C. Valderanis[102], E. Valdes Santurio[148a,148b], N. Valencic[109], S. Valentinetti[22a,22b], A. Valero[170], L. Valéry[13], S. Valkar[131], J.A. Valls Ferrer[170], W. Van Den Wollenberg[109], P.C. Van Der Deijl[109], H. van der Graaf[109], N. van Eldik[154], P. van Gemmeren[6], J. Van Nieuwkoop[144], I. van Vulpen[109], M.C. van Woerden[109], M. Vanadia[134a,134b], W. Vandelli[32], R. Vanguri[124], A. Vaniachine[160], P. Vankov[109], G. Vardanyan[180], R. Vari[134a], E.W. Varnes[7], T. Varol[43], D. Varouchas[83], A. Vartapetian[8], K.E. Varvell[152], J.G. Vasquez[179], G.A. Vasquez[34b], F. Vazeille[37], T. Vazquez Schroeder[90], J. Veatch[57], V. Veeraraghavan[7], L.M. Veloce[161], F. Veloso[128a,128c], S. Veneziano[134a], A. Ventura[76a,76b], M. Venturi[172], N. Venturi[161], A. Venturini[25], V. Vercesi[123a], M. Verducci[134a,134b], W. Verkerke[109], J.C. Vermeulen[109], A. Vest[47,aw], M.C. Vetterli[144,d], O. Viazlo[84], I. Vichou[169,*], T. Vickey[141], O.E. Vickey Boeriu[141], G.H.A. Viehhauser[122], S. Viel[16], L. Vigani[122], M. Villa[22a,22b], M. Villaplana Perez[94a,94b], E. Vilucchi[50], M.G. Vincter[31], V.B. Vinogradov[68], A. Vishwakarma[45], C. Vittori[22a,22b], I. Vivarelli[151], S. Vlachos[10], M. Vlasak[130], M. Vogel[178], P. Vokac[130], G. Volpi[126a,126b], M. Volpi[91], H. von der Schmitt[103], E. von Toerne[23], V. Vorobel[131], K. Vorobev[100], M. Vos[170], R. Voss[32], J.H. Vossebeld[77], N. Vranjes[14], M. Vranjes Milosavljevic[14], V. Vrba[129], M. Vreeswijk[109], R. Vuillermet[32], I. Vukotic[33], P. Wagner[23], W. Wagner[178], H. Wahlberg[74], S. Wahrmund[47], J. Wakabayashi[105], J. Walder[75], R. Walker[102], W. Walkowiak[143], V. Wallangen[148a,148b], C. Wang[35b], C. Wang[36b,ax], F. Wang[176], H. Wang[16], H. Wang[43], J. Wang[45], J. Wang[152], K. Wang[90], Q. Wang[115], R. Wang[6], S.M. Wang[153], T. Wang[38], W. Wang[36a], C. Wanotayaroj[118], A. Warburton[90], C.P. Ward[30], D.R. Wardrope[81], A. Washbrook[49], P.M. Watkins[19], A.T. Watson[19], M.F. Watson[19], G. Watts[140], S. Watts[87], B.M. Waugh[81], S. Webb[86], M.S. Weber[18], S.W. Weber[177],

S.A. Weber[31], J.S. Webster[6], A.R. Weidberg[122], B. Weinert[64], J. Weingarten[57], C. Weiser[51], H. Weits[109], P.S. Wells[32], T. Wenaus[27], T. Wengler[32], S. Wenig[32], N. Wermes[23], M.D. Werner[67], P. Werner[32], M. Wessels[60a], J. Wetter[165], K. Whalen[118], N.L. Whallon[140], A.M. Wharton[75], A. White[8], M.J. White[1], R. White[34b], D. Whiteson[166], F.J. Wickens[133], W. Wiedenmann[176], M. Wielers[133], C. Wiglesworth[39], L.A.M. Wiik-Fuchs[23], A. Wildauer[103], F. Wilk[87], H.G. Wilkens[32], H.H. Williams[124], S. Williams[109], C. Willis[93], S. Willocq[89], J.A. Wilson[19], I. Wingerter-Seez[5], F. Winklmeier[118], O.J. Winston[151], B.T. Winter[23], M. Wittgen[145], M. Wobisch[82,t], T.M.H. Wolf[109], R. Wolff[88], M.W. Wolter[42], H. Wolters[128a,128c], S.D. Worm[133], B.K. Wosiek[42], J. Wotschack[32], M.J. Woudstra[87], K.W. Wozniak[42], M. Wu[58], M. Wu[33], S.L. Wu[176], X. Wu[52], Y. Wu[92], T.R. Wyatt[87], B.M. Wynne[49], S. Xella[39], Z. Xi[92], D. Xu[35a], L. Xu[27], B. Yabsley[152], S. Yacoob[147a], D. Yamaguchi[159], Y. Yamaguchi[120], A. Yamamoto[69], S. Yamamoto[157], T. Yamanaka[157], K. Yamauchi[105], Y. Yamazaki[70], Z. Yan[24], H. Yang[36c], H. Yang[176], Y. Yang[153], Z. Yang[15], W-M. Yao[16], Y.C. Yap[83], Y. Yasu[69], E. Yatsenko[5], K.H. Yau Wong[23], J. Ye[43], S. Ye[27], I. Yeletskikh[68], E. Yildirim[86], K. Yorita[174], R. Yoshida[6], K. Yoshihara[124], C. Young[145], C.J.S. Young[32], S. Youssef[24], D.R. Yu[16], J. Yu[8], J.M. Yu[92], J. Yu[67], L. Yuan[70], S.P.Y. Yuen[23], I. Yusuff[30,ay], B. Zabinski[42], G. Zacharis[10], R. Zaidan[66], A.M. Zaitsev[132,ai], N. Zakharchuk[45], J. Zalieckas[15], A. Zaman[150], S. Zambito[59], D. Zanzi[91], C. Zeitnitz[178], M. Zeman[130], A. Zemla[41a], J.C. Zeng[169], Q. Zeng[145], O. Zenin[132], T. Ženiš[146a], D. Zerwas[119], D. Zhang[92], F. Zhang[176], G. Zhang[36a,ar], H. Zhang[35b], J. Zhang[6], L. Zhang[51], L. Zhang[36a], M. Zhang[169], R. Zhang[23], R. Zhang[36a,ax], X. Zhang[36b], Y. Zhang[35a], Z. Zhang[119], X. Zhao[43], Y. Zhao[36b,az], Z. Zhao[36a], A. Zhemchugov[68], J. Zhong[122], B. Zhou[92], C. Zhou[176], L. Zhou[38], L. Zhou[43], M. Zhou[35a], M. Zhou[150], N. Zhou[35c], C.G. Zhu[36b], H. Zhu[35a], J. Zhu[92], Y. Zhu[36a], X. Zhuang[35a], K. Zhukov[98], A. Zibell[177], D. Zieminska[64], N.I. Zimine[68], C. Zimmermann[86], S. Zimmermann[51], Z. Zinonos[57], M. Zinser[86], M. Ziolkowski[143], L. Živković[14], G. Zobernig[176], A. Zoccoli[22a,22b], M. zur Nedden[17], L. Zwalinski[32].

1   Department of Physics, University of Adelaide, Adelaide, Australia
2   Physics Department, SUNY Albany, Albany NY, U.S.A.
3   Department of Physics, University of Alberta, Edmonton AB, Canada
4   (a) Department of Physics, Ankara University, Ankara; (b) Istanbul Aydin University, Istanbul; (c) Division of Physics, TOBB University of Economics and Technology, Ankara, Turkey
5   LAPP, CNRS/IN2P3 and Université Savoie Mont Blanc, Annecy-le-Vieux, France
6   High Energy Physics Division, Argonne National Laboratory, Argonne IL, U.S.A.
7   Department of Physics, University of Arizona, Tucson AZ, U.S.A.
8   Department of Physics, The University of Texas at Arlington, Arlington TX, U.S.A.
9   Physics Department, National and Kapodistrian University of Athens, Athens, Greece
10 Physics Department, National Technical University of Athens, Zografou, Greece
11 Department of Physics, The University of Texas at Austin, Austin TX, U.S.A.
12 Institute of Physics, Azerbaijan Academy of Sciences, Baku, Azerbaijan
13 Institut de Física d'Altes Energies (IFAE), The Barcelona Institute of Science and Technology, Barcelona, Spain
14 Institute of Physics, University of Belgrade, Belgrade, Serbia
15 Department for Physics and Technology, University of Bergen, Bergen, Norway
16 Physics Division, Lawrence Berkeley National Laboratory and University of California, Berkeley CA, U.S.A.
17 Department of Physics, Humboldt University, Berlin, Germany
18 Albert Einstein Center for Fundamental Physics and Laboratory for High Energy Physics, University of Bern, Bern, Switzerland
19 School of Physics and Astronomy, University of Birmingham, Birmingham, U.K.

20 [a] *Department of Physics, Bogazici University, Istanbul;* [b] *Department of Physics Engineering, Gaziantep University, Gaziantep;* [d] *Istanbul Bilgi University, Faculty of Engineering and Natural Sciences, Istanbul,Turkey;* [e] *Bahcesehir University, Faculty of Engineering and Natural Sciences, Istanbul, Turkey*

21 *Centro de Investigaciones, Universidad Antonio Narino, Bogota, Colombia*

22 [a] *INFN Sezione di Bologna;* [b] *Dipartimento di Fisica e Astronomia, Università di Bologna, Bologna, Italy*

23 *Physikalisches Institut, University of Bonn, Bonn, Germany*

24 *Department of Physics, Boston University, Boston MA, U.S.A.*

25 *Department of Physics, Brandeis University, Waltham MA, U.S.A.*

26 [a] *Universidade Federal do Rio De Janeiro COPPE/EE/IF, Rio de Janeiro;* [b] *Electrical Circuits Department, Federal University of Juiz de Fora (UFJF), Juiz de Fora;* [c] *Federal University of Sao Joao del Rei (UFSJ), Sao Joao del Rei;* [d] *Instituto de Fisica, Universidade de Sao Paulo, Sao Paulo, Brazil*

27 *Physics Department, Brookhaven National Laboratory, Upton NY, U.S.A.*

28 [a] *Transilvania University of Brasov, Brasov, Romania;* [b] *Horia Hulubei National Institute of Physics and Nuclear Engineering, Bucharest;* [c] *National Institute for Research and Development of Isotopic and Molecular Technologies, Physics Department, Cluj Napoca;* [d] *University Politehnica Bucharest, Bucharest;* [e] *West University in Timisoara, Timisoara, Romania*

29 *Departamento de Física, Universidad de Buenos Aires, Buenos Aires, Argentina*

30 *Cavendish Laboratory, University of Cambridge, Cambridge, U.K.*

31 *Department of Physics, Carleton University, Ottawa ON, Canada*

32 *CERN, Geneva, Switzerland*

33 *Enrico Fermi Institute, University of Chicago, Chicago IL, U.S.A.*

34 [a] *Departamento de Física, Pontificia Universidad Católica de Chile, Santiago;* [b] *Departamento de Física, Universidad Técnica Federico Santa María, Valparaíso, Chile*

35 [a] *Institute of High Energy Physics, Chinese Academy of Sciences, Beijing;* [b] *Department of Physics, Nanjing University, Jiangsu;* [c] *Physics Department, Tsinghua University, Beijing 100084, China*

36 [a] *Department of Modern Physics, University of Science and Technology of China, Anhui;* [b] *School of Physics, Shandong University, Shandong;* [c] *Department of Physics and Astronomy, Key Laboratory for Particle Physics, Astrophysics and Cosmology, Ministry of Education; Shanghai Key Laboratory for Particle Physics and Cosmology, Shanghai Jiao Tong University, Shanghai (also at PKU-CHEP);, China*

37 *Université Clermont Auvergne, CNRS/IN2P3, LPC, Clermont-Ferrand, France*

38 *Nevis Laboratory, Columbia University, Irvington NY, U.S.A.*

39 *Niels Bohr Institute, University of Copenhagen, Kobenhavn, Denmark*

40 [a] *INFN Gruppo Collegato di Cosenza, Laboratori Nazionali di Frascati;* [b] *Dipartimento di Fisica, Università della Calabria, Rende, Italy*

41 [a] *AGH University of Science and Technology, Faculty of Physics and Applied Computer Science, Krakow;* [b] *Marian Smoluchowski Institute of Physics, Jagiellonian University, Krakow, Poland*

42 *Institute of Nuclear Physics Polish Academy of Sciences, Krakow, Poland*

43 *Physics Department, Southern Methodist University, Dallas TX, U.S.A.*

44 *Physics Department, University of Texas at Dallas, Richardson TX, U.S.A.*

45 *DESY, Hamburg and Zeuthen, Germany*

46 *Lehrstuhl für Experimentelle Physik IV, Technische Universität Dortmund, Dortmund, Germany*

47 *Institut für Kern- und Teilchenphysik, Technische Universität Dresden, Dresden, Germany*

48 *Department of Physics, Duke University, Durham NC, U.S.A.*

49 *SUPA - School of Physics and Astronomy, University of Edinburgh, Edinburgh, U.K.*

50 *INFN Laboratori Nazionali di Frascati, Frascati, Italy*

51 *Fakultät für Mathematik und Physik, Albert-Ludwigs-Universität, Freiburg, Germany*

52 *Departement de Physique Nucleaire et Corpusculaire, Université de Genève, Geneva, Switzerland*

[53] $^{(a)}$ *INFN Sezione di Genova;* $^{(b)}$ *Dipartimento di Fisica, Università di Genova, Genova, Italy*

[54] $^{(a)}$ *E. Andronikashvili Institute of Physics, Iv. Javakhishvili Tbilisi State University, Tbilisi;* $^{(b)}$ *High Energy Physics Institute, Tbilisi State University, Tbilisi, Georgia*

[55] *II Physikalisches Institut, Justus-Liebig-Universität Giessen, Giessen, Germany*

[56] *SUPA - School of Physics and Astronomy, University of Glasgow, Glasgow, U.K.*

[57] *II Physikalisches Institut, Georg-August-Universität, Göttingen, Germany*

[58] *Laboratoire de Physique Subatomique et de Cosmologie, Université Grenoble-Alpes, CNRS/IN2P3, Grenoble, France*

[59] *Laboratory for Particle Physics and Cosmology, Harvard University, Cambridge MA, U.S.A.*

[60] $^{(a)}$ *Kirchhoff-Institut für Physik, Ruprecht-Karls-Universität Heidelberg, Heidelberg;* $^{(b)}$ *Physikalisches Institut, Ruprecht-Karls-Universität Heidelberg, Heidelberg;* $^{(c)}$ *ZITI Institut für technische Informatik, Ruprecht-Karls-Universität Heidelberg, Mannheim, Germany*

[61] *Faculty of Applied Information Science, Hiroshima Institute of Technology, Hiroshima, Japan*

[62] $^{(a)}$ *Department of Physics, The Chinese University of Hong Kong, Shatin, N.T., Hong Kong;* $^{(b)}$ *Department of Physics, The University of Hong Kong, Hong Kong;* $^{(c)}$ *Department of Physics and Institute for Advanced Study, The Hong Kong University of Science and Technology, Clear Water Bay, Kowloon, Hong Kong, China*

[63] *Department of Physics, National Tsing Hua University, Taiwan, Taiwan*

[64] *Department of Physics, Indiana University, Bloomington IN, U.S.A.*

[65] *Institut für Astro- und Teilchenphysik, Leopold-Franzens-Universität, Innsbruck, Austria*

[66] *University of Iowa, Iowa City IA, U.S.A.*

[67] *Department of Physics and Astronomy, Iowa State University, Ames IA, U.S.A.*

[68] *Joint Institute for Nuclear Research, JINR Dubna, Dubna, Russia*

[69] *KEK, High Energy Accelerator Research Organization, Tsukuba, Japan*

[70] *Graduate School of Science, Kobe University, Kobe, Japan*

[71] *Faculty of Science, Kyoto University, Kyoto, Japan*

[72] *Kyoto University of Education, Kyoto, Japan*

[73] *Department of Physics, Kyushu University, Fukuoka, Japan*

[74] *Instituto de Física La Plata, Universidad Nacional de La Plata and CONICET, La Plata, Argentina*

[75] *Physics Department, Lancaster University, Lancaster, U.K.*

[76] $^{(a)}$ *INFN Sezione di Lecce;* $^{(b)}$ *Dipartimento di Matematica e Fisica, Università del Salento, Lecce, Italy*

[77] *Oliver Lodge Laboratory, University of Liverpool, Liverpool, U.K.*

[78] *Department of Experimental Particle Physics, Jožef Stefan Institute and Department of Physics, University of Ljubljana, Ljubljana, Slovenia*

[79] *School of Physics and Astronomy, Queen Mary University of London, London, U.K.*

[80] *Department of Physics, Royal Holloway University of London, Surrey, U.K.*

[81] *Department of Physics and Astronomy, University College London, London, U.K.*

[82] *Louisiana Tech University, Ruston LA, U.S.A.*

[83] *Laboratoire de Physique Nucléaire et de Hautes Energies, UPMC and Université Paris-Diderot and CNRS/IN2P3, Paris, France*

[84] *Fysiska institutionen, Lunds universitet, Lund, Sweden*

[85] *Departamento de Fisica Teorica C-15, Universidad Autonoma de Madrid, Madrid, Spain*

[86] *Institut für Physik, Universität Mainz, Mainz, Germany*

[87] *School of Physics and Astronomy, University of Manchester, Manchester, U.K.*

[88] *CPPM, Aix-Marseille Université and CNRS/IN2P3, Marseille, France*

[89] *Department of Physics, University of Massachusetts, Amherst MA, U.S.A.*

[90] *Department of Physics, McGill University, Montreal QC, Canada*

[91] *School of Physics, University of Melbourne, Victoria, Australia*

[92] *Department of Physics, The University of Michigan, Ann Arbor MI, U.S.A.*

[93] *Department of Physics and Astronomy, Michigan State University, East Lansing MI, U.S.A.*

[94] $^{(a)}$ *INFN Sezione di Milano;* $^{(b)}$ *Dipartimento di Fisica, Università di Milano, Milano, Italy*

[95] B.I. Stepanov Institute of Physics, National Academy of Sciences of Belarus, Minsk, Republic of Belarus

[96] Research Institute for Nuclear Problems of Byelorussian State University, Minsk, Republic of Belarus

[97] Group of Particle Physics, University of Montreal, Montreal QC, Canada

[98] P.N. Lebedev Physical Institute of the Russian Academy of Sciences, Moscow, Russia

[99] Institute for Theoretical and Experimental Physics (ITEP), Moscow, Russia

[100] National Research Nuclear University MEPhI, Moscow, Russia

[101] D.V. Skobeltsyn Institute of Nuclear Physics, M.V. Lomonosov Moscow State University, Moscow, Russia

[102] Fakultät für Physik, Ludwig-Maximilians-Universität München, München, Germany

[103] Max-Planck-Institut für Physik (Werner-Heisenberg-Institut), München, Germany

[104] Nagasaki Institute of Applied Science, Nagasaki, Japan

[105] Graduate School of Science and Kobayashi-Maskawa Institute, Nagoya University, Nagoya, Japan

[106] $^{(a)}$ INFN Sezione di Napoli; $^{(b)}$ Dipartimento di Fisica, Università di Napoli, Napoli, Italy

[107] Department of Physics and Astronomy, University of New Mexico, Albuquerque NM, U.S.A.

[108] Institute for Mathematics, Astrophysics and Particle Physics, Radboud University Nijmegen/Nikhef, Nijmegen, Netherlands

[109] Nikhef National Institute for Subatomic Physics and University of Amsterdam, Amsterdam, Netherlands

[110] Department of Physics, Northern Illinois University, DeKalb IL, U.S.A.

[111] Budker Institute of Nuclear Physics, SB RAS, Novosibirsk, Russia

[112] Department of Physics, New York University, New York NY, U.S.A.

[113] Ohio State University, Columbus OH, U.S.A.

[114] Faculty of Science, Okayama University, Okayama, Japan

[115] Homer L. Dodge Department of Physics and Astronomy, University of Oklahoma, Norman OK, U.S.A.

[116] Department of Physics, Oklahoma State University, Stillwater OK, U.S.A.

[117] Palacký University, RCPTM, Olomouc, Czech Republic

[118] Center for High Energy Physics, University of Oregon, Eugene OR, U.S.A.

[119] LAL, Univ. Paris-Sud, CNRS/IN2P3, Université Paris-Saclay, Orsay, France

[120] Graduate School of Science, Osaka University, Osaka, Japan

[121] Department of Physics, University of Oslo, Oslo, Norway

[122] Department of Physics, Oxford University, Oxford, U.K.

[123] $^{(a)}$ INFN Sezione di Pavia; $^{(b)}$ Dipartimento di Fisica, Università di Pavia, Pavia, Italy

[124] Department of Physics, University of Pennsylvania, Philadelphia PA, U.S.A.

[125] National Research Centre "Kurchatov Institute" B.P.Konstantinov Petersburg Nuclear Physics Institute, St. Petersburg, Russia

[126] $^{(a)}$ INFN Sezione di Pisa; $^{(b)}$ Dipartimento di Fisica E. Fermi, Università di Pisa, Pisa, Italy

[127] Department of Physics and Astronomy, University of Pittsburgh, Pittsburgh PA, U.S.A.

[128] $^{(a)}$ Laboratório de Instrumentação e Física Experimental de Partículas - LIP, Lisboa; $^{(b)}$ Faculdade de Ciências, Universidade de Lisboa, Lisboa; $^{(c)}$ Department of Physics, University of Coimbra, Coimbra; $^{(d)}$ Centro de Física Nuclear da Universidade de Lisboa, Lisboa; $^{(e)}$ Departamento de Fisica, Universidade do Minho, Braga; $^{(f)}$ Departamento de Fisica Teorica y del Cosmos and CAFPE, Universidad de Granada, Granada (Spain); $^{(g)}$ Dep Fisica and CEFITEC of Faculdade de Ciencias e Tecnologia, Universidade Nova de Lisboa, Caparica, Portugal

[129] Institute of Physics, Academy of Sciences of the Czech Republic, Praha, Czech Republic

[130] Czech Technical University in Prague, Praha, Czech Republic

[131] Charles University, Faculty of Mathematics and Physics, Prague, Czech Republic

[132] State Research Center Institute for High Energy Physics (Protvino), NRC KI, Russia

[133] Particle Physics Department, Rutherford Appleton Laboratory, Didcot, U.K.

[134] $^{(a)}$ INFN Sezione di Roma; $^{(b)}$ Dipartimento di Fisica, Sapienza Università di Roma, Roma, Italy

135 [a] *INFN Sezione di Roma Tor Vergata;* [b] *Dipartimento di Fisica, Università di Roma Tor Vergata, Roma, Italy*

136 [a] *INFN Sezione di Roma Tre;* [b] *Dipartimento di Matematica e Fisica, Università Roma Tre, Roma, Italy*

137 [a] *Faculté des Sciences Ain Chock, Réseau Universitaire de Physique des Hautes Energies - Université Hassan II, Casablanca;* [b] *Centre National de l'Energie des Sciences Techniques Nucleaires, Rabat;* [c] *Faculté des Sciences Semlalia, Université Cadi Ayyad, LPHEA-Marrakech;* [d] *Faculté des Sciences, Université Mohamed Premier and LPTPM, Oujda;* [e] *Faculté des sciences, Université Mohammed V, Rabat, Morocco*

138 *DSM/IRFU (Institut de Recherches sur les Lois Fondamentales de l'Univers), CEA Saclay (Commissariat à l'Energie Atomique et aux Energies Alternatives), Gif-sur-Yvette, France*

139 *Santa Cruz Institute for Particle Physics, University of California Santa Cruz, Santa Cruz CA, U.S.A.*

140 *Department of Physics, University of Washington, Seattle WA, U.S.A.*

141 *Department of Physics and Astronomy, University of Sheffield, Sheffield, U.K.*

142 *Department of Physics, Shinshu University, Nagano, Japan*

143 *Department Physik, Universität Siegen, Siegen, Germany*

144 *Department of Physics, Simon Fraser University, Burnaby BC, Canada*

145 *SLAC National Accelerator Laboratory, Stanford CA, U.S.A.*

146 [a] *Faculty of Mathematics, Physics & Informatics, Comenius University, Bratislava;* [b] *Department of Subnuclear Physics, Institute of Experimental Physics of the Slovak Academy of Sciences, Kosice, Slovak Republic*

147 [a] *Department of Physics, University of Cape Town, Cape Town;* [b] *Department of Physics, University of Johannesburg, Johannesburg;* [c] *School of Physics, University of the Witwatersrand, Johannesburg, South Africa*

148 [a] *Department of Physics, Stockholm University;* [b] *The Oskar Klein Centre, Stockholm, Sweden*

149 *Physics Department, Royal Institute of Technology, Stockholm, Sweden*

150 *Departments of Physics & Astronomy and Chemistry, Stony Brook University, Stony Brook NY, U.S.A.*

151 *Department of Physics and Astronomy, University of Sussex, Brighton, U.K.*

152 *School of Physics, University of Sydney, Sydney, Australia*

153 *Institute of Physics, Academia Sinica, Taipei, Taiwan*

154 *Department of Physics, Technion: Israel Institute of Technology, Haifa, Israel*

155 *Raymond and Beverly Sackler School of Physics and Astronomy, Tel Aviv University, Tel Aviv, Israel*

156 *Department of Physics, Aristotle University of Thessaloniki, Thessaloniki, Greece*

157 *International Center for Elementary Particle Physics and Department of Physics, The University of Tokyo, Tokyo, Japan*

158 *Graduate School of Science and Technology, Tokyo Metropolitan University, Tokyo, Japan*

159 *Department of Physics, Tokyo Institute of Technology, Tokyo, Japan*

160 *Tomsk State University, Tomsk, Russia*

161 *Department of Physics, University of Toronto, Toronto ON, Canada*

162 [a] *INFN-TIFPA;* [b] *University of Trento, Trento, Italy*

163 [a] *TRIUMF, Vancouver BC;* [b] *Department of Physics and Astronomy, York University, Toronto ON, Canada*

164 *Faculty of Pure and Applied Sciences, and Center for Integrated Research in Fundamental Science and Engineering, University of Tsukuba, Tsukuba, Japan*

165 *Department of Physics and Astronomy, Tufts University, Medford MA, U.S.A.*

166 *Department of Physics and Astronomy, University of California Irvine, Irvine CA, U.S.A.*

167 [a] *INFN Gruppo Collegato di Udine, Sezione di Trieste, Udine;* [b] *ICTP, Trieste;* [c] *Dipartimento di Chimica, Fisica e Ambiente, Università di Udine, Udine, Italy*

168 *Department of Physics and Astronomy, University of Uppsala, Uppsala, Sweden*

169 Department of Physics, University of Illinois, Urbana IL, U.S.A.

170 Instituto de Fisica Corpuscular (IFIC) and Departamento de Fisica Atomica, Molecular y Nuclear and Departamento de Ingeniería Electrónica and Instituto de Microelectrónica de Barcelona (IMB-CNM), University of Valencia and CSIC, Valencia, Spain

171 Department of Physics, University of British Columbia, Vancouver BC, Canada

172 Department of Physics and Astronomy, University of Victoria, Victoria BC, Canada

173 Department of Physics, University of Warwick, Coventry, U.K.

174 Waseda University, Tokyo, Japan

175 Department of Particle Physics, The Weizmann Institute of Science, Rehovot, Israel

176 Department of Physics, University of Wisconsin, Madison WI, U.S.A.

177 Fakultät für Physik und Astronomie, Julius-Maximilians-Universität, Würzburg, Germany

178 Fakultät für Mathematik und Naturwissenschaften, Fachgruppe Physik, Bergische Universität Wuppertal, Wuppertal, Germany

179 Department of Physics, Yale University, New Haven CT, U.S.A.

180 Yerevan Physics Institute, Yerevan, Armenia

181 Centre de Calcul de l'Institut National de Physique Nucléaire et de Physique des Particules (IN2P3), Villeurbanne, France

a Also at Department of Physics, King's College London, London, U.K.

b Also at Institute of Physics, Azerbaijan Academy of Sciences, Baku, Azerbaijan

c Also at Novosibirsk State University, Novosibirsk, Russia

d Also at TRIUMF, Vancouver BC, Canada

e Also at Department of Physics & Astronomy, University of Louisville, Louisville, KY, U.S.A.

f Also at Physics Department, An-Najah National University, Nablus, Palestine

g Also at Department of Physics, California State University, Fresno CA, U.S.A.

h Also at Department of Physics, University of Fribourg, Fribourg, Switzerland

i Also at Departament de Fisica de la Universitat Autonoma de Barcelona, Barcelona, Spain

j Also at Departamento de Fisica e Astronomia, Faculdade de Ciencias, Universidade do Porto, Portugal

k Also at Tomsk State University, Tomsk, Russia, Russia

l Also at The Collaborative Innovation Center of Quantum Matter (CICQM), Beijing, China

m Also at Universita di Napoli Parthenope, Napoli, Italy

n Also at Institute of Particle Physics (IPP), Canada

o Also at Horia Hulubei National Institute of Physics and Nuclear Engineering, Bucharest, Romania

p Also at Department of Physics, St. Petersburg State Polytechnical University, St. Petersburg, Russia

q Also at Borough of Manhattan Community College, City University of New York, New York City, U.S.A.

r Also at Department of Physics, The University of Michigan, Ann Arbor MI, U.S.A.

s Also at Centre for High Performance Computing, CSIR Campus, Rosebank, Cape Town, South Africa

t Also at Louisiana Tech University, Ruston LA, U.S.A.

u Also at Institucio Catalana de Recerca i Estudis Avancats, ICREA, Barcelona, Spain

v Also at Graduate School of Science, Osaka University, Osaka, Japan

w Also at Fakultät für Mathematik und Physik, Albert-Ludwigs-Universität, Freiburg, Germany

x Also at Institute for Mathematics, Astrophysics and Particle Physics, Radboud University Nijmegen/Nikhef, Nijmegen, Netherlands

y Also at Department of Physics, The University of Texas at Austin, Austin TX, U.S.A.

z Also at Institute of Theoretical Physics, Ilia State University, Tbilisi, Georgia

aa Also at CERN, Geneva, Switzerland

ab Also at Georgian Technical University (GTU),Tbilisi, Georgia

ac Also at Ochadai Academic Production, Ochanomizu University, Tokyo, Japan

^{ad} Also at Manhattan College, New York NY, U.S.A.

^{ae} Also at Academia Sinica Grid Computing, Institute of Physics, Academia Sinica, Taipei, Taiwan

^{af} Also at School of Physics, Shandong University, Shandong, China

^{ag} Also at Departamento de Fisica Teorica y del Cosmos and CAFPE, Universidad de Granada, Granada (Spain), Portugal

^{ah} Also at Department of Physics, California State University, Sacramento CA, U.S.A.

^{ai} Also at Moscow Institute of Physics and Technology State University, Dolgoprudny, Russia

^{aj} Also at Departement de Physique Nucleaire et Corpusculaire, Université de Genève, Geneva, Switzerland

^{ak} Also at Eotvos Lorand University, Budapest, Hungary

^{al} Also at International School for Advanced Studies (SISSA), Trieste, Italy

^{am} Also at Department of Physics and Astronomy, University of South Carolina, Columbia SC, U.S.A.

^{an} Also at Institut de Física d'Altes Energies (IFAE), The Barcelona Institute of Science and Technology, Barcelona, Spain

^{ao} Also at School of Physics, Sun Yat-sen University, Guangzhou, China

^{ap} Also at Institute for Nuclear Research and Nuclear Energy (INRNE) of the Bulgarian Academy of Sciences, Sofia, Bulgaria

^{aq} Also at Faculty of Physics, M.V.Lomonosov Moscow State University, Moscow, Russia

^{ar} Also at Institute of Physics, Academia Sinica, Taipei, Taiwan

^{as} Also at National Research Nuclear University MEPhI, Moscow, Russia

^{at} Also at Department of Physics, Stanford University, Stanford CA, U.S.A.

^{au} Also at Institute for Particle and Nuclear Physics, Wigner Research Centre for Physics, Budapest, Hungary

^{av} Also at Giresun University, Faculty of Engineering, Turkey

^{aw} Also at Flensburg University of Applied Sciences, Flensburg, Germany

^{ax} Also at CPPM, Aix-Marseille Université and CNRS/IN2P3, Marseille, France

^{ay} Also at University of Malaya, Department of Physics, Kuala Lumpur, Malaysia

^{az} Also at LAL, Univ. Paris-Sud, CNRS/IN2P3, Université Paris-Saclay, Orsay, France

* Deceased